FACULTY
OF MATHEMATICS
AND PHYSICS
Charles University

HABILITATION THESIS

Martin Veis

Magneto-optical spectroscopy as a probe of the electronic structure and magnetism of materials and nanostructures

Institute of Physics of Charles University

Prague 2025

To Filip, David, Linda, and Eva, who make my life meaningful every day.

Contents

Introduction

This habilitation thesis summarizes the research activities of the author in the field of magneto-optical spectroscopy, with a focus on materials and physical phenomena that show potential for applications in integrated photonics and spintronics. After his Ph.D., the author established a magneto-optical group at the Institute of Physics of Charles University and developed an experimental technique able to measure magneto-optical effects with high precision in a broad spectral range. This allowed him to use magneto-optical spectroscopy as a powerful tool to investigate the interplays between structural, electronic, magnetic, and optical properties, offering new insights into the underlying physical phenomena. These findings have not only broadened fundamental understandings but also contributed to the optimization of material preparation, improving their performance and applicability.

The results were concluded in 17 impacted publications and presented at numerous conferences. The studies were also subjects of several successfully defended Ph.D. theses of M. Zahradník, E. Jesenská, L. Beran and K. Tikuišis supervised by the author. Finally, the work was also financially supported by several grants awarded to the author as PI or co-PI from the Czech Grant Agency and Ministry of Education and Youth of the Czech Republic.

This work would never have been possible without the continuous support of a large number of people. Therefore, I would like to use this opportunity and express my gratitude to my Ph.D. supervisors Prof. Š. Višňovský (Charles University), who introduced me the beautiful field of magneto-optics, and Prof. A. Ishida (Shizuoka University), who broadened my expertise in semiconductors and solid state growth.

The great thanks belongs to my true friends, Dr. M. Orlita (LNCMI CNRS Grenoble), Dr. K Výborný (FZU AV ČR) and Dr. O. Heczko (FZU AV ČR) who kept my toughs forward and positive.

I also would like to thank former and current directors of the Institute of Physics of Charles University, Prof. V. Baumruk, Prof. J. Franc and Prof. P. Heřman, who always supported my research activities and created a pleasant working environment.

My huge gratitude belongs to my close colleagues at Charles University, Dr. R. Antoš, Dr. J. Hamrle, Doc. M. Kučera and Dr. K. Uhlířová with special thanks to Dr. J. Zázvorka for his friendship and support.

I also would like to thank our international collaborators, namely Prof. T. Ishibashi (NUT Japan), Prof. Ph. Lecoeur, Prof. G. Agnus, and Dr. T. Maroutian from Université Paris-Saclay, Prof. L. Bi (UEST China), Prof. L. Cohen and Dr. F. Johnson from Imperial College, London, for their exciting samples and ideas. A very special thanks belongs to Prof. C. A. Ross (MIT), who always supported me without a blink of an eye.

The work would not be possible without the collaborations with Doc. J. Mistrík (UPCE), Dr. M. Urbánek (CEITEC), Dr. M. Zelený (VUT Brno) and Dr. J. Zemen (FEL ČVUT).

I also would like to thank my formal and current students who stayed with me in the laboratory and did not allow me to get old, especially to L. Beran, M. Zahradník, E. Jesenská, K. Tikuišis, L. Ohnoutek, T. Maleček and M. Hubert.

My final thanks goes to my parents, brother, wife, and children for their everlasting love.

1. Magneto-optical phenomena linear in magnetization

On September 13^{th} 1845, Michael Faraday discovered the influence of the magnetized medium on the polarization of light after its propagation through the heavy glass made of silico-borate of lead. He wrote to his diary:

*A piece of heavy glass which was 2 inches by 1.8 inches, and 0.5 of an inch thick, being silico borate of lead, and polished on the two shortest edges, was experimented with. It gave no effects when the same magnetic poles or the contrary poles were on opposite sides (as respects the course of the polarized ray) – nor when the same poles were on the same side, either with a constant or intermitting current – BUT, when contrary magnetic poles were on the same side, there was an effect produced on the polarized ray, **and thus magnetic force and light were proved to have relation to each other**. This fact will most likely prove exceedingly fertile and of great value in the investigation of both conditions of natural force* [1].

That time, the discovery was really groundbreaking since the picture of light as an electromagnetic wave was not developed yet. The general idea was that light propagates by means of mechanical waves, similar to sound waves in fluids, or in a corpuscular manner. Faraday in his well known paper interconnected for the first time magnetism and light and proved to be related to each other:

*Thus is established, I think for the first time, **a true, direct relation and dependence between light and the magnetic and electric forces**; and thus, a great addition made to the facts and considerations which tend to prove that all natural forces are tied together, and have one common origin* [2].

This stimulated the first ideas, which led to the present picture of light as an electromagnetic wave, developed later by Maxwell and others. The pioneering works in magneto-optics have been conducted by Verdet and Becquerel, who formulated well-known linear relation between the magneto-optical Faraday rotation, applied magnetic field and length of the medium

$$\theta_F = V \cdot L \cdot B, \tag{1.1}$$

where V is so-called Verdet constant, L is the length of the medium and B is applied magnetic field.

Several decades later in 1876, John Kerr discovered an analogy to the Faraday effect on reflection. He observed a polarization change of linearly polarized light reflected from the polished pole of the electromagnet. In addition, he discovered that the reflected light was elliptically polarized. The magneto-optical phenomena started to play an important role in many experimental and theoretical discoveries in the first half of the 20^{th} century, involving famous physicists, such as Zeeman, Hall, Lorentz, and others. Today, magneto-optical phenomena refer to the interaction between light and magnetically altered materials, leading to changes in the properties of light (such as polarization or intensity) due to the magnetic state of the material, or vice versa. These include already mentioned Faraday and Kerr effects, Voight and Cotton-Mouton effects (quadratic in magnetization), optical reorientation (photo-induced change in magnetization of solid or gas-like paramagnets affected by circularly polarized emission), the inverse Faraday effect (magnetizing the medium after its irradiation by intense circularly polarized light), etc. They are widely used as experimental techniques for academic research in materials

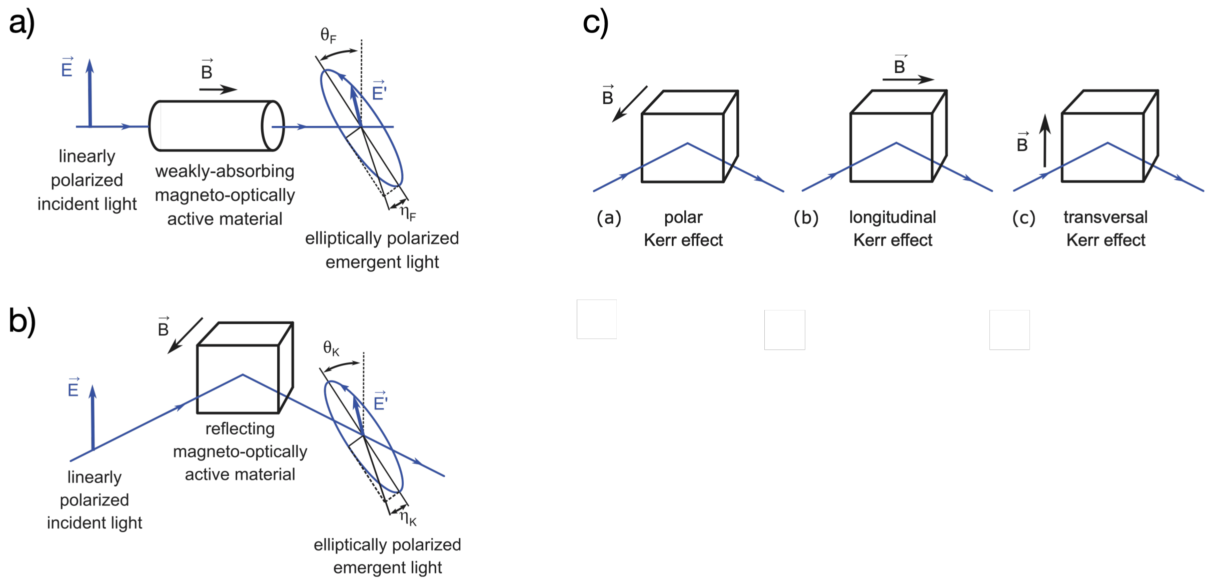

Figure 1.1: Schematic description of the a) Faraday geometry and b) Kerr geometry. Common magneto-optical Kerr geometries are shown in c). Adapted from [3].

physics, or industrial applications.

Phenomenologically the magneto-optical response of a medium can be described using permittivity tensor. When a material is placed into an external magnetic field, the magnetization induced by the field induces optical anisotropy in the material. The field is only a small perturbation and therefore the permittivity tensor of the material for the case of collinear magnetic order can be expressed as [4]

$$\varepsilon_{ij} = \varepsilon_{ij}^0 + K_{ijk}M_k + G_{ijkl}M_kM_l + ..., \tag{1.2}$$

where ε_{ij}^0 is non-magnetic permittivity tensor of the material (which describes anisotropic optical properties in the absence of net magnetization), $M_{k,l}$ are components of magnetization vector, and K_{ijk} and G_{ijkl} are elements of linear and quadratic magneto-optical tensors. Taking into account Onsager principle of reciprocity [5], the elements of permittivity tensor fulfill

$$\varepsilon_{ij}(\mathbf{M}) = \varepsilon_{ji}(\text{-}\mathbf{M}), \tag{1.3}$$

leading to its antisymmetric form. Since the applied magnetic field breaks the time-reversal symmetry, the propagation of light in magneto-optical medium becomes non-reciprocal. As a result, the polarization rotation of light propagating forward and backward in the magneto-optical medium has still the same sign, which is a crucial difference from classical optical activity. This non-reciprocity phenomenon is a basis of optical isolation described in following chapters.

With respect to the nature of the research presented in this thesis, we limit ourselves only to the introduction of the magneto-optical effects linear in magnetization. These include the most prominent magneto-optical phenomena:

- **Magneto-optical Faraday rotation and magnetic circular dichroism:** First discovered magneto-optical effect, which manifest itself as a rotation of the linear polarization of light upon its transmission through a magnetized medium. The direction of magnetization vector (or applied magnetic field) is parallel to the light

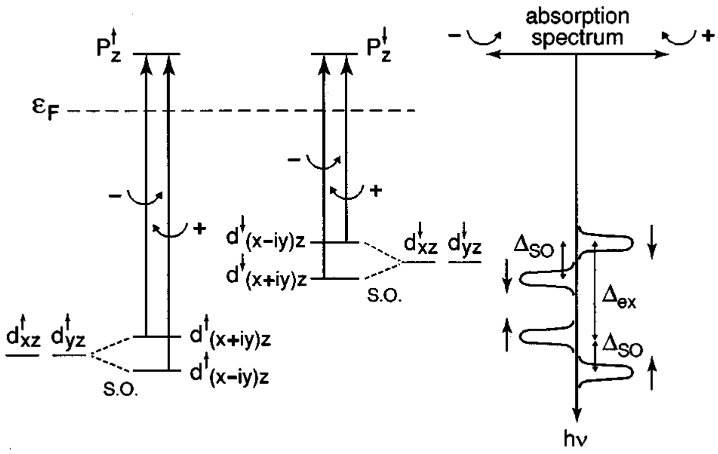

Figure 1.2: Schematic representation of electric dipolar optical transitions in ferromagnet with highlighted difference for left and right circularly polarized light. This induces magneto-optical response [6].

propagation. The schematic description of such geometry is depicted in Fig. 1.1a. Phenomenologically, the Faraday rotation can be explained by different refractive index of the material for left- and right- circularly polarized light. This difference is induced by the applied magnetic field (and subsequent magnetization). Since the circular polarizations of light form a basis in which any arbitrary polarization can be superposed, the Faraday rotation can be written in the form

$$\theta_F = \frac{\omega}{2c}(n_+ - n_-)L, \tag{1.4}$$

where ω is the angular frequency, c is the speed of light in vacuum and L is the length of the magneto-optically active medium. Equation (1.4) describe a basic principle of the non-reciprocal phase shift induced by magneto-optical phenomena and used in non-reciprocal isolation. Different absorption for left- and right- circularly polarized light also leads to the change of its polarization state after propagation in magneto-optical medium. This results in magnetic circular dichroism (MCD) so the outcoming light is elliptically polarized as sketched in Fig. 1.1a.

- **Complex magneto-optical Kerr effect:** The analogy to the Faraday effect upon the reflection. A linearly polarized incident light becomes elliptically polarized with the azimuth called Kerr rotation and ellipticity called Kerr ellipticity as schematically shown in Fig. 1.1b. Contrary to Faraday effect, one can distinguish three main geometries of Kerr magneto-optical effect based on the orientation of applied magnetic field and the plane of incident light. These are (i) polar, (ii) longitudinal, and (iii) transversal (schematically shown in Fig. 1.1c).

  In the approximation of small angles, the relation between the reflection coefficients (in the basis of s and p polarizations) and complex magneto-optical Kerr effect Φ_K for p polarized incident light can be written as

$$\frac{r_{sp}}{r_{pp}} = \Phi_K \approx \theta_K - i\epsilon_K, \tag{1.5}$$

  where r_{sp} and r_{pp} are the elements of Jones reflection matrix and θ_K and ϵ_K are the Kerr rotation and ellipticity angles.

Microscopically, the linear magneto-optical effects arise mainly from the electric dipole transitions that satisfy the selection rules $\Delta l = \pm 1$ and $\Delta m_l = \pm 1$. While the angular momentum rule implies only transitions between s and p, p and d, or d and f states, its z-projection selects the helicity of the light polarization ($\Delta m_l = 1$ for left- and $\Delta m_l = -1$ right-circular polarization). In the case of ferromagnetic materials, the exchange interactions lead to splitting of the d states, resulting in different optical absorptions for the majority and minority spins. However, such absorption is not sensitive to light polarization and does not induce magneto-optical response. To observe magneto-optical effects, the simultaneous existence of spin-orbit coupling is necessary to lift the orbital degeneracy of the d states and resolve different helicity of light polarization. This situation is schematically shown in Fig. 1.2. Therefore, elements with large spin-orbit coupling are often used to increase the magneto-optical response of ferri- and ferromagnetic materials.

Detailed descriptions of the physics of magneto-optical phenomena, including quadratic effects, can be found in various textbooks [3, 7, 8].

2. Employing magneto-optical phenomena in experimental research and industrial applications

Due to their high sensitivity to magnetism and electronic structure, magneto-optical phenomena are widely used in academic research. In addition, the induced change of light polarization can be utilized in optoelectronic or photonic devices that rely on this light property. This chapter summarizes experimental and theoretical magneto-optical approaches commonly used in academic research together with several industrial applications in which the magneto-optical phenomena play a crucial role. This outlines one of the main motivations for the research presented in the following chapters.

2.1 Precise measurements as a key for successful materials research

The drive for miniaturization in modern technology has led to extensive research on magnetic materials in the form of thin layers (with thickness typically in the nanometer range) that are key components in various spintronic, magneto-photonic and magnetic storage devices. 2D magnetic materials are another exciting and rapidly growing class of materials that have attracted significant attention in recent years [9]. These materials combine the unique properties of two-dimensional systems with intrinsic magnetism, promising for a broad range of potential applications in spintronics, quantum computing, and energy-efficient data storage. The discovery of ferromagnetism and antiferromagnetism in atomically thin layers, such as CrI_3 [10] and Fe_3GeTe_2 [11], has stimulated intense interest due to their tunable magnetic properties, which can be controlled by external stimuli such as electric fields, strain, or stacking configurations. However, such ultrathin films and atomically thin layers typically exhibit small magneto-optical effects (with amplitudes in order of 10^{-4} - 10^{-3} deg) as a result of their reduced thickness and volume. Such small angles make them challenging to detect in a wide spectral range and therefore to analyze the physical properties of investigated materials and their nanostructures. Consequently, there is a growing need for highly sensitive and precise magneto-optical measurement tools that can reliably capture these subtle effects.

Over the decades, several approaches have been developed to measure magneto-optical effects, each with its advantages and limitations. A detailed overview of the methods can be found in textbooks; see, e.g., [3, 8]. Here we summarize commonly used magneto-optical techniques:

- **Intensity based techniques:** Most basic techniques usually use only two nearly crossed polarizers: (i) input polarizer to define the polarization of incident light and (ii) analyzer to analyze the polarization state of the light transmitted/reflected from the magnetized sample. Nearly crossed polarizers are widely used in magneto-optical imaging of magnetic domains. The rotating analyzer approach, described in detail in the following paragraph, can reach high sensitivity and is capable of spectroscopic measurements.

- **Differential techniques:** They utilize a Wollaston prism or optical bridge to analyze the polarization state of reflected/transmitted light by detecting the intensity of two orthogonal polarizations. The magneto-optical effect is then proportional to the intensity difference between two detected polarizations. Such sensitive and precise techniques are commonly used in magneto-optical magnetometry or time-resolved magneto-optical measurements, where the laser is used as a light source.

- **Interferometric techniques:** Rely on non-reciprocal phase shift induced by the interaction of probe beam with magnetized sample, which induces small changes in its interference pattern with the reference beam. This approach, which has only non-reciprocal sensitivity, is able to detect magneto-optical effect with high precision at single wavelength of laser light. The commonly used interferometer is the Sagnac interferometer [12].

- **Polarization modulation techniques:** In all the above mentioned approaches, the DC signal arising from the impact of the transmitted/reflected light on the detector is detected. Despite nowadays available high-stability light sources, one can still improve the signal-to-noise ratio utilizing the polarization modulation element (such as photo-elastic modulator or Faraday cell) in the optical path and synchronic detection with a lock-in amplifier. Such an approach can be combined with all the above-mentioned techniques.

In the following paragraphs, we present a short description of an experimental setup which was developed in our magneto-optical laboratory at the Institute of Physics of Charles University and which is routinely used for spectroscopic purposes. This intensity-based technique employs a rotating analyzer and is schematically shown in Fig. 2.1. The light from the laser-driven broadband light source passes through the linear polarizer, which defines the polarization state of incident light (usually s or p polarization). After its transmission/reflection on the sample in an external magnetic field, it passes through the wave plate and analyzer (linear polarizer oriented near the crossed position with the first polarizer) which is mounted on the rotational stage. Finally, the light is detected by a CCD spectrometer and the intensity of the detected light is given by

$$I \approx \frac{T}{2}[\sin^2\alpha + (\theta_K \cos\delta + \epsilon_K \sin\delta)\sin 2\alpha] + C, \tag{2.1}$$

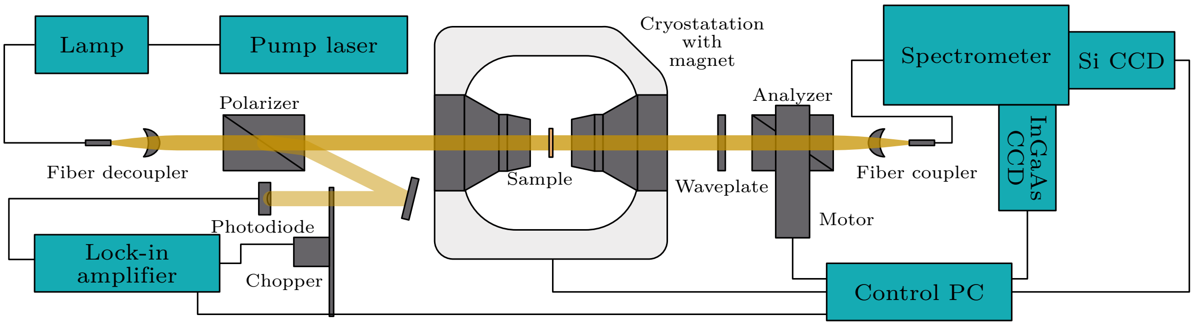

Figure 2.1: Schematics of a magneto-optical spectrometer based on the rotating analyzer method [13]. This experimental setup was used to acquire most of the experimental data presented in this thesis.

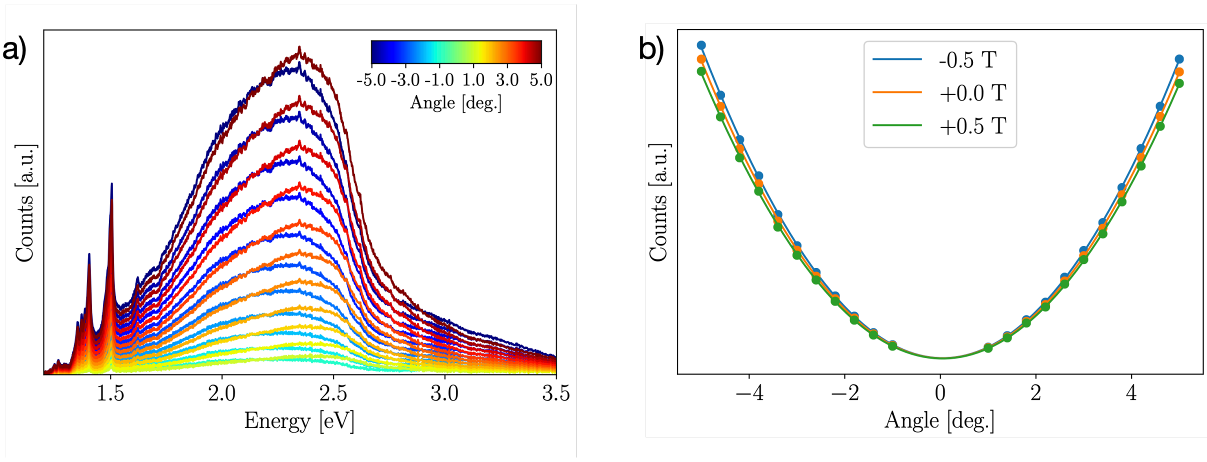

Figure 2.2: a) Angular dependence of intensity spectra rerecorded by CCD spectrometer after the reflection on garnet thin film at applied magnetic field of 0.5 T, b) angular dependence of recorded intensity for light energy of 2.5 eV and different applied magnetic fields. Adapted from [13]

where R denotes the reflectivity of the sample, α is the rotation angle of the analyzer, δ is phase shift of the wave plate, C is additionally added term to account for dark current of the detector, and θ_K and ϵ_K are the magneto-optical rotation and ellipticity.

Using a combination of measurements with and without the wave plate in the optical path, and knowing the phase shift δ in the entire measured spectral range, one can derive a spectrally dependent complex magneto-optical effect (rotation and ellipticity) from the intensity spectra recorded at different angles α, employing equation (2.1). Typical recorded intensity spectra and angular dependence of the intensity at fixed light energy and various applied magnetic fields are shown in Fig. 2.2. Since a CCD spectrometer is used as a detector, one can get the whole spectrum in one measurement, which is different from commonly used approaches based on a monochromator coupled with a photodiode or photomultiplier. This allows for relatively fast measurements and acquisition of large amounts of data for statistical processing.

The sensitivity and accuracy of the presented method depend on the particular measurement sequence and the number of recorded angles α together with chosen spectra averaging. When properly set up, the sensitivity can reach approx. 5×10^{-5} deg as demonstrated in Fig. 2.3. The equipment used in our laboratory enables measurements in the temperature range from 2K to 700K and magnetic fields up to 14T. Moreover, we have also proven that this approach is extendable for spatially and time-resolved measurements. Fully functional spatially and time-resolved experimental setups are now under construction in our laboratory.

2.2 Theoretical apparatus for the analysis of experimental data

To gather maximum information about investigated materials and nanostructures, experimental magneto-optical data are often confronted with theoretical modeling. These can offer additional insight or confirm hypotheses based on the experimental results. Since the magneto-optical response can be described within the spectrally dependent permittivity

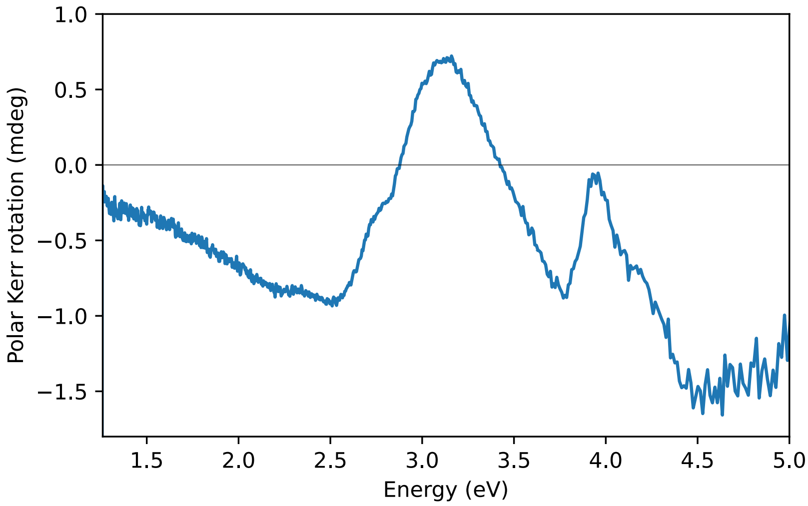

Figure 2.3: Polar Kerr rotation spectrum of ultrathin film of $LuFeO_3$ [14], demonstrating the sensitivity and accuracy of our rotating analyzer method. One should note that maximal amplitude of the Kerr rotation is approx. 10^{-3} deg.

tensor, one can adopt several theoretical approaches.

- **Electromagnetic simulations:** Commonly used theoretical approach to simulate magneto-optical effects on macroscopic level. There is a wide variety of approaches that can be used [15, 16, 17, 18] and we limit ourselves only to the short description of the transfer matrix formalism, which was used for the research presented in this thesis. This formalism was introduced in 1980 by Yeh [19] to describe the propagation of light in layered non-absorbing anisotropic media and later extended by Višňovský for absorbing media and magneto-optical effects [20]. The workflow of the transfer matrix formalism calculations for anisotropic multilayers is depicted in Fig. 2.4.

  The solution of a wave equation in each anisotropic layer characterized by a permittivity tensor is found in the form of four eigenmodes, which provides a basis to describe an arbitrary plane wave field within the medium. Using classical boundary conditions at the interfaces, the electric fields at adjacent layers are related to each other. This leads to the 4×4 matrix representation. Multiplying together matrices for all layers relate together the electric fields at two half-spaces surrounding the multilayer. Finally, the fields at the front and back interfaces of the multilayer can be described in terms of Fresnel reflection and transmission coefficients. The knowledge of Jones reflection/transmission matrix serves for the final calculation of magneto-optical quantities with respect to Eq. (1.5). This powerful theoretical tool can serve to calculate (i) theoretical values of magneto-optical effects if the material parameters of all layers are known (for simulations of interfaces), or (ii) off-diagonal elements of permittivity tensor if the complex magneto-optical effect and diagonal elements of permittivity tensor are known (for subsequent microscopic analysis of electronic structure).

- **Semiclassical theory of magneto-optical transitions:** Widely used from 60's to 10's to analyze the magneto-optical properties of various substances in terms

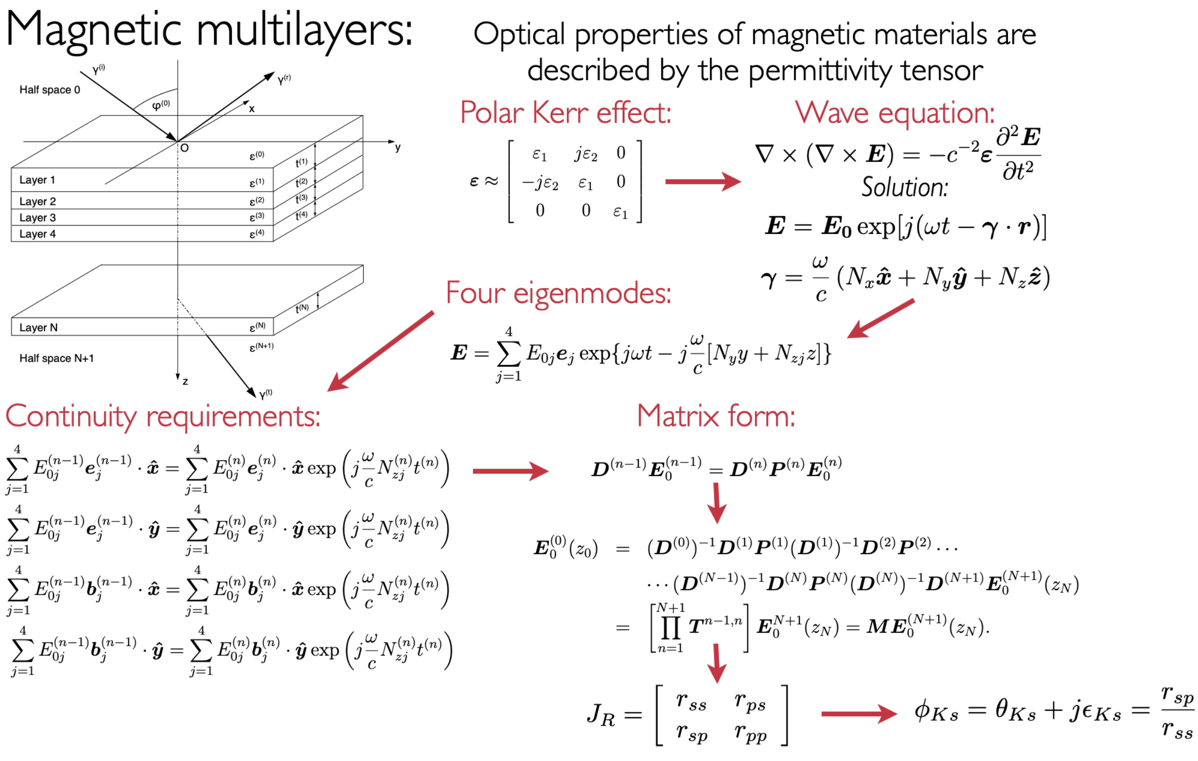

Figure 2.4: Scheme of the magneto-optical calculation workflow using transfer matrix formalism for anisotropic multilayers based on Yeh and Višňovský.

of the spectral dependence of the off-diagonal elements of the permittivity tensor [21, 22]. The dispersion of optical conductivity or electric permittivity tensors can be obtained either by applying the Fermi golden [23] rule or through the Kubo formalism [24]. Such a theoretical approach is still valuable today for fitting the spectra of off-diagonal permittivity tensor elements and deducing the energies and amplitudes of particular magneto-optical transitions. These can be later mapped to the electronic structure with the help of *ab initio* calculations, or their values can be monitored with respect to changes in external conditions (applied voltage/current, induced strain, composition, temperature, magnetic field, etc.).

- **Calculations from the first principles:** In the last decade, the increasing computing power allowed for the application of advanced Density Functional Theory (DFT) codes to model the magneto-optical response via the calculations of electronic structure and the following spectral dependence of the full permittivity tensor. The magneto-optical effect spectra are then calculated using standard electromagnetic simulations with a DFT-calculated permittivity tensor as input. Since modern DFT codes are capable of deriving element- and orbital-resolved density of states (DOS), it is possible to map particular magneto-optical transitions to the electronic structure of the investigated material.

All of the approaches mentioned above have been successfully used in the research presented in this thesis.

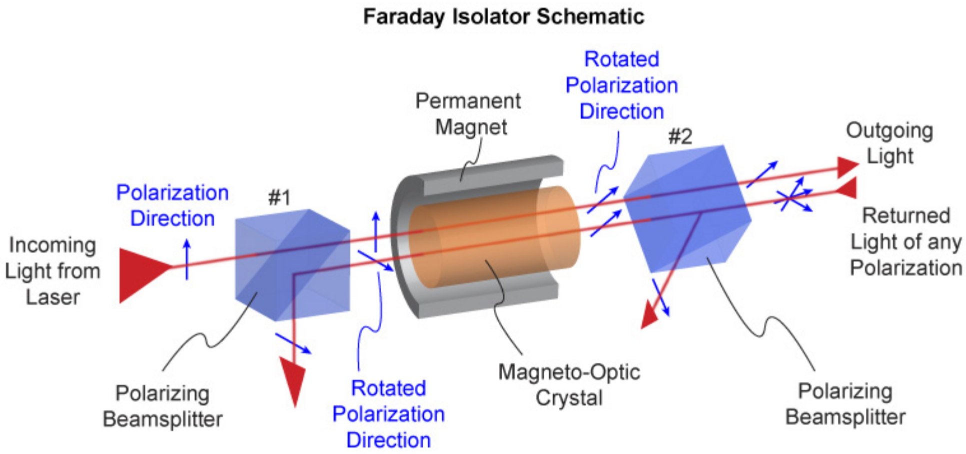

Figure 2.5: Schematic explanation of the functionality of a bulk magneto-optical isolator [25].

2.3 Non-reciprocity for optical isolation

The non-reciprocal nature of linear magneto-optical effects can be utilized for optical isolation. The optical isolator consists of an active magneto-optical material (usually ferrimagnetic garnet) placed in an external magnetic field and two linear polarizers (shown schematically in Fig. 2.5). When light enters the isolator, it is vertically linearly polarized by the polarizer. Afterwards, its polarization is rotated by 45 degrees in the magneto-optical medium via the Faraday effect. Finally, the light exits the Faraday rotator and passes through an output polarizer that is oriented to transmit the 45-degree rotated light. This ensures that the forward-traveling light passes through without significant losses. If any light propagates backward to the isolator (e.g., due to back-reflections from optical element), owing to the time-reversal symmetry breaking by the static magnetic field, which is now pointing opposite to the propagation direction, light undergoes another 45 degrees rotation in the same means as it travels back through the Faraday rotator. As a result, the polarization of the backward-propagating light is rotated by a total of 90 degrees relative to the input polarizer and is blocked. Magneto-optical isolators in bulk form are commercially available and are commonly used mainly in high-power laser systems to protect resonator cavities.

However, the demand for advanced photonic technologies has driven the development of integrated photonic circuits that combine multiple functionalities on a single chip. These circuits are essential for applications ranging from high-speed optical communication and quantum computing to sensing and artificial intelligence. One critical aspect of photonic integration is combining III-V semiconductor lasers, which are the most efficient light sources, with silicon-based photonic platforms. The imperfections of the lithographic processes increase the light scattering and back-reflections, which are unwanted parasitic effects that can influence the stability of the laser source and limit the overall functionality of the photonic chip. Therefore, integrated optical isolation devices are of great interest in the photonics community.

Unfortunately, the standard bulk approach to magneto-optical isolators, which relies on Faraday rotation in a magneto-optical medium, is challenging to implement in integrated photonic systems because of its requirement for long path lengths to achieve sufficient Faraday rotation, and polarizing filters for operation. Moreover, shape-induced

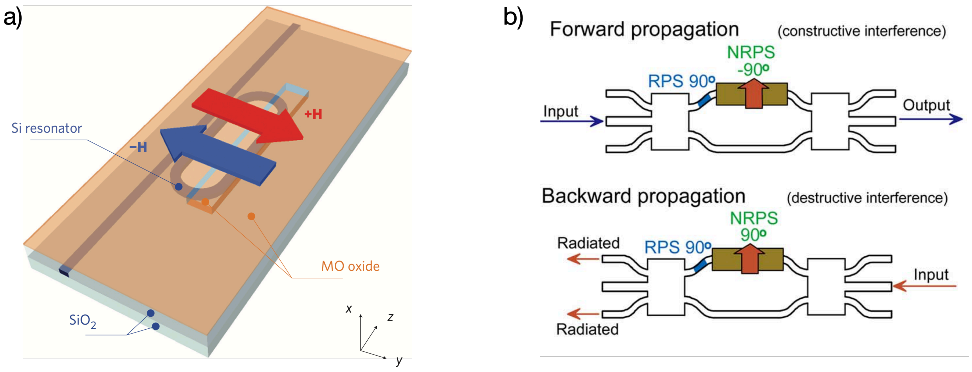

Figure 2.6: Schematic illustrations of two approaches employing non-reciprocal phase shift, a) ring resonator [28], b) Mach-Zender interferometer [34].

birefringence is a major obstacle for non-reciprocal waveguide devices, since it results in different propagations of transverse electric (TE) and transverse magnetic (TM) modes. For an effective Faraday rotation, the conversion between the TE and TM modes must be coherent, which is not possible for a birefringent waveguide. Therefore, complete energy transfer between the modes is not possible.

For this reason, integrated magneto-optical isolators typically employ two primary design approaches: non-reciprocal phase shift (NRPS) and non-reciprocal mode conversion (NRMC). NRPS designs, such as Mach-Zehnder interferometers and ring resonators (schematically shown in Fig. 2.6), leverage the phase difference induced by magneto-optical effects to achieve isolation. These designs have demonstrated wideband isolation ratios of up to 30 dB and insertion losses of as low as 5 dB [26, 27, 28, 29, 30]. Notable advances include compact ring resonators with footprints below 1 mm^2 and integrated designs using SiN waveguides for improved mode matching.

NRMC-based resonators, on the other hand, utilize magneto-optical claddings to convert between TE and TM modes. This approach simplifies fabrication and enables magnet-free operation, making it suitable for applications requiring low thermal budgets. Recent studies have shown that such designs can achieve isolation ratios of 20-30 dB with insertion losses comparable to NPRS designs [31, 32]. More detailed information on recent progress and various types of realization can be found in review papers [33, 34].

Recent works aim to reduce the size of these isolators while improving their performance by incorporating nanoscale resonant photonic structures, such as photonic crystals or metasurfaces, to strengthen light-matter interactions [35]. These designs enable efficient, compact, and scalable isolators that are compatible with integrated photonic platforms, opening the way for robust optical systems in telecommunications, quantum computing, and sensing applications.

Despite advanced, complex, and efficient designs of integrated non-reciprocal devices, there is still a major technological challenge, which originates from the incompatibility of traditional magneto-optical materials with silicon technology. Commonly used rare-earth iron garnets are not naturally compatible with silicon technology because of their large lattice mismatch with silicon substrates and high annealing temperatures required for their proper crystallization together with mismatched thermal expansion coefficients.

For this reason, scientific research in this field is very active and the attention of the community focuses on (i) innovations in the integration of standard garnet magneto-optical materials, such as seed-layer engineering and deposition optimization, wafer bond-

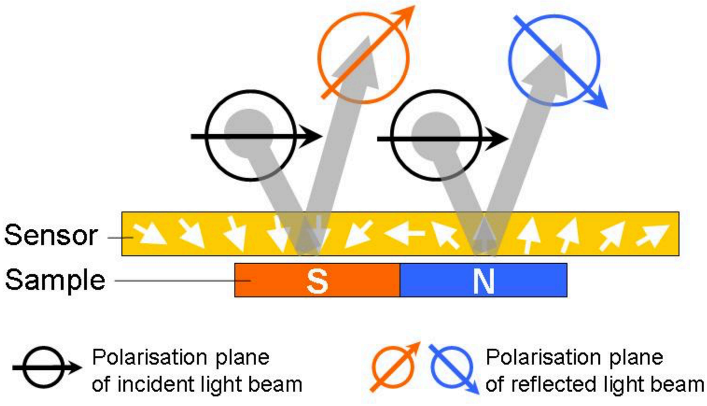

Figure 2.7: Schematic illustration of the principle of magneto-optical indicator [36].

ing, and transfer printing of garnet nanosheets, and (ii) exploring alternative materials that are compatible with silicon technology, such as ferrite thin films or hybrid structures.

To evaluate the performance of particular material in magneto-optical isolation, a quantity Figure-of-Merit (FoM) is often deduced using the following equation

$$FoM = \frac{\theta_F}{\alpha_{dB}} = \frac{\theta_F}{4.34\alpha}[deg/dB], \tag{2.2}$$

where α is the absorption coefficient in dB or cm^{-1}.

2.4 Visualization of magnetic fields and holographic imaging via magneto-optical effects

Another commercially successful application of the Faraday effect is a magneto-optical indicator. Such a device takes advantage of the polarization rotation in the magneto-optical layer to visualize stray magnetic fields generated by investigated objects. The schematic of its principle is shown in Fig. 2.7. By placing the indicator near a magnetic source, the stray magnetic field magnetizes the indicator, which alters the polarization state of the transmitted light in a spatially dependent manner. This change can be detected using crossed polarizers, creating a visible intensity pattern corresponding to the magnetic field distribution. An example of visualization is shown in Fig. 2.8. The advantage is a real-time and non-invasive insight into the magnitude and direction of magnetic field, making magneto-optical indicators invaluable in applications like quality control of magnetic materials, imaging of magnetic flux leakage, and studies of complex field interactions in devices.

Despite existing commercial products, the search for novel transparent magnetic materials with a higher magneto-optical response and a fast magnetization response (to work in tens of GHz), which can be grown on large lateral scales, is still the subject of active scientific research [37].

2.5 Approaches of magneto-optical research

Magneto-optical effects linear in magnetization depend mainly on two extrinsic variables: (i) external magnetic field and (ii) photon energy of incident light. Based on the particular

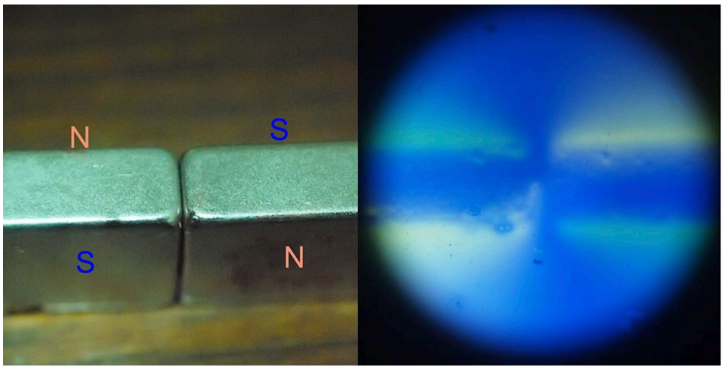

Figure 2.8: A photo of two permanent magnets together with the image of their stray magnetic fields obtained with magneto-optical indicator. Courtesy of T. Ishibashi, Nagaoka University of Technology, Japan.

goal of the research, one can choose the following experiments:

- **Magneto-optical magnetometry**. The measurements at constant energy of incident light while varying the external magnetic field [38, 39, 40]. Since the magneto-optical effects of interest are linear in magnetization, their field dependence provides useful information about magnetic properties of investigated materials.
- **Magneto-optical spectroscopy**. The measurements at a constant magnetic field (usually on a magnetically saturated sample) while varying the energy of incident light. Because the magneto-optical response is driven by electronic transitions, the spectral dependence provides us with insight into the electronic structure of the investigated material. The confrontation of the experimental results with *ab initio* calculations may allow us to map the particular transitions to the band structure.
- **Magneto-optical spectroscopy and theoretical modeling**. Comparing the experimental data with phenomenological theoretical modeling, such as transfer matrix formalism, one may describe small magnetic and structural changes at interfaces, which are otherwise hardly accessible by other experimental techniques.

Depending on the scenario, magneto-optical phenomena may serve as powerful tools to provide important information for:

- Basic research of physical phenomena related to the band structure and magnetism of investigated materials
- Search for novel magnetic materials and their nanostructures
- Optimization of magneto-optical properties for direct applications in terms of ideal material composition, substrate, or growth conditions
- Optimization of growth conditions to obtain proper magnetic properties of the materials and their external control
- Optimization of material composition for desired applications

The following chapters illustrate the magneto-optical research in several above-mentioned scenarios, to provide an idea of how useful magneto-optical phenomena may be and how important information they can provide.

3. Magnetic oxides for non-reciprocal photonics and imaging

This chapter summarizes the results of our work on rare-earth iron garnets in the form of thin films on various substrates and their nanostrucures. The main motivation of the research were potential applications of these materials in integrated non-reciprocal devices or imaging.

Rare-earth iron garnets $Re_3Fe_5O_{12}$ are ferrimagnetic materials known for decades. They crystallize in a cubic crystal structure with three sublattices: the dodecahedral (c) site usually occupied by the rare-earth ions and the octahedral (a) and tetrahedral (d) sites usually occupied by iron ions. The schematic of the crystal structure of garnet is shown in Fig. 3.1 for the case of $Y_3Fe_5O_{12}$. The possibility of choosing various rare-earth ions in the dodecachedral sites allows for large tuning of magnetic, optical, and magneto-optical properties, making these materials ideal for applications in magneto-photonics.

3.1 From bulk to nanostructures: enhanced magneto-optical response of garnet thin films

To successfully adapt non-reciprocal phenomena into the integrated photonics concepts, an enormous effort was focused to the growth of high-quality garnet thin films, firstly on lattice matched garnet substrates. There are three main growth methods established for growth: pulsed laser deposition (PLD) [28, 41, 42], liquid phase epitaxy (LPE) [43, 44], and magnetron sputtering [45, 46, 47], each having its advantages and disadvantages.

Our magneto-optical investigations of ferrimagnetic garnets started with PLD grown $Bi_xY_{3-x}Fe_5O_{12}$ (Bi:YIG) films with $x = 1$ and 2 on $Gd_3Ga_5O_{12}$ (GGG) substrates (**PUBLICATION A1**). The thickness of the films varied between 70 and 200 nm. X-ray diffraction (XRD) and magnetization measurements revealed a nano-granular structure of the layers under compressive strain with reduced saturation magnetizations

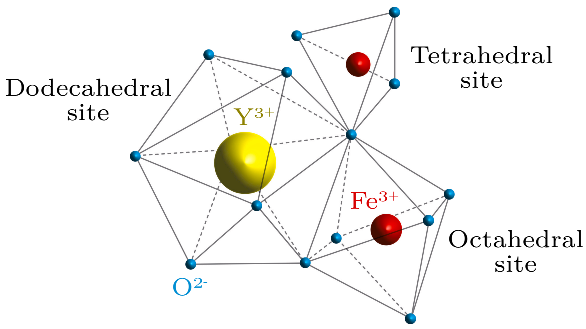

Figure 3.1: Simplified sketch of $Y_3Fe_5O_{12}$ unit cell highlighting three different sublattices made of oxygen arrangements [13].

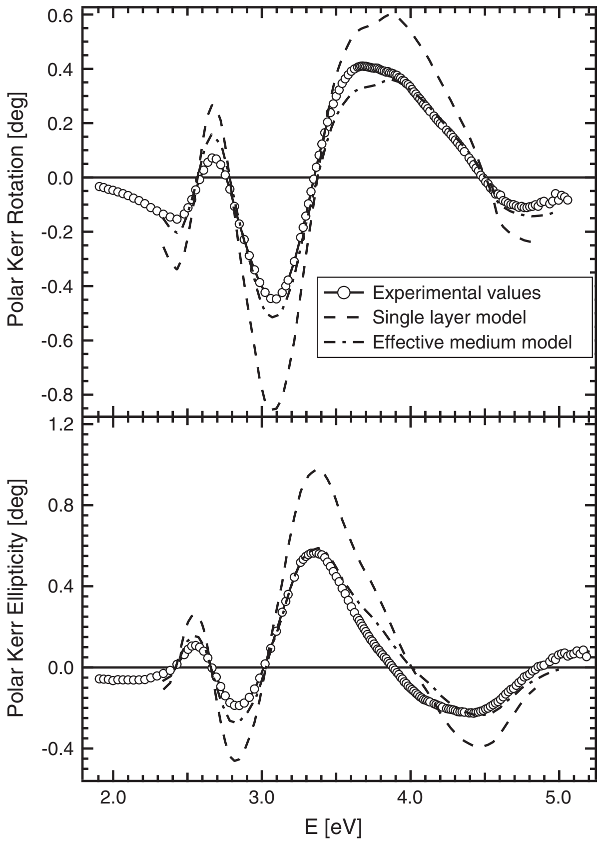

Figure 3.2: Experimental and theoretical polar Kerr rotation and ellipticity of 73 nm thick $Bi_1Y_2Fe_5O_{12}$ film as a function of the photon energy. In the effective medium model, the volume fraction f equals 0.6 [48].

compared to their bulk counterparts. Room temperature polar Kerr rotation and ellipticity spectra of 73 nm thick $Bi_1Y_2Fe_5O_{12}$ layer taken in saturation at nearly normal incidence are displayed in Fig. 3.2. The measured magneto-optical spectra of all investigated samples resembled those obtained in thick films and bulk [22], with extrema between 2.5 and 4.5 eV. In this spectral region the magneto-optical activity is mainly driven by electronic transitions involving Fe ions, namely O $2p \rightarrow$ Fe $3d$ charge transfer transitions and Fe inter-sublattice transitions. The lower energy side of the spectra exhibited interference patterns that depended strongly on the thickness of the film. To analyze the experimental data and address the lower magnetization of the films, we have calculated the theoretical dependence of the magneto-optical Kerr effect using a transfer matrix formalism. Taking into account a model structure of a single layer on a semi-infinite bulk substrate with material parameters taken from literature, the resulting theoretical spectra described the experimental results reasonably well with higher amplitudes at maxima and minima (see Fig. 3.2).

This result confirmed suppressed exchange interactions due to the presence of the substrate and the nano-granular nature of the samples. One can consider broken interactions of Fe ions at octa- and tetrahedral sub-lattices in the surface layers of the nanograins [49]. Similarly, these interactions can be suppressed at the interface with a mismatched substrate raising the so-called magnetically dead interface layer. Finally, vacancies at tetrahedral sites can also reduce saturation magnetization and therefore magneto-optical activity. To reflect such behavior, revised model structures of a Bi:YIG layer consisting of magneto-optically active Bi:YIG surrounded by magneto-optically passive Bi:YIG medium, or a multilayer of magneto-optically passive Bi:YIG top and bottom layers sandwiching the magneto-optically active Bi:YIG layer were proposed. The ratios f between the passive and active medium were the same as the saturation magnetizations of the samples to the bulk. The resulting MOKE spectra for these revised model structures exhibited better agreement with the experimental data, as demonstrated in Fig. 3.2, confirming the presence of Bi:YIG with suppressed magnetism in the investigated samples. The same results were achieved for measurements in longitudinal configuration (in-plane applied magnetic field) on the same samples. Magnetically dead layers at the layer/substrate interface were later studied in detail by other groups [50, 51, 52, 53] building on our results.

As an addition to well established growth techniques a simple and scalable metal-organic decomposition (MOD) technique appeared to be promising in producing high-quality epitaxial films of ferrimagnetic garnets [54]. Unlike vacuum based techniques, MOD requires only a standard chemical laboratory equipped with fume hood, spin coater, and a laboratory oven. A mixture of metal-organic liquids in a desired ratio is deposited on the substrate and spin-coated to produce a wet film. Afterwards, the film is heated several times (drying and preannealing) to remove remaining solvents that did not evaporate and to decompose metal-organic liquids. Since spin coating allows one to prepare only thin films (with a thickness of maximally several tens of nanometers), this procedure is repeated several times to stack the layers and achieve thicker films. In the end, the resulting layer is finally annealed to control oxygen stoichiometry and crystallization. The main advantage of the method is its scaleability, since it can produce homogeneous films with large surface size and is limited only by the physical size of the spin-coater. However, the growth of thick films requires an enormous amount of time. This stimulated our interest in MOD grown garnet thin films.

We have investigated a series of $Bi_xY_{3-x}Fe_5O_{12}$ thin films where x varied from 1.5 to 3 (**PUBLICATION A2**). The samples were grown on (100) GGG substrates and their nominal thickness was 200 nm. Optical properties were characterized by a combination of transmission measurements and spectroscopic ellipsometry, and the resulting spectral dependence of complex dielectric function (diagonal element of permittivity tensor) systematically varied with respect to Bi content. The amplitude of both, real and imaginary parts increased with increasing Bi content. Moreover, the onset of absorption was slightly shifting toward lower energies. Similar behavior was observed for LPE-grown epitaxial films [22]. Substitution by Bismuth leads to considerable lattice expansion due to its large ionic radius [55] resulting in a lattice parameter of 12.624 Å. This is approximately 2% larger than for $Y_3Fe_5O_{12}$ (YIG) (12.376 Å). It was experimentally confirmed that the expansion of the lattice broadens the width of the electronic transitions responsible for optical and magneto-optical response [22, 56], which results in a red-shift of the absorption.

Magneto-optical characterization employed Faraday and polar Kerr magneto-optical spectroscopies, which allowed us to deduce the off-diagonal elements of permittivity tensor in a relatively broad spectral range from 1.5 to 5 eV. Polar Kerr spectra exhibited visible magneto-optical interference up to 3.3 eV, making them suitable for higher energy region analysis, while Faraday spectra showed a large magneto-optical response between 2.5 and 3.5 eV, reaching 70 deg/μm in the case of $Bi_3Fe_5O_{12}$, as depicted in Fig. 3.3. Such value confirms the high crystalline quality of the sample, as it belongs to the highest reported

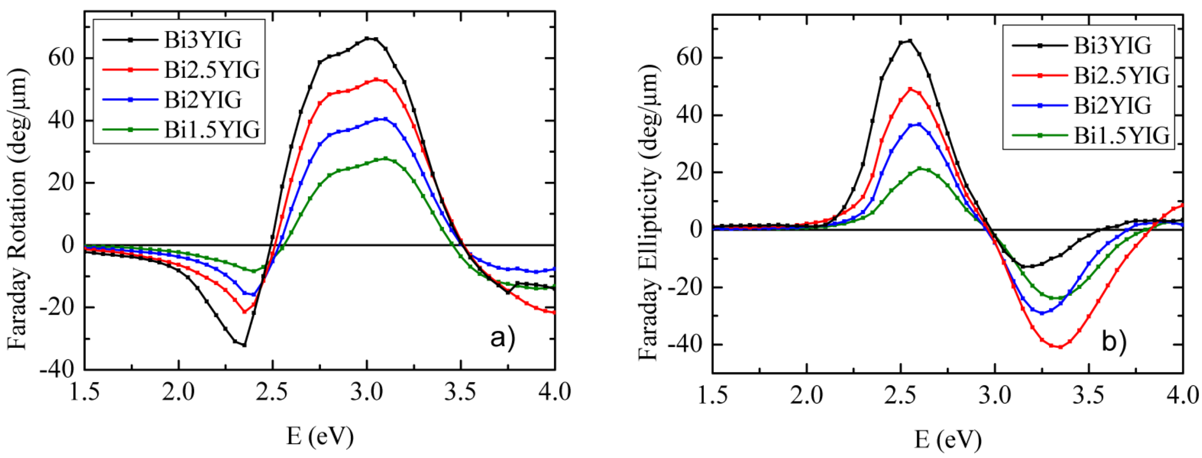

Figure 3.3: Magneto-optical Faraday a) rotation and b) ellipticity spectra of Bi:YIG thin films grown on GGG substrates by MOD method [66].

values for thin films [57, 47]. The good crystallographic quality of the investigated films was confirmed by transmission electron microscopy (TEM).

The deduced spectra of the off-diagonal elements of the permittivity tensor showed a significant amplitude dependence on the Bismuth composition. Two main spectral structures around 2.7 and 3.1 eV were clearly visible in the spectra of the imaginary part, where the latter one becomes more prominent with increasing Bismuth content. This demonstrated a key role of the hybridization between the Bi^{3+} and Fe^{3+} states in the magneto-optically active electron transitions. With respect to the symmetry of molecular orbitals [22] and spin-orbit coupling [58, 59], these transitions belong to Fe^{2+} t_e and Fe^{2+} t_{2g} exited states of the tetrahedral and octahedral sublattices.

The results presented MOD as a capable growth technique for high-quality epitaxial thin films of ferrimagnetic garnets with high concentrations of Bismuth, which are not easily reachable by well established methods, such as LPE. This stimulated a greater interest in this technique and was later used even for other garnet compositions [60, 61, 62]. Moreover, the spectra of the full permittivity tensor in a relatively broad spectral range allowed for the theoretical design of novel magneto-photonic nanostructures [63, 64] or first-principles calculations [65].

Motivated by potential applications in optical communication, yttrium iron garnet is commonly doped with Ce^{3+} ions to increase the magneto-optical response at the 1550 nm telecommunication wavelength. This doping raises Ce $4f$ states in the band gap, resulting in an electronic transition Ce^{3+} $(4f)\rightarrow$ Fe^{3+} ($3d$, tetrahedral), responsible for a significant increase in magneto-optical response around 1.4 eV [67, 68]. Large Faraday rotations have been reported for magnetron sputtered films with Ce compositions reaching 2.5 [47]. However, these films showed a large absorption coefficient in the spectral range of interest, making them unsuitable for optical isolation. On the other hand, epitaxial strain induced by the substrate can be used to engineer and tailor the magnetic properties of garnets. Therefore, we aimed (**PUBLICATION A3**) to systematically study the influence of substrate crystallographic orientation on the optical and magneto-optical properties of $Ce_1Y_2Fe_5O_{12}$ (Ce:YIG).

The investigated samples were PLD grown on (100), (110) and (111) oriented GGG substrates. Their thickness was 80 nm and their crystalline quality was checked by means

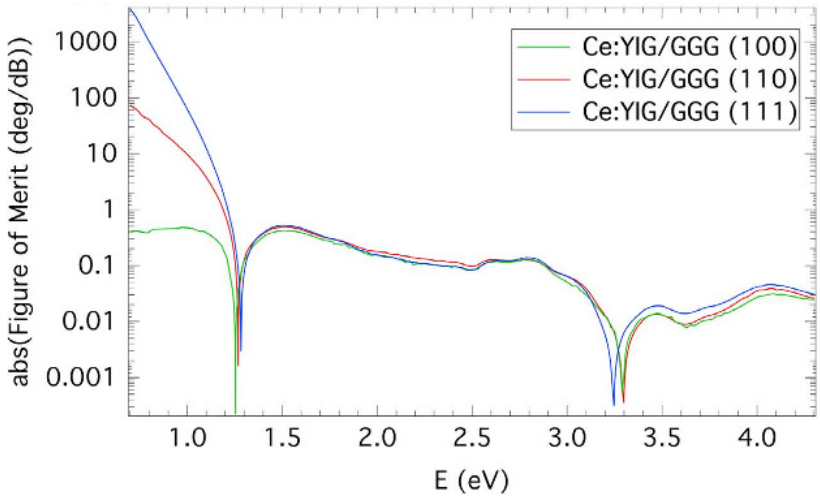

Figure 3.4: Spectral dependence of FoM of Ce:YIG films on GGG substrates with various crystallographic orientation [70].

of standard X-ray tools, such as XRD and XRR. No secondary phases were detected, and all layers were epitaxially grown. Subsequent magnetic characterization showed an in-plane easy axis in all samples regardless of the substrate orientation. The hard axis saturation field varied from 2 kOe to 8 kOe depending on the substrate orientation. This confirmed the role of magnetocrystalline and magnetoelastic anisotropies as they are angularly dependent. Magneto-optical characterization employed both Faraday and Kerr spectroscopies. Hysteresis loops of the Faraday effect were measured for 1550 and 780 nm incident wavelength, and the saturation fields were in line with magnetometry measurements. The (111) oriented sample had an anisotropy field $H_K = 2$ kOe closest to that expected from shape anisotropy (H_K for YIG is 1.78 kOe [69]). Higher anisotropy fields for other samples suggested non-vanishing influence of magnetocrystalline or magnetoelastic anisotropies.

Above 2.5 eV the Faraday spectra showed a spectral behavior typical for ferrimagnetic garnets since at these energies the magneto-optical response is mediated by Fe^{3+} states at the tetrahedral and octahedral sites. A notable enhancement of the magneto-optical response was found around 1.4 eV, originating in the Ce^{3+} f states. The amplitude of the effect did not vary too much, but was highest for the film on the (111) oriented substrate. A value of approx. 5800 deg/cm at 1550 nm wavelength was exceptionally high for this composition, exceeding the bulk values. This was promising from an application point of view.

To evaluate the performance (namely FoM) of investigated samples for non-reciprocal photonic devices, their optical response was characterized by means of spectroscopic ellispometry. Using a layered model structure, we deduced the spectral dependence of diagonal elements of the permittivity tensor together with the absorption coefficient from the experimental data. Subsequently, by combining the Faraday spectra and diagonal elements of permittivity tensor, the off-diagonal elements were calculated as well. Using the knowledge of the Faraday rotation and absorption coefficient spectra, the spectral dependence of FoM was calculated and is shown in Fig. 3.4. Although in the visible and UV part of the spectra the difference in the FoM across the samples is subtle, the influence of the crystallographic orientation of the substrate is clearly visible in the IR region. This is partially due to the higher magneto-optical response of the (111) oriented sample,

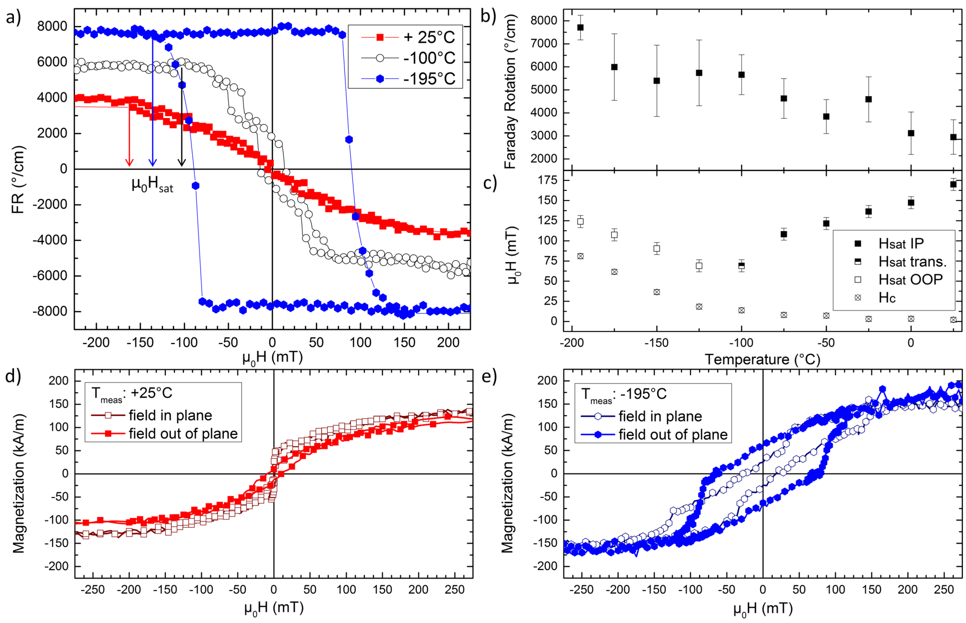

Figure 3.5: Temperature dependent magnetic and magneto-optical properties of Ce:YIG film. (a) Faraday loops at 1550 nm obtained at +25°C (red squares), 100°C (black circles), and 195°C (blue hexagons) for out-of-plane magnetic field. (b) The saturation Faraday rotation as a function of temperature. (c) The coercive field (circles) and the saturation field (squares) measured from the out-of-plane Faraday rotation loops. Filled squares correspond to an in-plane easy axis, open squares an out-of-plane easy axis, and the half-filled square a transition between them. Magnetization loops obtained at +25°C (d) and 195°C (e) for in-plane (open symbols) and out-of-plane (filled symbols) fields[82].

but mainly due to its notably lower absorption coefficient. Obtained FoM of approx. 943 dB·cm^{-1} at 1550 nm for this crystallographic orientation is more than 3 times higher than the values reported on various materials for optical isolation and is approx. two thirds of a value for high quality bulk crystal with extremely low optical absorption.

Our selection of the most suitable substrate orientation for the growth of Ce doped $Y_3Fe_5O_{12}$ helped later optimize the growth of other garnet compounds [71, 72, 73, 74, 75], as well as the knowledge of the permittivity tensor spectra allowed the numerical design of advanced photonic devices for optical isolation [76, 77, 78, 79, 80].

Experimental studies on Ce:YIG thin films showed a larger magnetic moment than pure YIG [81]. Detailed X-ray and magnetometry experiments revealed in-plane strain and in-plane uniaxial anisotropy for samples grown on (111) GGG substrates. This uniaxial magnetoelastic anisotropy originates from the presence of the substrate and is an additional term to consider in the general magnetic properties of Ce:YIG.

Since the magneto-crystalline and magneto-elastic anisotropy terms should have a notable dependence on temperature, the temperature-dependent magneto-optical, magnetic and structural properties of 80 nm thick $Ce_{0.6}Y_{2.9}Fe_{4.5}O_{12}$ thin films on GGG (111) substrates down to liquid nitrogen temperatures were correlated in our investigations (**PUBLIACTION A4**). Room temperature reciprocal space mapping revealed a very good in-plane adaptation of the Ce:YIG layer to the GGG lattice with only minor strain relaxation. The out-of-plane lattice parameter was found to be larger than the in-plane lattice spacing, which indicated a rhombohedral distortion of the Ce:YIG lattice with tensile strain along the [111] direction and a compressive strain in-plane. Temperature-dependent $\theta - 2\theta$ XRD scans showed a small monotonous shift of the diffraction peaks of GGG substrate and a change in the facet angle along the [111] direction of rhombohedrally distorted lattice. The results clearly demonstrated the decrease in in-plane compressive strain when lowering the temperature. This was explained by the higher thermal expansion coefficient of Ce:YIG than GGG for temperatures above -100°C.

Temperature-dependent Faraday rotation loops revealed notable changes in the magnetic anisotropy of the layer with decreasing temperature, as shown in Fig. 3.5. They suggested a magnetic reorientation from in-plane magnetic anisotropy at room temperature to out-of-plane anisotropy at -195°C. A gradual transition between these two states has been observed across the temperature range where below -100°C the in-plane saturation field becomes smaller than the out-of-plane one. This was followed by an increase in coercivity below this temperature and agrees with the changes in the rhombohedral distortion of the Ce:YIG unit cell. A detailed analysis of magnetic anisotropy terms revealed a notably higher increase of magnetocrystalline and magnetoelastic terms with decreasing temperature. They favor out-of-plane magnetization alignment and overcome the shape anisotropy (which favors the in-plane easy axis) term at low temperatures.

The spectral dependence of the Faraday rotation and MCD spectra in the photon energy range from 0.7 to 4.2 eV at room temperature resembled our previously published results [70], showing the spectral structures originating from intra-ionic transitions of Ce^{3+} at low energies and crystal field and charge transfer transitions of Fe 3*d* and O 2*p* states at high energies. Low-temperature spectra exhibited red shifts of the crystal-field transitions as a consequence of temperature-induced lattice distortions, resulting in changes in octahedral and tetrahedral arrangements. The tetrahedral arrangements seemed to be more susceptible to deformations compared to the octahedral one. Our results later stimulated the scientific community to design garnets with particular compositions on selected substrates to increase the magnetocrystalline and magnetoelatic terms of magnetic anisotropy to obtain thin garnet films with perpendicular magnetic anisotropy [83, 84, 85, 86]

3.2 Towards the integrated photonics: garnets on Si substrate

Although the optimization of the deposition processes allowed the growth of high-quality thin films of ferrimagnetic garnets on substrates with compatible lattice parameters (such as GGG), the integration of garnets on Si (or other semiconductor) platform remained very challenging, mainly due to incompatible lattice parameters and the thermal expansion coefficient mismatch between garnets and common semiconductors [28, 87, 88, 89, 90, 91]. Therefore, polycrystalline layers with higher optical absorption and lower magneto-optical response compared to single-crystal films are formed on semiconductor substrates. In addition, various impurity phases such as $YFeO_3$, Fe_2O_3, CeO_2 or Bi_2O_3 can be formed during the crystallization process [92]. Therefore, optimization of the growth process in terms of oxygen partial pressure, substrate temperature, or post-deposition annealing is crucial to obtain films with good crystalline quality, high magneto-optical response, and low optical absorption at telecommunication wavelengths.

Our investigations of magneto-optical properties of garnets grown on Si (100) substrates started with PLD deposited layers of YIG and Ce:YIG (**PUBLICATION**

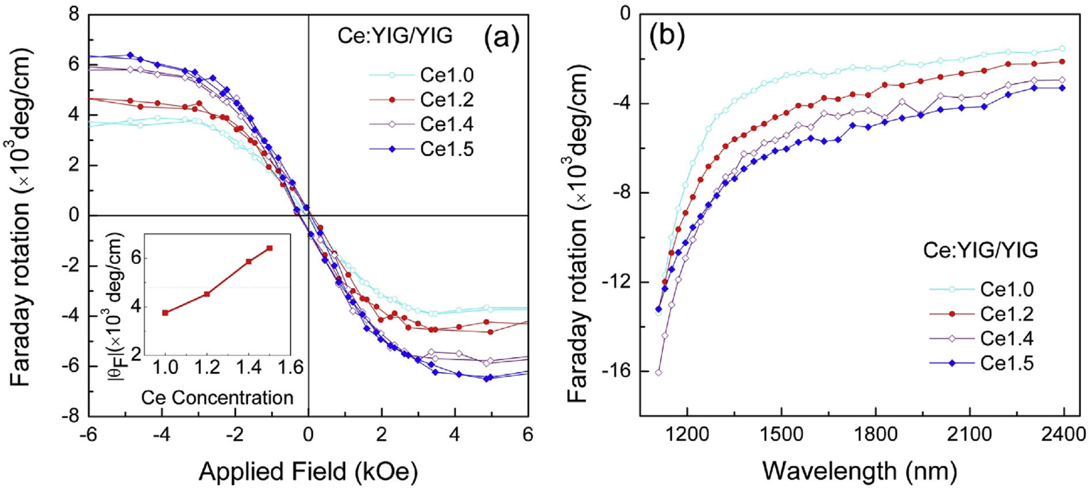

Figure 3.6: a) Faraday rotation hysteresis loops of $Y_{3-x}Ce_xFe_5O_{12}$/YIG films measured at 1550 nm. The inset shows the dependence of saturation Faraday rotation on the Ce concentration. b) Faraday rotation spectra in the near IR region. The thickness of x = 1.0, 1.2, 1.4, 1.5 samples are 219 nm, 192 nm, 179 nm, and 162 nm respectively [95].

A5). Ce concentrations ranged from x = 1.0 to x = 1.5 and all samples contained a 56 nm thick YIG seed layer. Post-deposition rapid thermal annealing has been employed to crystallize all films. Structural and chemical characterization confirmed the polycrystalline and single Ce:YIG phase nature of the films. It was found that lowering the oxygen partial pressure during the deposition leads to better crystallinity of the films due to better Ce solubility. Magnetization measurements revealed in-plane magnetic anisotropy of all samples and increased coercivity with increasing Ce content. Magneto-optical Faraday hysteresis loops measured at 1550 nm showed monotonous increase of the Faraday rotation with the Ce concentration. The $Ce_{1.5}Y_{1.5}Fe_5O_{12}$ thin film exhibited highest Faraday rotation of 6410 deg/cm due to more Ce^{3+} ions incorporated into the lattice (see Fig. 3.6). This incorporation enhances the paramagnetic electric dipole transition from Ce^{3+} $(4f)$ states to Fe^{3+} $(3d)$ states centered around 860 nm, the tail of which reaches the IR region. The spectral dependence of the refractive index and the extinction coefficient demonstrated an increase in the absorption coefficient for higher Ce concentrations. This was not fully explained by the Ce concentration and was addressed to the formation of oxygen vacancies or Fe^{2+} centers due to the low partial oxygen pressure during the deposition process. Higher absorption coefficients led to low FoM values, suggesting that more growth optimizations are necessary to fulfill the requirements for photonic applications. This was later done by several research groups inspired by our results [93, 94, 27], achieving reasonable FoM values.

Motivated by attempts to grow Ce:YIG on silicon, other types of ferrimagnetic garnets became of particular interest. As a garnet with the highest magneto-optical response, Bi-doped YIG was a natural choice (**PUBLICATION A6**). Epitaxial and polycrystalline $Bi_xY_{3-x}Fe_5O_{12}$ thin films were synthesized using PLD on GGG and Si substrates with x = 0.8, 1.2, and 1.5. The thickness of the films ranged from 20 to 130 nm. In the case of the Si substrate, two growth approaches have been used, since the annealing of a single Bi:YIG layer on the Si substrate did not produce a garnet phase. In the first case, the YIG seed layer was deposited on the substrate prior to the Bi:YIG layer deposition

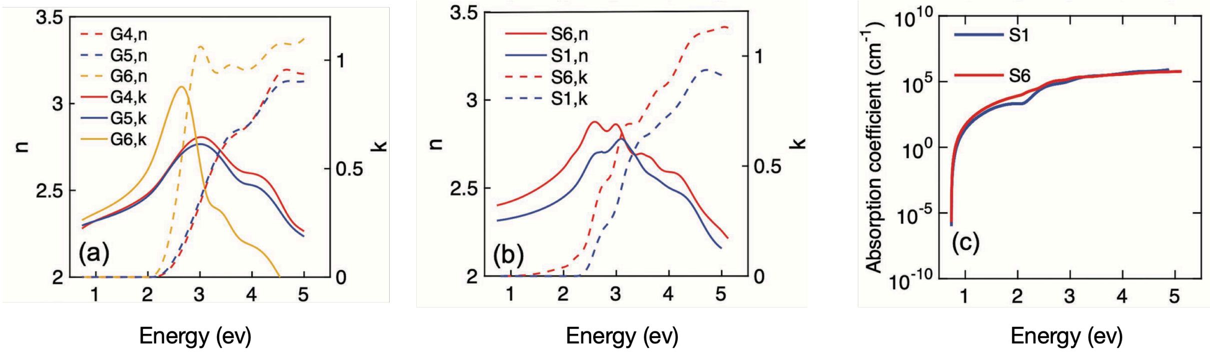

Figure 3.7: Refractive index (n) and extinction coefficient (k) spectra of a) Bi:YIG/GGG, b) Bi:YIG/YIG/Si and YIG/Bi:YIG/Si films characterized by spectroscopic ellipsometry. c) Spectral dependence of absorption coefficient of Bi:YIG/YIG/Si and YIG/Bi:YIG/Si films. Adapted from [96]

(bottom-up crystallization), while in the second case, the seed layer was deposited on top of the Bi:YIG layer (top-down crystallization). In both cases, the samples were rapidly thermally annealed to obtain the proper crystallinity of the layers. In the beginning, special attention was paid to the (Bi+Y)/Fe ratio in the samples on GGG substrates and its relation to the deposition conditions in terms of O_2 pressure and substrate temperature. For growth temperatures from 520 to 600°C at P_{O_2} of 20 mTorr, the ratio was close to a stoichiometric value of 0.6 and XRD analysis confirmed growth of a single phase garnet layer. The magneto-optical Faraday rotation was found to be almost a linear function of P_{O_2} as more Bi content is incorporated in the layer at higher deposition pressures. The Faraday rotation spectra resembled those already reported in the literature and therefore confirmed the epitaxial quality of the layers deposited on GGG substrates. The samples grown on Si substrates showed the same cation ratios as those found in films grown on GGG substrates.

Structural characterization of the layers grown on Si substrates by XRD revealed notable differences between the top-down and bottom-up approaches. While the bottom-up crystallization produced polycrystalline layers without secondary phases, the layer produced by top-down crystallization contained secondary phases of Bi_2O_3 and Fe_2O_3. This was explained by the volatility of Bi. During annealing of the top-down structure, Bi cannot escape as in the case of the bottom-up approach. The excess of Bi therefore forms Bi_2O_3 phases. An additional annealing step was necessary after the growth of the Bi:YIG layer, but before the YIG layer, to achieve single-phase layers with proper composition. On the other hand, the top-down method leads to larger grains of approx. 5 μm compared to 2 μm of bottom-up and allows placing the Bi:YIG layer in direct contact with an underlying waveguide in order to increase optical coupling and improve the performance of integrated optical isolator. TEM images demonstrated the possibility of the growth of Bi:YIG on the sidewalls of the waveguide for optical isolation of the TE mode.

After the structural characterization, the Bi:YIG films on Si substrates were characterized by optical and magneto-optical spectroscopies. Magneto-optical Faraday rotation hysteresis loops at 1550 nm showed a similar dependence of the amplitude on the Bi content for both top-down and bottom-up approaches, reaching approx. 2000 deg/cm for $Bi_{1.5}Y_{1.5}Fe_5O_{12}$. The shape of the loops resembled an in-plane magnetic anisotropy of the layers. Spectroscopic ellipsometry was utilized to characterize the optical response of the samples. The resulting spectral dependence of the complex refractive index of the layers showed a red shift of the optical absorption edge for samples with a higher content of Bi, as shown in Fig. 3.7. This led to a higher optical loss of the layers at a wavelength of 1550 nm. However, the higher Bi content induced a higher Faraday rotation, which resulted in a FoM of 769 deg/dB at 1550 nm. This value was one order of magnitude higher than previously reported values for the garnet films on Si substrates, highlighting the Bi:YIG as a promising candidate for integrated nonreciprocal photonic devices. This has led to an increase in the attention to this material in recent years thanks to our work [97, 98, 99].

As a next step, our following efforts focused on garnet materials, which can be grown directly on Si substrates, without the necessity of the YIG seed layer [100, 101]. This material was terbium iron garnet $Tb_3Fe_5O_{12}$ (TbIG) and its variations doped by Ce and Bi (**PUBLICATION A7**). Polycrystalline layers were PLD deposited on Si substrates at a temperature of 750°C and subsequently crystallized by rapid thermal annealing at a temperature of 900°C. The composition ratio defined as R = (Tb+Ce+Bi)/Fe was used to optimize the growth of the layers. Although pure TbIG crystallized well without secondary phases and R close to stoichiometric 0.6, Ce and Bi doped TbIG layers with only compositions of $Ce_{0.36}$TbIG and $Bi_{0.03}$TbIG could be prepared without secondary phases and R close to 0.6. In addition, an iron-deficient TbIG layer was prepared to study the influence of the redistribution of Tb^{3+} ions within the unit cell on the optical and magneto-optical response. The thicknesses of the investigated layers ranged from 70 to 300 nm.

Atomic force microscopy (AFM) images confirmed a polycrystalline nature of all investigated layers with grain sizes of 100-150 nm, 20-100 nm, and 10-30 nm for TbIG, Ce:TbIG and Bi:TbIG, respectively. Magnetic characterization of the layers showed in-plane magnetic easy axis, which was ascribed to the interplay of shape and magnetoelastic anisotropy terms. The presence of Tb ions with magnetic moment in dodecahedral sublattice induced a compensation temperature, T_{comp}, which was observed for all layers. The nearly stoichimetric samples exhibited T_{comp} values close to the bulk T_{comp}, while Fe-rich TbIG showed lower T_{comp}. This agreed with previously reported conclusions that an increase in Tb:Fe ratio increases the magnetization below T_{comp} [103]. This trend can be explained by the excess Tb that occupies the octahedral sites. Since high-resolution X-ray Photoelectron Spectroscopy (XPS) found that tetravalent Tb^{4+} ions ($4f^7$) are present in the layers, these prefer to occupy smaller octahedral sites and exhibit stronger exchange coupling to Fe^{3+} and less canting than Tb ions at dodecahedral positions. Replacement of Tb^{3+} ($4f^8$) ions with Bi^{3+} ($5d^{10}6s^2$) or Ce^{3+} ($4f^1$) reduced the magnetic moment and lowered the values of T_{comp} in doped samples. The measured values of T_{comp} were lower than in the non-doped samples, and the difference corresponded to the amount of doping.

All samples were characterized by Faraday magneto-optical spectroscopy in the near-IR spectral region to obtain the values of Faraday rotation in saturation at a wavelength of 1550 nm. Non-doped TbIG and Bi-doped TbIG samples exhibited notably larger Faraday rotation than Ce-doped samples as follows from Fig. 3.8. Since both Bi^{3+} and Ce^{3+} have a negative contribution to the Faraday rotation of YIG [22, 67, 104], it was expected that the doped samples will exhibit lower values of Faraday rotation than TbIG. Polar and longitudinal magneto-optical spectroscopies resembled previous results on bulk crystals[105]. The spectra exhibited spectral structures located in the spectral region from 2 to 4 eV that originate from crystal field Fe^{3+} optical transitions. Temperature-dependent magneto-optical measurements demonstrated the presence of magnetic compensation by

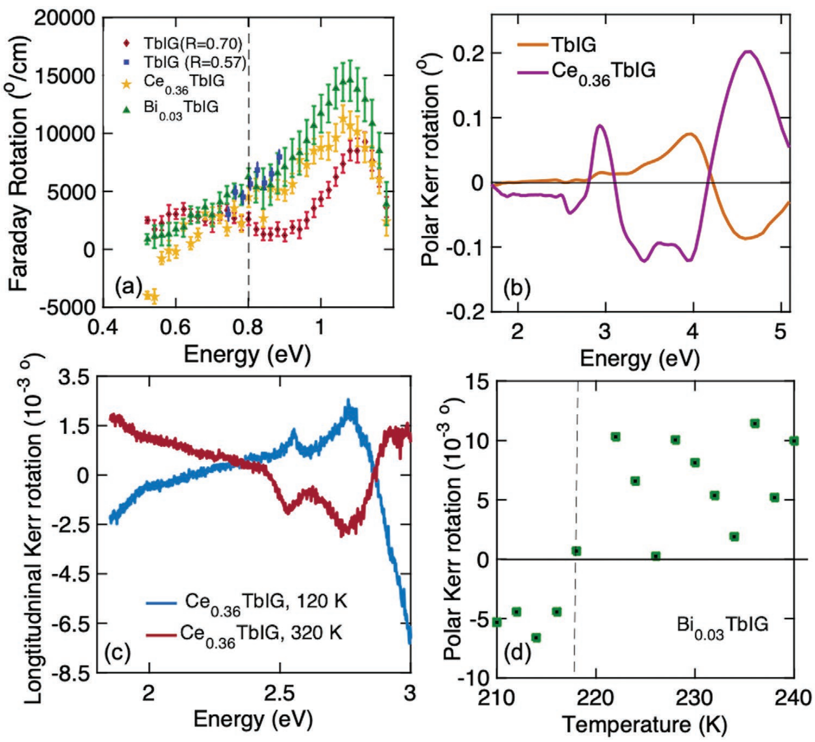

Figure 3.8: a) Room-temperature Faraday rotation spectra of TbIG, $Ce_{0.36}$TbIG, and $Bi_{0.03}$TbIG films. b) Room temperature polar Kerr rotation spectra of TbIG and $Ce_{0.36}$TbIG films. c) Temperature-dependent longitudinal Kerr rotation of $Ce_{0.36}$TbIG. d) Polar Kerr rotation versus temperature of $Bi_{0.03}$TbIG at energy 2.5 eV, showing a sign change at T_{comp} in the range of ≈220 K [102].

sign reversal of the magneto-optical polar and longitudinal Kerr effect when crossing the T_{comp}. To evaluate the functionality of investigated layers from the point of view of photonic applications, their optical properties were examined by means of spectroscopic ellipsometry to estimate the values of the FoM. The Ce and Bi-doped TbIG layers exhibited lower absorption than pure TbIG layers. This phenomenon was explained mainly in terms of higher concentrations of Tb^{4+} and Fe^{2+} which may enhance the absorption via Fe^{3+}-Fe^{2+} relaxation and charge transfer from ligand orbitals. Replacement of Tb with Ce and Bi reduces the absorption pathways related to Tb^{4+} and enhances the FoM. Therefore, this work pointed out the necessity to control the Tb^{3+}/Tb^{4+} ratio to maximize the functionality of these materials for nonreciprocal photonics, which has been done in the following works stimulated by our results [106, 107, 108].

3.3 Beyond the layered concept: Complex and nanostructured materials

To further increase the magneto-optical response of the materials, novel photonic concepts of nanostructures have been introduced, utilizing strong optical resonances at subwavelength scales. Resonant structures like photonic crystals, cavities, or surface plasmon resonances can concentrate the electromagnetic field of light within the magneto-optical material, increasing the effective interaction of light and matter. This

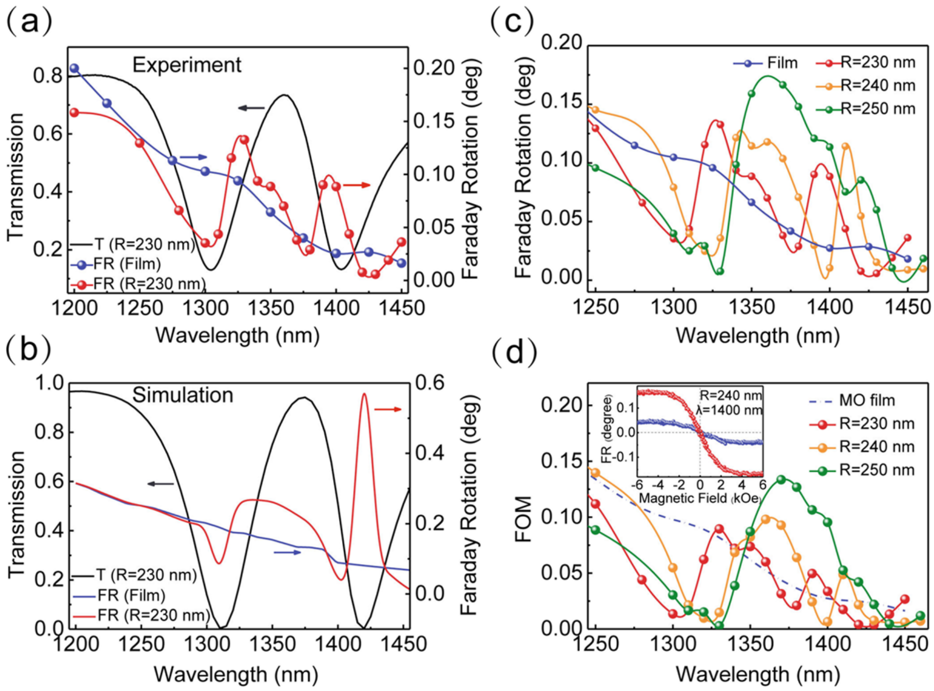

Figure 3.9: a) Measured Faraday rotation and transmission spectra of the metasurface with R = 230 nm compared with bare Ce:YIG/YIG thin films. The black and red curves indicate the transmission and spectra Faraday rotation spectra of the metasurface, while the blue curve shows the Faraday rotation spectra of the bare magneto-optical films as the reference. b) Simulation results of the same structure are also displayed here for comparison. The curves are in correspondence to a) by the colors. c) Measured Faraday rotation spectra of the magneto-optical dielectric metasurfaces as a function of the wavelength and the radius. d) FoM of the metasurface compared to the Ce:YIG/YIG film for different radiuses of silicon disks. Also, the inset shows measured FR hysteresis loops for the metasurface with R = 240 nm and the bare MO film at 1370 nm wavelength [112].

leads to significant amplification of magneto-optical effects and increases non-reciprocal functionality. Furthermore, engineering resonant phenomena, such as defect modes [109], optical Tamm states [110], or Borrmann effects [111], allow light confinement to magneto-optically active regions while minimizing losses. The ability to tune these resonances also allows for precise control of the enhancement, which makes resonant structures important in modern applications. Despite huge benefits, some resonant nanostructures also have drawbacks in the form of high optical losses.

To overcome the difficulties with high optical losses of magneto-plasmonic resonant structures, one can utilize another type of resonance, such as the Mie resonance. This allowed us to design all dielectric magneto-optical metasurfaces consisting of high-refractive-index materials to avoid the issues of absorption losses. Moreover, apart from electric mode resonance, high-refractive-index nanostructures can also produce magnetic mode resonances. We therefore focused on the study of the resonant enhancement of the magneto-optical response in all-dielectric magneto-optical metasurfaces consisting of periodic amorphous silicon nanodisks on Ce:YIG thin films on SiO_2 substrates (**PUBLICATION A8**).

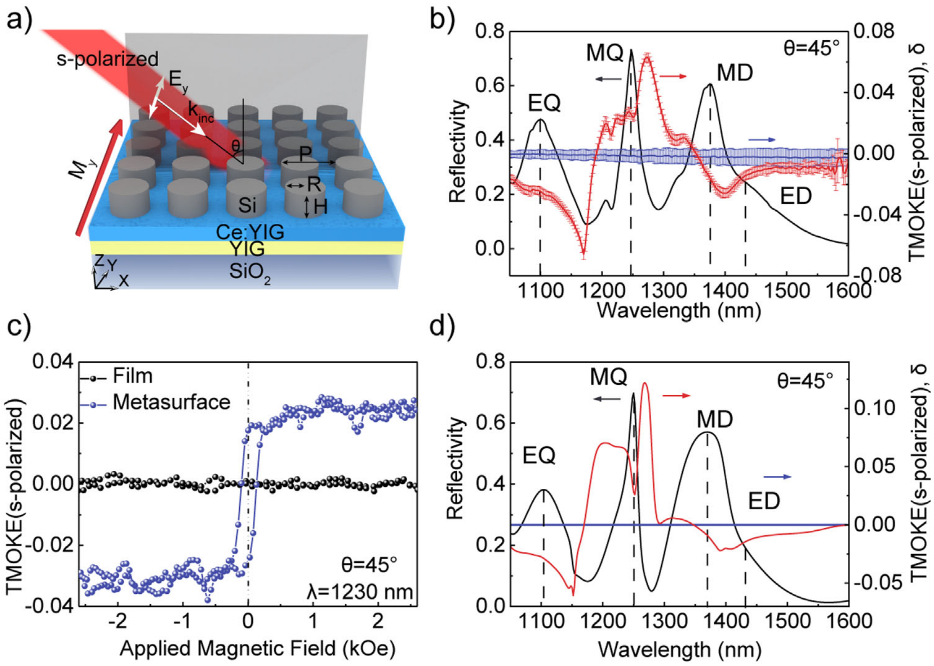

Figure 3.10: Reflection spectrum and giant transverse Kerr effect for *s*-polarized incident light. a) Schematic diagram of the *s*-polarized transverse Kerr effect characterization setup. All measurements are obtained for *s*-polarized light at an incidence angle of $\theta = 45°$. b) Measured *s*-polarized transverse Kerr effect and reflection spectra of the metasurface compared with bare Ce:YIG/YIG thin films. The error bars represent the standard deviation from five consecutive measurements. c) Measured transverse Kerr effect hysteresis for the metasurface and the bare magneto-optical films at a wavelength of 1230 nm. d) Simulated reflection spectra and transverse Kerr effect response of the metasurface for *s*-polarized light at an incidence angle of $\theta = 45°$ [35].

The Ce:YIG layers were deposited on silica substrates using a standard PLD technique, YIG seed layer, and post-deposition annealing to achieve proper crystallization. Afterward, an amorphous silicon layer was grown on top of Ce:YIG by plasma-enhanced chemical vapor deposition, and electron beam litography was used to fabricate nanodisk patterns using the HSQ resist. Deep reactive ion etching was employed subsequently to obtain the final metasurface structure.

Our observed enhancement via the hybridization of Mie resonances with waveguide modes stimulated research activity in the direction of the use of Mie scattering in nonreciprocal photonic devices [113] as an effective way to overcome the limits of plasmonic nanostructures.

Optical transmission data in the near-IR spectral region showed two resonant modes (see Fig. 3.9(a)), which changed their energy with the change in the radius of the nanodisk. Theoretical calculations based on the rigorous coupled-wave analysis method predicted optical resonances attributed to TM0(±1,0) and TE0(0,±1) guided modes at the same energies. Moreover, simulated electromagnetic field distributions showed that the higher energy resonance resembles the magnetic dipole Mie resonance, whereas the lower energy resonance resembles the electric dipole Mie resonance. Based on theoretical analysis, the experimentally observed resonances in the metasurface were considered to be hybridized Mie resonances and waveguide modes (TM0-MD and TE0-ED). Interestingly, these excited modes were strongly confined in the magneto-optical Ce:YIG/YIG layer,

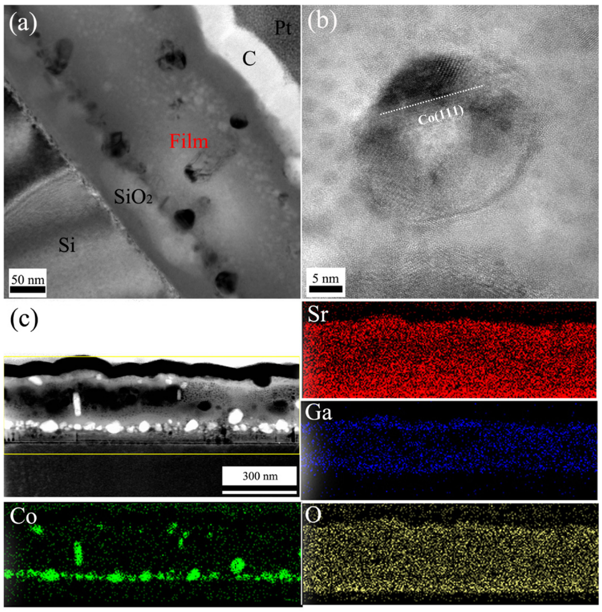

Figure 3.11: TEM and elemental mapping of films on (001) Si substrates. a) Bright field TEM image of the 180 nm thick film on Si. b) High-resolution TEM image of a single Co particle in the film. c) Scanning TEM image and STEM-EDX element mapping of the 180 nm thick film on Si [114].

which was explained by the higher refractive index of magneto-optical materials compared to SiO_2. This led to the enhancement of electromagnetic field in the magneto-optical medium resulting in an increase of Faraday rotation in the vicinity of resonant energies compared to the simple magneto-optical layer, as shown in Fig. 3.9. The enhancement energies changed with the radius of the nanodisk, as expected. The metasurface with R = 250 nm exhibited a Faraday rotation more than four times higher at λ = 1370 nm, while keeping a reasonable transmittance of 64%. The theoretical simulations describe well the experimental data.

The Mie resonances may not only enhance the conventional magneto-optical effects but can also induce anomalous phenomena that do not exist in planar arrangements. For this purpose a metasurface consisting of Si nanodisks on a magneto-optical bilayer with YIG and Ce:YIG films was fabricated on quartz substrate (**PUBLICATION A9**). The YIG layer was deposited as a seed layer to promote crystallization of Ce:YIG films. Experimental optical transmission spectra at normal incidence exhibited three resonant peaks at 1100, 1310 and 1420 nm. Theoretically simulated transmission spectra as a function of the incident angle for $s-$ and $p-$ polarized light showed different dispersive behavior, and together with planar waveguide theory and multipoole analysis various waveguide modes and electric and magnetic dipoles and quadrupoles were identified. Magneto-optical experiments on the metasurfaces revealed a large transverse magneto-optical Kerr effect for $s-$polarized incident light, which does not exist for simple planar structures (see Fig. 3.10). Moreover, a giant enhancement of longitudinal Kerr effect for nearly normal incidence was observed for the investigated metasurface as well. Such behavior originates from circular displacement currents in the Ce:YIG layer induced by magnetic dipoles and quadrupoles at Mie resonances. Electromagnetic simulations showed the characteristic circular electric field distribution when the

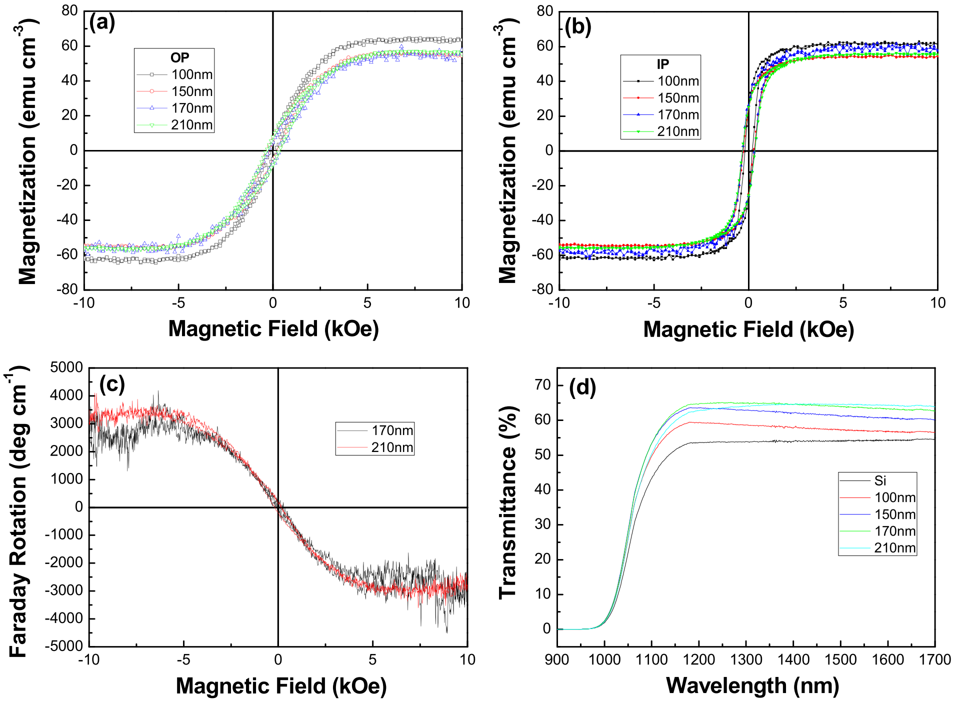

Figure 3.12: Properties of the films on Si deposited at 3 μTorr oxygen and 760°C. a) Out-of-plane (OP) and b) in-plane (IP) hysteresis loops of films with different thicknesses. The hysteresis loops of the three thickest films overlap. c) The Faraday rotation of films measured with an applied field perpendicular to the film plane at 1550 nm wavelength. d) The optical transmission spectra of the films [114].

intensity E_z was enhanced and confined in the Ce:YIG layer. These observations again highlight the important role of circular displacement currents in the observed anomalous magneto-optical effects. The results clearly demonstrated the possibility of utilizing the complex Mie resonance modes to realize novel magneto-optical effects, which can allow unprecedented opportunity to control light propagation with magnetization and vice versa. They highlighted Mie resonances and all-dielectric metasurfaces for future research in the field of integrated photonics [115, 116, 117, 118].

Apart from the design of magneto-optical metasurfaces, one can also utilize another approach of hybrid, two-phase films to achieve a suitable magneto-optical material with silicon compatibility. We have focused on the study of two-phase nanocomposite films of metallic nanoparticles with diameters bellow 50 nm in perovskite $Sr(Ga_{1-x}Co_x)O_{3-\delta}$ (**PUBLICATION A10**). The investigated layers were grown by PLD on (001) $(LaAlO_3)_{1/3}(Sr_2AlTaO_6)_{2/3}$ (LSAT) and Si substrates from a $Sr(Ga_{0.73}Co_{0.27})O_3$ target. The substrate temperature during the deposition was chosen to be 720°C for LSAT and 760°C for Si to optimize the deposition process and avoid the formation of other oxide phases. Structural characterization by XRD revealed diffraction peaks corresponding to the perovskite structure and to metallic Co. The layers on LSAT substrates were single crystals, whereas on Si they were pollycrystaline. High-resolution TEM analysis together with element mapping by EDX confirmed the presence of sub-50 nm Co nanoparticles both at the substrate/layer interface and within the volume of the layer (see Fig. 3.11 for the case of layers on Si substrates). The biding energy spectra of Co 2p3 obtained by XPS showed two peak components corresponding to metallic Co as well as ionic

Co^{3+} of the perovskite matrix. The volume fraction of metallic Co was estimated to be approximately 6%.

Magneto-optical loops of Faraday rotation and both in-plane and out-of-plane magnetic hysteresis loops showed a decrease in saturation magnetization, M_S, with increasing thickness. Since the M_S originating mainly from Co and considering the volume fraction of 6%, the estimated M_S was in agreement with the experiential values for thinner samples. The layers exhibited weak magnetic anisotropy, probably arising from the spatial distribution of the Co particles. Therefore, the closely spaced Co nanoparticles at the substrate/layer interface might be responsible for in-plane easy axis of the samples. The saturated Faraday rotation of the films at a wavelength of 1550 nm followed a thickness dependence similar to M_S (see Fig. 3.12), as expected. The highest Faraday rotation was observed for the thinnest layers and was approx. 3000 deg/cm for layers on both LSAT and Si substrates. Spectroscopic ellispometry was employed to deduce the spectral dependence of complex refractive index of the layers and to estimate the values of the absorption coefficient at 1550 nm in order to calculate the FoM. Due to a relatively complex structure of the layers, a two layer model utilizing the effective medium approximation was used to evaluate experimental ellipsometric data. The resulting absorption coefficients confirmed relatively high optical absorption, which was ascribed to the absorption of metallic Co at the layer/substrate interface. Therefore, the values of FoM were modest in comparison to those of other perovskite materials on Si substrates.

4. Metallic and half-metallic materials for spintronics

Rapid development in the field of information technologies put enormous pressure on the development of high power, low energy consumption, and affordable computing devices. While the approaches of the classical electronics start to hit their quantum-mechanical limits, novel concepts such as photonic computing or spin electronics (spintronics) take place. In contrast to classical electronics, spintronics employs a spin of an electron as a carrier of one bit of information, making devices faster, non-volatile, and with lower energy consumption. For the successful implementation of spintronic devices in consumable electronics, one has to master and dynamically control the magnetic order of materials. For that purpose, various elements (such as spin-filters, magnetic tunneling junctions (MTJs), spin valves, spin-transfer torque devices, spin-orbit torque devices, spin pumping devices, giant magnetoresistance (GMR) devices, etc.) are crucial to fabricate with proper functionality.

This chapter summarizes our research of magneto-optical properties of metallic and half-metallic materials, which because of their unique properties (high spin polarization and strain-induced changes of magnetic properties, compensation point, modifiable interfaces, etc.) can serve well for purposes of novel spintronics devices.

4.1 An interplay between the structure and magnetism: magneto-optical properties of strained manganites thin films

Hole doped manganites $La_{1-x}M_xMnO_3$ (M = Ca, Sr, Ba) emerge as ideal model systems for studying phenomena underlying strain-controlled magnetic properties. These perovskite structure oxides exhibit colossal magnetoresistance [119] and nearly fully spin-polarized carriers. They also contain manganese ions with mixed valence states (Mn^{3+}/Mn^{4+}), resulting in metallic conductivity along with ferromagnetic ordering. This phenomenon is explained by the double exchange interaction [120], which is strongly tied to the crystal lattice and depends on the Mn-O bond length and bond angle. This dependency leads to different physical properties of manganites deposited on different substrates and opens the possibility for future integration with piezoelectric buffer layers for dynamic control of magnetism.

Our interest was focused on the half-metallic and ferromagnetic $La_{2/3}Sr_{1/3}MnO_3$ (LSMO), which exhibits a high Currie temperature, $T_C \approx 370K$ [121] and nearly 100% spin polarization [122]. We investigated the magneto-optical properties of LSMO thin films grown on $SrTiO_3$ (STO) substrates with (100) and (110) crystallographic orientations (**PUBLICATION A11**). Our goal was to analyze the dependence of the permittivity tensor elements on film thickness and substrate orientation, as well as to evaluate how strain and surface morphology influence the magneto-optical properties.

The LSMO films were deposited using PLD with thicknesses ranging from 10 to 50 nm. Using magneto-optical Kerr spectroscopy in both polar and longitudinal configurations, combined with spectroscopic ellipsometry, we examined the optical and magneto-optical

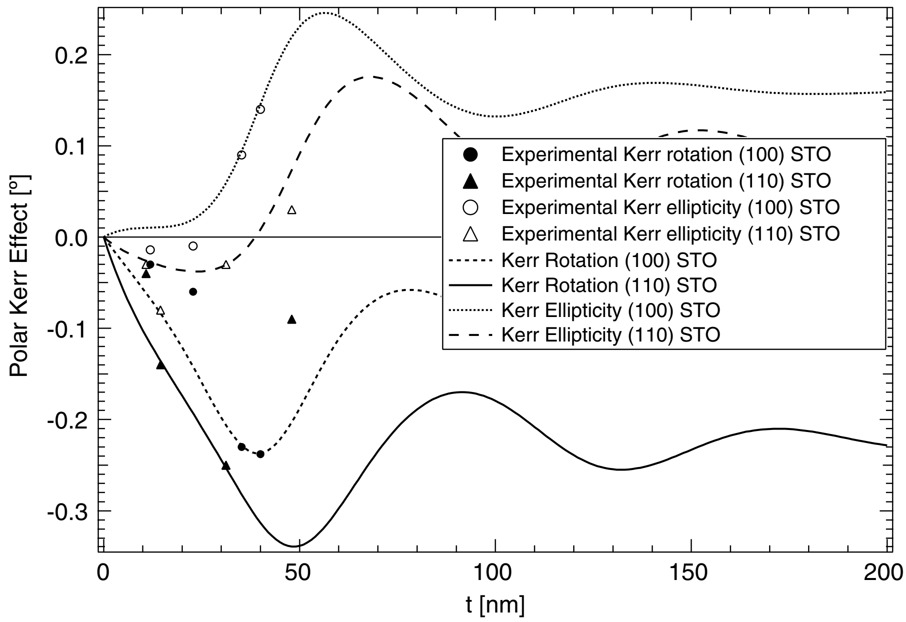

Figure 4.1: Computed polar Kerr rotation and ellipticity as a function of thickness of the LSMO films on STO substrate at a fixed photon energy. The points correspond to experimental values [124].

response of investigated films in the photon energy range from 1.2 to 4.8 eV. The combination of the techniques allowed for deduction of the spectral dependence of the full permittivity tensor for each film. The spectral behavior agreed well with the results reported on sintered samples and thick films [123], demonstrating the epitaxial quality of the investigated samples.

The experimental magneto-optical Kerr spectra showed a clear dependence on film thickness and substrate orientation, as shown in Fig. 4.1 for the fixed energy of incident light. A thickness-dependent theoretical polar Kerr effect was calculated using the material parameters obtained on 35.2 nm (STO (100) substrate) and 31.2 nm (STO (110) substrate) thick samples and considering a model structure of a thin LSMO film on semi-infinite STO substrate (included in Fig. 4.1).

Comparison with experimental data revealed that films grown on STO(110) exhibited a faster onset of the polar Kerr effect compared to those on STO(100), as follows from Fig. 4.1. This behavior is likely related to the lower strain in STO(110) films, which facilitates the development of ferromagnetic order. In LSMO films, the ferromagnetic order is mainly driven by double-exchange interactions between the Mn^{3+} and Mn^{4+} ions [125]. These interactions are highly sensitive to strain induced by lattice mismatch with the substrates [126]. Consequently, deviations from the linearity of the polar Kerr effect were attributed to tensile strain, which can vary with the increasing thickness of the LSMO films. The off-diagonal permittivity element spectra, extracted from magneto-optical spectroscopy, confirmed this trend by showing higher amplitudes in thinner films on STO (110), whereas in films on STO (100), the magneto-optical response developed more gradually with increasing thickness.

The analysis of the longitudinal Kerr effect spectra revealed that for the films grown on STO (100), the longitudinal Kerr spectra could be reasonably explained by assuming the off-diagonal elements of the permittivity tensor deduced from polar Kerr spectroscopy. However, for films grown on STO (110), while the expected spectral shape was obtained,

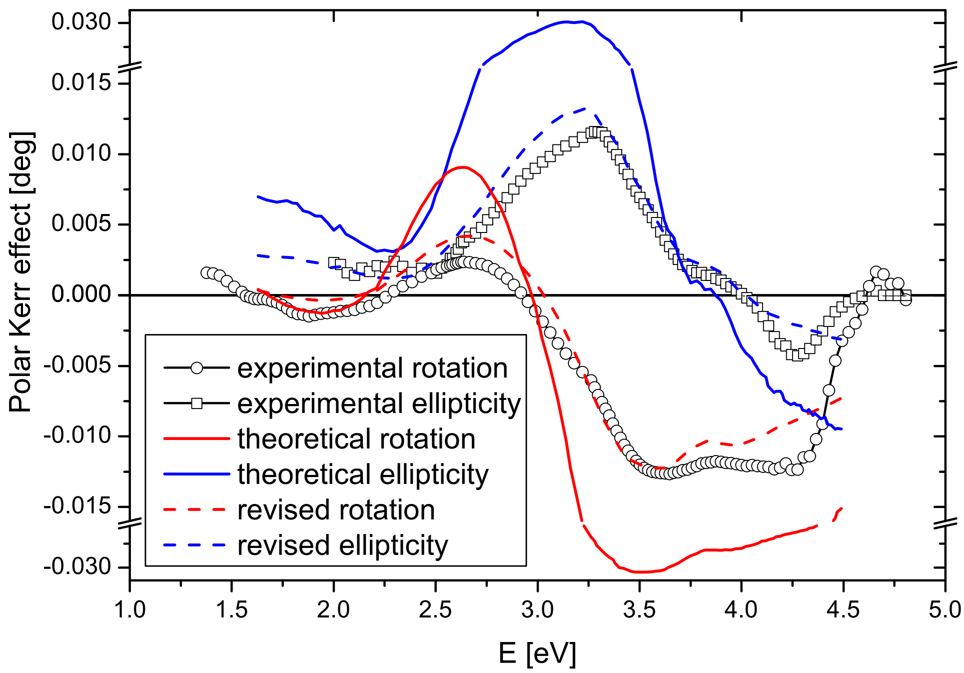

Figure 4.2: Experimental and theoretical polar Kerr rotation and ellipticity spectra of 5 nm thick LSMO film. The theoretical model (solid curves) employed transfer matrix formalism and material parameters of a 35 nm thick LSMO layer. The revised theoretical model (dashed curves) considered a more realistic structure [134].

the computed amplitudes were higher than the measured ones, suggesting a more pronounced surface morphology induced by slightly different growth on this substrate orientation. At the oblique light incidence, the amplitude of the Kerr effect is usually influenced by light scattering on the surface roughness.

Importantly, the experimental results showed that even for 10 nm thick sample, the magneto-optical spectra exhibited characteristic LSMO spectral structures, confirming the presence of room-temperature ferromagnetism. The good agreement between the deduced permittivity tensor spectra with those obtained from bulk and thick film samples [127, 123] further supported the conclusion that the perovskite structure of LSMO was well developed even at such small thicknesses.

The findings of our study broadened the knowledge about the corelation between the strain induced by different substrate orientations and the optical and magneto-optical properties of LSMO. They were later used in following research related to strain modifications and growth optimization of manganite thin films [128, 129, 130, 131, 132].

Stimulated by the results on the strain-influenced thickness-dependent magneto-optical Kerr effect in LSMO, we moved our attention to the layer/substrate interface to get more insight into the creation and evolution of magnetism from the interface across the layer. Our primary focus was to understand the impact of interface effects on the evolution of ferromagnetism and magneto-optical properties in ultrathin films since the existence of a magnetically dead layer was reported [133]. To achieve this, we performed polar and longitudinal Kerr magneto-optical spectroscopy, complemented by theoretical modeling based on the transfer matrix formalism.

We examined PLD deposited LSMO films on (100) STO substrates with thicknesses of 5 nm (13 monolayers) and 10.7 nm (27 monolayers) (**PUBLICATION A12**). The magneto-optical Kerr effect, which is proportional to the film magnetization, was measured in the photon energy range from 1.2 to 4.6 eV. For the 10.7 nm film, the experimental polar Kerr spectra showed excellent agreement with theoretical simulations using bulk-like permittivity tensor parameters. This indicated that the LSMO layer exhibited magneto-optical properties comparable to those of bulk crystals, suggesting a well-developed perovskite structure with a strong ferromagnetic order.

However, for the 5 nm film, a significant reduction in Kerr effect amplitudes with respect to the theoretical model was observed (see Fig. 4.2), indicating suppressed ferromagnetism due to interface effects. To explain such behavior, a revised theoretical model with monolayer resolution was employed. This model revealed that the suppression of the double-exchange interactions occurs within the first three monolayers, where the out-of-plane Mn e_g $(3z^2 - r^2)$ orbitals are stabilized against in-plane e_g $(x^2$ - $y^2)$ making a local C-type antiferromagnetic structure at the interface [135]. Beyond these interfacial layers, the double-exchange mechanism gradually restores, reaching full ferromagnetic order within approximately nine monolayers. The revised theoretical polar Kerr effect spectra agreed well with experimental data as shown in Fig. 4.2.

The agreement of the revised theoretical model with the experimental longitudinal Kerr rotation spectrum further supported our explanations. Moreover, the presence of a measurable magneto-optical Kerr effect at room temperature in the 5 nm thick film underscored the effectiveness of this simple experiential technique in detecting ferromagnetic ordering even in extremely thin LSMO layers, where otherwise advanced magnetomety techniques, such as SQUID, must be used.

Our gained knowledge of interface effects and the onset and evolution of magnetism across the ultrathin LSMO layer was later utilized in the following research on heterostructures of magnetic oxides [136, 137, 138].

Oxygen octahedral rotations (OOR) in LSMO are key structural features that significantly influence its magnetic and electronic properties [139, 140, 141, 142, 143]. These rotations, which involve tilting of the MnO_6 octahedra, are strongly linked to the lattice and strain conditions. Near interfaces, such as with STO, OOR can be modified due to the mismatch between the oxygen octahedral tilting patterns of the two materials. For example, suppression of OOR in thin LSMO layers has been shown to alter ferromagnetic ordering, leading to phenomena such as canted magnetism [141]. By tuning the OOR through strain engineering or interfacial coupling, it is possible to control magnetocrystalline anisotropy and other functional properties of LSMO for spintronic and multi-ferroic applications. Such phenomena attracted our attention and we investigated the magneto-optical properties of LSMO films grown on different substrates to analyze the effects of epitaxial strain and OOR on their electronic structure (**PUBLICATION A13**).

Four different substrates were used to impose varying levels of epitaxial strain on the films: $LaAlO_3$ (LAO) for large compressive strain, LSAT for small compressive strain, STO for small tensile strain, and $DyScO_3$ (DSO) for large tensile strain. All films exhibited single-crystalline growth with low surface roughness. The thicknesses were consistent across all substrates, approximately 20 nm, as confirmed by XRD and spectroscopic ellipsometry. XRD was used to verify crystallinity and determine the lattice parameters of the films. Reciprocal Space Mapping revealed the strain states of investigated films. The films were coherently strained according to the substrates, with compressive strain observed for films on LAO and LSAT substrates and tensile strain for those on STO and

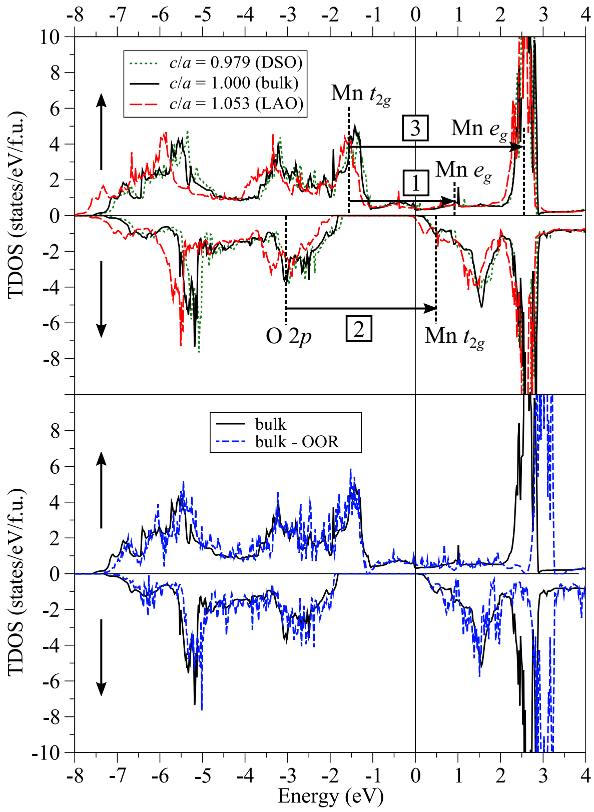

Figure 4.3: Spectra of total DOS obtained by *ab initio* calculations. Top panel shows unstrained bulk LSMO and strained LSMO corresponding to growth on LAO and DSO substrates. Magneto-optically active transitions are highlighted by arrows. Bottom panel shows bulk LSMO with no OOR and bulk LSMO with quasireal tilt [144].

DSO substrates. The strain induced by the paritucular substrate resulted in distortions of the LSMO unit cell, with compressive strain decreasing the angle γ_m of the deformed monoclinic unit cell (toward orthorhombicity) and tensile strain increasing it. The OOR patterns were found to change depending on the type of strain induced by the substrates. AFM assessed the surface morphology and roughness, with most films showing surface roughness below 0.5 nm, except for the LAO substrate, which exhibited a roughness of approximately 1.4 nm. SQUID magnetometry was used to estimate the Curie temperature, T_C, and magnetic moment of the investigated films. Magnetic properties deteriorated with increasing epitaxial strain, which was attributed to unit cell distortions and the formation of a magnetically dead layer at the film/substrate interface. Therefore, the films grown under larger strains exhibited reduced T_C and smaller magnetic moments.

We employed a combination of spectroscopic ellipsometry and magneto-optical spectroscopy to determine the spectra of both the diagonal and off-diagonal elements of the permittivity tensor and to get useful insight into the electronic structure of LSMO under different strains. Additionally, we used *ab initio* calculations to distinguish between the contributions of strain-induced distortions and OOR to the observed electronic transitions. Magneto-optical polar Kerr spectroscopy revealed that the strength of the Kerr effect depended strongly on the type and magnitude of the epitaxial strain. Films grown under high compressive strain exhibited a significant suppression of their ferromagnetic ordering, leading to weaker Kerr signals. This effect was attributed to unit cell distortions and the presence of a magnetically dead layer at the film/substrate interface. In contrast, films grown under tensile strain retained stronger ferromagnetic properties, as indicated by higher polar Kerr rotation and ellipticity values.

To gain further insight into the changes in electronic structure induced by strain, we used *ab initio* calculations. Confrontation of the off-diagonal permittivity element spectra with *ab initio* calculated DOS (shown in Fig. 4.3) confirmed the presence of two previously reported electronic transitions in all studied LSMO films, corresponding to charge-transfer and crystal-field excitations. Furthermore, we identified a new electronic transition at approximately 4.3 eV, which was observed only in films grown under compressive strain. This was classified as a crystal-field paramagnetic Mn $t_{2g} \rightarrow e_g$ transition, based on its spectral characteristics and behavior under different strain conditions. Theoretically calculated magneto-optical spectra showed that oxygen octahedra rotations had a negligible effect on the magneto-optical properties of LSMO (see Fig. 4.3). Instead, the dominant factor influencing the magneto-optical response was strain-induced distortions, which modified the occupation of Mn t_{2g} orbitals and consequently altered the selection rules for magneto-optical transitions. The ability to tune magnetic and magneto-optical properties via strain engineering has important implications for the development of oxide-based spintronics and optoelectronic devices, which confirms the following research on this topic, based on our findings [145, 146, 147].

4.2 Metallic thin films

Metallic materials play a crucial role in spintronics due to their ability to generate, transport, and manipulate spin-polarized currents, and metallic ferromagnetic layers are crucial building blogs of various spintronics devices. Among ferromagnetic metals, permalloy ($\approx$ 80% nickel and 20% iron alloy) is widely used in spin valves, MTJs and GMR sensors, where it serves as a key ferromagnetic layer for generating and detecting spin-polarized currents. Despite being widely used, the spectral dependence of the full permittivity tensor of permalloy in the form of thin films remained unknown. Therefore, we systematically investigated the optical and magneto-optical properties of permalloy thin films with thicknesses of 10 nm and 150 nm over a broad spectral range from 0.7 to 6.4 eV (**PUBLICATION A14**). The samples were prepared by ion beam sputtering on Si (100) substrates.

Spectroscopic ellipsometry and magneto-optical Kerr effect spectroscopy were used to extract the optical and magneto-optical parameters of the films in the form of a spectral dependence of the full permittivity tensor. This information might be essential for the future design of novel spintronics and optoelectronic devices. Furthermore, we examined the effects of oxidation by comparing the samples with and without a protective Au capping layer. Polar Kerr magneto-optical spectroscopy was measured in the energy range from 1.3 to 5.5 eV at nearly normal light incidence and in the fully magnetically saturated state. The results showed that the thick films (150 nm) exhibited smooth and nearly monotonic Kerr spectra, while thin films (10 nm) displayed spectroscopic structures around 3.2 eV and 4.2 eV due to optical reflections at the substrate/layer interface. The penetration depth of light in permalloy was found to be significant compared to the small thickness of thin films, allowing light reflections at the film/substrate interface, which modified the observed magneto-optical response.

The extracted off-diagonal elements of the permittivity tensor (shown in Fig. 4.4) further revealed that the strongest magneto-optical response occurred in the lower energy region (below 3 eV), indicating dominant Drude-like contributions from free carriers. The

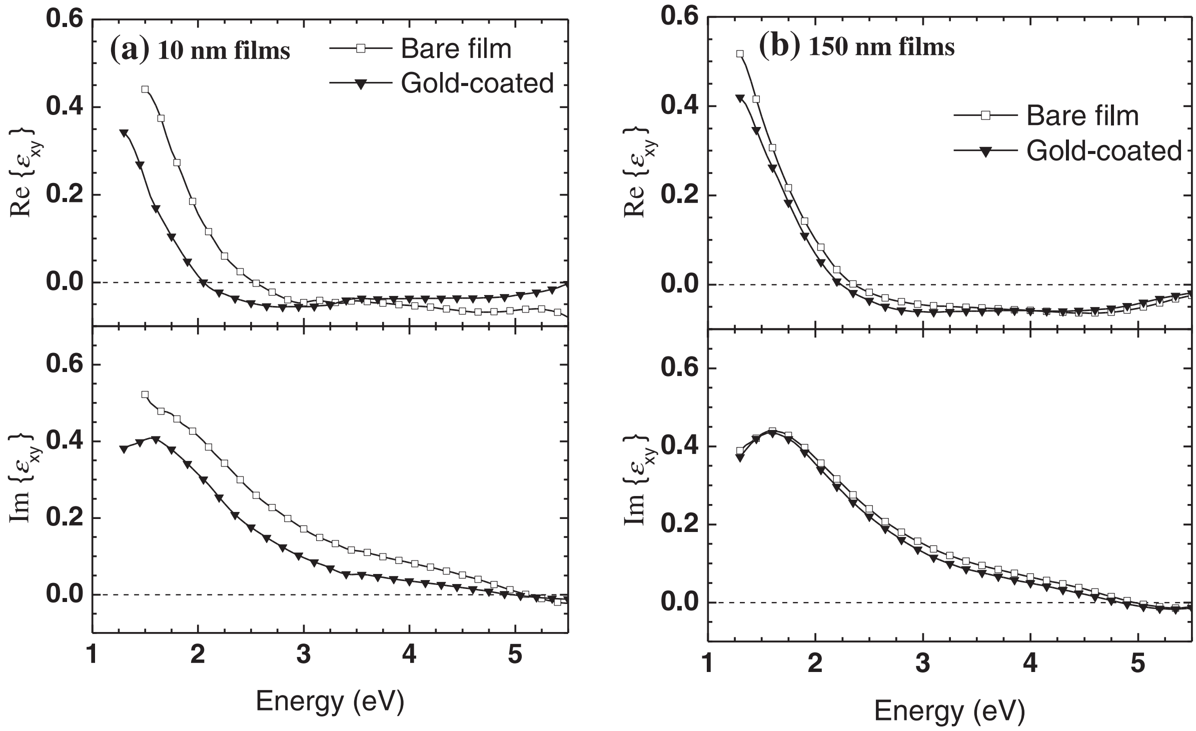

Figure 4.4: Deduced spectra of complex off-diagonal elements of permittivity tensor of permalloy thin films [148].

real part of the off-diagonal permittivity crossed zero at approximately 2.35 eV, significantly lower than the 5 eV zero crossing found in pure Ni, reflecting a different band structure of permalloy. Unlike pure Ni or Fe, no distinct zigzag structures [149] were observed around 5 eV, suggesting different interband transition behaviors.

The maximal Kerr rotation for thick permalloy films was found to be around 2.3–2.5 eV, corresponding to wavelengths of 495–540 nm, easily accessible with commercial laser sources. For thin films, the maximum Kerr rotation occurred at 1.5 eV and 4.5 eV, further confirming the influence of back-reflections from the Si substrate. The calculated FoM, which is important for magneto-optical applications, peaked around 2 eV, demonstrating that permalloy thin films could be used in specific optoelectronic devices.

Moreover, a strong impact of surface oxidation on the magneto-optical properties of 10 nm films was observed. The presence of a surface oxide layer modified the diagonal elements of the permittivity tensor and reduced the magneto-optical response due to the presence of antiferromagnetic NiO and FeO. An evident shift of the spectral features in the off-diagonal permittivity elements is also visible in Fig. 4.4. This underscores the necessity of surface protection strategies (such as Au capping).

Our comprehensive characterization of the magneto-optical response of permalloy thin films across a wide spectral range and derived permittivity tensor was utilized by the following research in the field of magnetic sensing, magneto-plasmonics and neuromorphic computing [150, 151, 152, 153, 154].

Ferrimagnetic metals are highly attractive due to their magnetic properties and electronic structure, which combine the benefits of ferromagnets and antiferromagnets. Unlike ferromagnetic materials, which suffer from stray fields and relatively slow magnetization

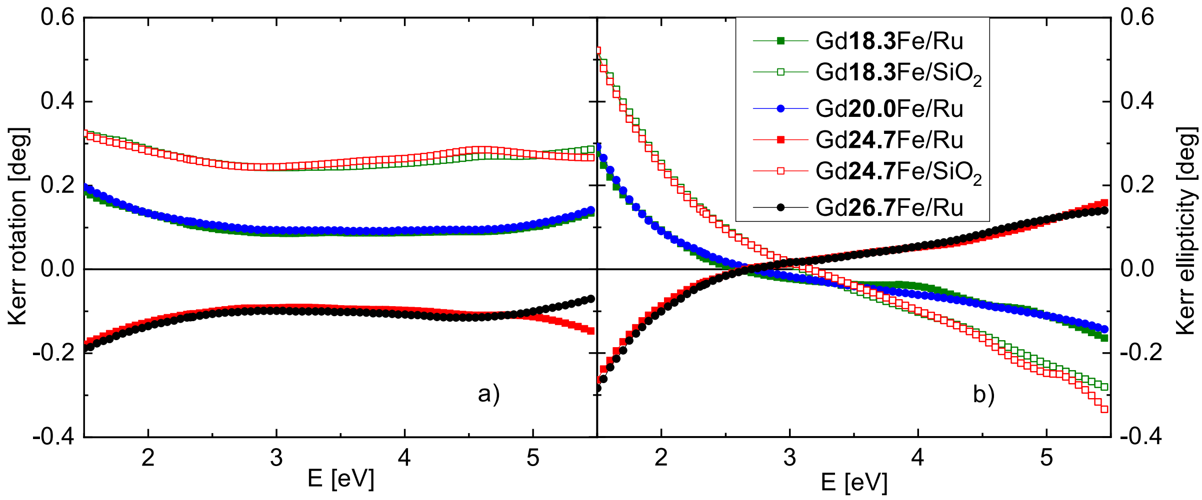

Figure 4.5: Polar magneto-optical Kerr (a) rotation and (b) ellipticity spectra of investigated Gd_xFe_{100-x} thin films with various compositions. The signe reversal of the effect confirms a compensation point [156].

dynamics, ferrimagnetic metals exhibit faster switching speeds and reduced stray fields because of their antiparallel magnetic sublattices. Furthermore, ferrimagnetic metals often exhibit compensation points where the magnetic moments on antiparallel sublattices cancel each other and the net magnetization vanishes. This allows for efficient spin manipulation under specific conditions. These properties are particularly advantageous for applications such as all-optical switching and spin-transfer-torque devices. In addition, their tunable magnetic properties, achieved by adjusting the material composition, enable precise control over performance metrics.

Motivated by low current density switching in $Gd_{22}Fe_{78}$ - MgO MTJs [155], we investigated the optical and magneto-optical properties of amorphous Gd_xFe_{100-x} thin films with varying compositions near the magnetic compensation point (**PUBLICATION A15**). The investigated films of different Gd concentrations (x = 18.3, 20.0, 24.7, 26.7) were prepared by DC magnetron sputtering. Two different materials, Ru and SiO_2, were used for capping to prevent surface oxidation of the layers. The thicknesses of Gd_xFe_{100-x} ranged from 87 to 132 nm. The thickness of the Ru capping was approx. 3 nm, while the SiO_2 capping was approx. 10 nm thick.

A combination of spectroscopic ellipsometry and magneto-optical polar Kerr spectroscopy allowed us to determine the spectra of the full permittivity tensor in a broad spectral range from 1.5 to 5.5 eV. The diagonal elements of the permittivity tensor obtained by spectroscopic ellipsometry showed a spectral behavior influenced by both Drude-like free carrier absorption and interband transitions. In particular, we observed a dominant Lorentz oscillator contribution centered around 1.9 eV, which was attributed to electronic transitions between the Fe 3*d* and Gd 5*d* states. As the concentration of Gd increased, the amplitude of this oscillator decreased, indicating a suppression of these transitions due to changes in the electronic structure.

Magneto-optical measurements of the polar Kerr effect at nearly normal incidence revealed significant variations in the Kerr rotation and ellipticity spectra across different compositions, as shown in Fig. 4.5, with a clear sign reversal at the compensation point, confirming a change in the net magnetization direction. The compensation point of the Gd_xFe_{100-x} at room temperature was estimated to be approx. $x = 24.5$.

The spectral dependence of the deduced off-diagonal permittivity tensor elements further supported this behavior, showing a zero crossing near 1.8 eV, which remained consistent across different compositions. This suggests just minor changes in the band structure of the material with composition variations. Polar Kerr effect hysteresis loops showed sharp transitions and increased coercivity as the composition approached the compensation point, reflecting the effects of reduced net magnetization and strong perpendicular magnetic anisotropy in the samples.

Finally, the variation of the capping layers (Ru and SiO_2) showed that the samples with SiO_2 capping exhibited stronger magneto-optical signals than those with Ru capping. This was attributed to different optical properties of the capping and, therefore, different reflection coefficients at the film/capping interface. Additionally, small variations in the measured coercivity for the same Gd concentration but different capping suggested potential minor compositional inhomogeneities or strain effects induced by the capping layer.

Our demonstration of the possibility to tune magnetic, optical and magneto-optical properties of Gd_xFe_{100-x} compounds by a simple variation of composition stimulated the following research in this field to obtain the material with desired physical properties required by applications [157, 158, 159, 160].

Interface effects in magnetic multilayers often define magnetic properties of the whole stack. Controlling the interfaces is therefore a key to enhanced magnetic properties of multilayered systems. There are various ways how to modify interfaces, among which Ga^+ ions irradiation provided interesting results when applied to Pt/Co systems with perpendicular magnetic anisotropy [161]. Building on already published results [162], we investigated the magneto-optical properties of Pt/Co/Pt, Pt/Co/Au, Au/Co/Au, and Au/Co/Pt trilayers with a Co thickness of 3 nm (**PUBLICATION A16**). Our aim was to investigate the differences in interfacial mixing of Pt/Co and Au/Co.

The samples were grown by molecular beam epitaxy on single crystal (0001) sapphire substrates. The thickness of the cobalt layer induced an in-plane magnetic anisotropy of the as-grown samples. After deposition, the samples were irradiated with a conventional ion implanter using 30 keV Ga^+ ions in a controlled manner to induce intermixing at interfaces and modify magnetic anisotropy. The ion fluence ranged from 10^{13} to 10^{16} ions/cm^2, enabling systematic investigation of fluence-dependent effects. XRD was used to measure lattice strain, interplanar spacing, and orientation, providing insights into the structural modifications induced by ion irradiation. XRR was utilized to evaluate layer thicknesses, surface roughness, and the extent of interface mixing. MFM provided high-resolution imaging of magnetic domain structures in irradiated samples, and positron annihilation spectroscopy analyzed vacancy-like defects and their chemical surroundings, revealing the effects of ion irradiation on defect distribution and interface quality.

We employed magneto-optical polar Kerr effect magnetometry and spectroscopy in the spectral range from 1.2 to 4.5 eV together with theoretical modeling based on transfer matrix formalism to analyze how irradiation alters the magnetic and magneto-optical behavior of the multilayers with emphasis on the interface changes.

Magneto-optical magnetometry measurements showed that ion irradiation significantly alters magnetic anisotropy, particularly enhancing perpendicular magnetic anisotropy in Pt/Co/Pt, Pt/Co/Au, and Au/Co/Pt structures. The choice of cover layer material, either Pt or Au, significantly impacted the magnitude and dependence of magnetic anisotropy changes on the ion fluence. The most pronounced changes in mag-

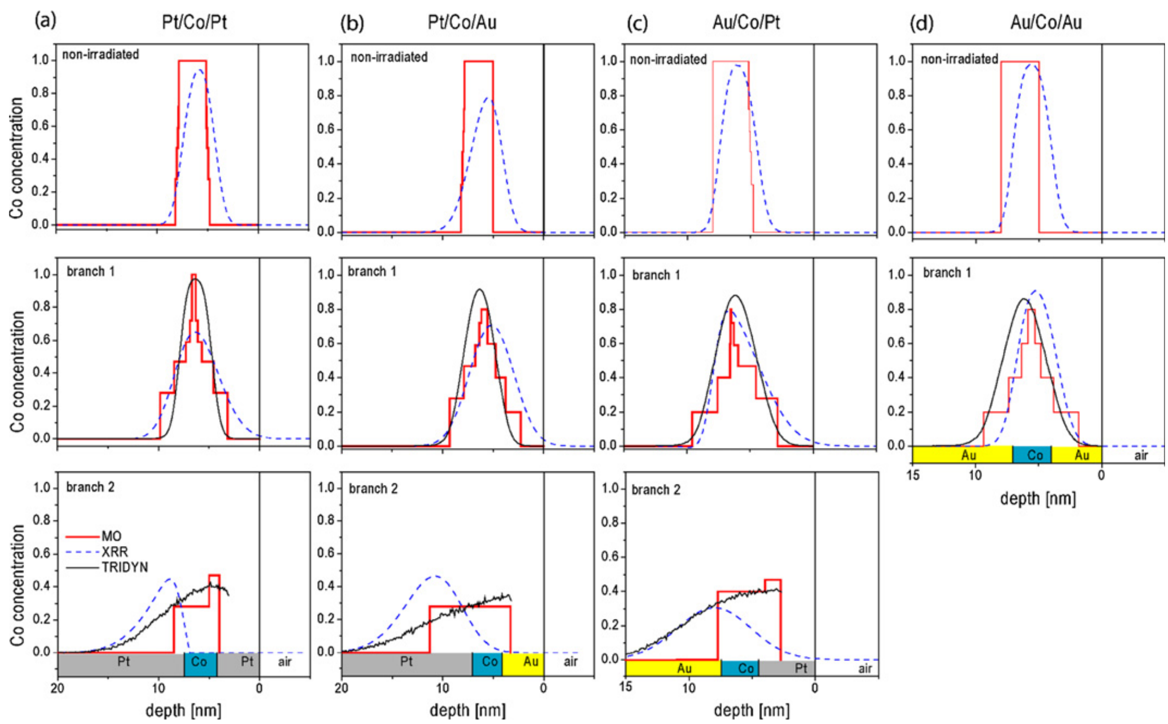

Figure 4.6: The depth profiles of Co concentration in a) Pt/Co/Pt, b) Pt/Co/Au/, c) Au/Co/Pt/, d) Au/Co/Au samples calculated as: the best fit step-like function to the experimentally obtained magneto-optical spectra (red line), XRR fitting (dashed blue line), and TRIDYN simulations (black line). Non-irradiated sample structures obtained from XRR fits are schematically shown at the bottom [163].

netic anisotropy were observed when Pt was replaced by Au as a capping or buffer layer (Pt/Co/Au and Au/Co/Pt). An ion fluence-induced increase in the polar Kerr rotation was observed for all Co layers capped with Pt, with the highest increase occurring in the Pt/Co/Pt structure, while smaller increases were observed for Pt/Co/Au and Au/Co/Pt. In contrast, no changes were detected for the Au/Co/Au system. Such effects were explained by different interfacial broadenings and disorder induced by ion irradiation.

Fluence-dependent polar Kerr rotation and ellipticity spectra of Pt/Co/Pt, Pt/Co/Au, and Au/Co/Pt trilayers exhibited non-monotonic behavior, with a strong increase at intermediate fluences followed by a decrease at higher fluences, likely due to ion-induced material removal and increased roughness. The Au/Co/Au system displayed negligible changes, confirming that Co and Au remain largely immiscible even under irradiation.

To explain such fluence-dependent behavior, theoretical magneto-optical spectra were calculated using a multilayer model consisting of 21 layers. This model reflected a real sample structure with gradual change in the material compositions, taking into account Co-Pt alloys with various compositions and their intermixing. The thicknesses of particular layers and intermixing ratios were adjusted to fit the experimental spectra of complex polar Kerr effect. Reasonably good agreement between the theoretical model and the experimental data was achieved, providing direct evidence of Co-Pt alloying under ion irradiation, which significantly modifies the magnetic properties of the trilayers and their magneto-optical response. The maximum enhancement of the magneto-optical Kerr rotation was observed for Pt/Co/Pt structures after moderate irradiation, demonstrating a correlation between the formation of magnetic Co-Pt alloys and enhanced magneto-optical properties. The cross-sectional Co-Pt compositional profiles of each trialyer obtained from magneto-optical analysis were compared to XRR and TRIDYN simulations showing reasonable agreement, as shown in Fig. 4.6. This clearly demonstrated the ability of magneto-optical spectroscopy as an effective tool to probe subtle changes at the interfaces between two materials, not only from the structural and compositional point of view but also from the magnetic point of view. This can not be done by other single experimental technique.

Since interfaces between magnetic layers and Pt or Au are attractive because of the existence of a Dzyaloshinskii-Moriya interaction, necessary to stabilize skyrmion structures, our obtained results served as a starting point for further investigations on how to tune these interfaces for applications in novel spintronic devices [164, 165, 166, 167].

4.3 Beyond the collinear magnetic order:magneto-optics of non-collinear antiferrimagnets

In recent years, the attention of the spintronics community was attracted by the non-collinear antiferromagnetic (AFM) order [168]. Non-collinear antiferromagnets manifest many advantages of antiferromagnets, such as vanishing net magnetization, which makes them insensitive to external magnetic fields. However, they still preserve several characteristics of ferromagnets, showing non-vanishing k-space Berry curvature and a consequent large anomalous Hall effect (AHE) [169] or magneto-optical Kerr effect [170]. Among non-collinear antiferromagnetic materials, the cubic antiperovskite Mn_3NiN gathered considerable attention due to its giant piezomagnetism [171]. This linear magneto-mechanic coupling effect can open the possibility to alter the magneto-optical response by applied strain, similarly to ferromagnetic LSMO.

Our interest from the magneto-optical spectroscopy point of view was focused on 100 nm thick epitaxial films of Mn_3NiN grown on (001) $BaTiO_3$ substrates using PLD (**PUBLICATION A17**). Neutron diffraction experiments confirmed a compressive in-plane biaxial strain of approx -0.007%. The Néel temperature, T_N, of 240 K has been deduced from zero-field-cooled magnetization measurements. The magnetization-field loops at various temperatures below and above T_N showed the film transition from the soft ferrimagnetic (FIM) phase existing above T_N to the AFM Γ^{4g} phase with a large coercive field. The non-vanishing small finite magnetization in the AFM phase was ascribed to the strain-induced canting of local magnetic moments. The temperature-dependent anomalous Hall effect measurements showed a gradual decrease of the anomalous Hall resistivity with decreasing temperature. This is related to the transition from the FIM phase with the highest AHE to the AFM Γ^{4g} phase followed by the transition to the AFM Γ^{5g} in which the AHE is forbidden by symmetry. The magneto-optical spectra were measured in polar geometry at nearly normal incidence. This time, a static out-of-plane magnetic field of $\pm$200 mmT was produced by a permanent magnet placed in contact with the sample. The direction of the magnetic field was alternated by a mechanical rotation of the permanent magnet. The sample was cooled down in the field to various temperatures ranging from 180 K to 300 K.

The resulting polar Kerr rotation spectra are shown in Fig. 4.7. The existence of magneto-optical spectra above T_N confirmed the existence of the FIM phase at room temperature. The amplitude of polar Kerr rotation was slightly decreasing with decreasing temperature, revealing spectral features near 1.7, 2 and 3.7 eV. A vanishing Kerr rotation

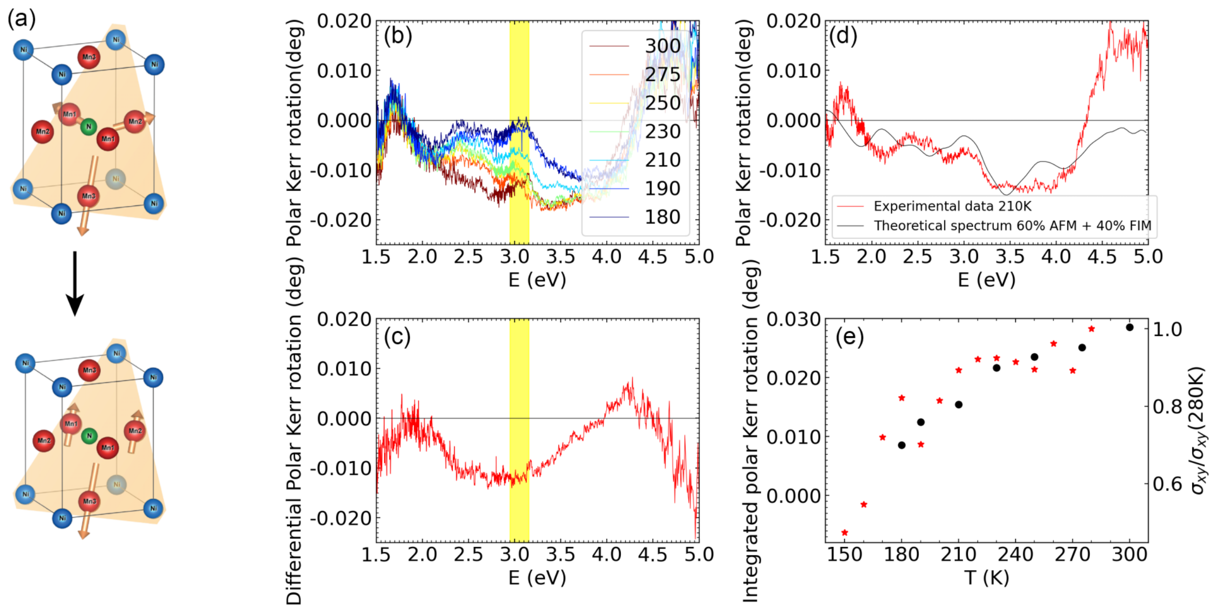

Figure 4.7: a) Schematic picture of the unit cell of Mn_3NiN together with the manganese magnetic moment alignment across the transition from the AFM to FIM phase induced by the change of temperature. b) Temperature evolution of experimental spectra of polar Kerr rotation, obtained from data taken at ±200 mT. The yellow region is the position of the gap-like feature in the manganese DOS of the AFM phase taken from nickel states. c) Differential polar Kerr rotation spectrum at 300 K to 180 K with marked position of the gap-like feature in the manganese DOS of the AFM phase. d) Experimental polar Kerr rotation spectrum taken at 210 K together with theoretical calculation when taking into account 60% of the AFM and 40% of the FIM phase; theory is multiplied by 0.1. e) A comparison of the temperature evolution of AHE conductivity (red stars) and integrated MOKE (black circles) between 1.5 and 4.3 eV [172].

was observed around 3 eV in the AFM phase. DFT calculations employing the GGA + U approach with Hubbard parameter, U, varying from 0 to 1.2 eV provided theoretical polar Kerr rotation spectra. The comparison between experimental and theoretical polar Kerr rotation spectra together with element-resolved calculations of the DOS for Mn and Ni 3*d* orbitals allowed us to map possible electronic states involved in magneto-optically active transitions. We have found relatively narrow Ni bands in DOS located only around 1.4 eV below the Fermi energy. This indicated that the excited states responsible for magneto-optical activity should be of Mn origin, which have a more rich energy-dependent DOS above the Fermi energy. Therefore, we were able to assign all the spectral structures observed in the polar Kerr rotation spectra to 3*d* electronic transitions from the ground state of nickel to various states of manganese. The vanishing Kerr rotation around 3 eV in the AFM phase nicely followed a notable gap in the 3*d* Mn DOS. Based on that, the difference in the spectra between the FIM and AFM phases was explained by the suppression of this gap in the FIM phase. In this phase, the Mn DOS have a peak, which explains a gain in the polar Kerr rotation amplitude at this energy. The differential Kerr rotation spectrum between 300 K and 180 K with the marked position of the gap-like feature in manganese DOS of the AFM phase is shown in Fig. 4.7c. The gradual change in the polar Kerr rotation spectra was simulated and explained by different mixtures of AFM and FIM phases, as shown in 4.7d for the case 60% AFM and 40% FIM. Finally, the temperature-dependent integral polar Kerr rotation was compared to the temperature-dependent anomalous Hall conductivity, which showed striking similarity as depicted in Fig. 4.7e. This result underscores that the intrinsic properties of the band structure (nonzero Berry curvature) dominate the large MOKE response in the soft FIM phase at room temperature and vanish for the Γ^{5g} AFM phase. It is also important to note that the FIM phase exhibits relatively small magnetic moment of 0.08 μ_B per formula unit, and therefore a ratio of the Kerr angle to the magnetic moment is comparable to or larger than other well-known ferrimagnets (such as CoPt, Bi_3Fe_5, NiMnSb, AuMnSb and others).

The experimental proof of the room temperature FIM phase in strained Mn_3NiN on BTO substrates is important with respect to the existence of piezomagnetism in this material. This opens up various possibilities to design and build devices for applications where the fast magnetization dynamics and dynamic control of magnetism are required, such as magnetic tunneling junctions or high-frequency magneto-optical spatial light modulators [173]. Our results also stimulated detailed work on the influence of the strain and its local variations on magnetic properties [174] or on the explanation of the anomalous Nernst effect in Mn_3NiN thin films [175].

Conclusion

The magneto-optical spectroscopy applied in the research of novel materials and nanostructures can provide valuable insights into magnetism and electronic structure and help to understand the underlying physical phenomena.

In Chapter 3 we showed that fine-tuning of the composition of ferrimagnetic iron garnets leads to an enhancement of their magneto-optical response and alternations in magnetic anisotropies. Moreover, using proper deposition conditions, optimized by feedback from magneto-optical spectroscopy measurements, growth on lattice mismatched silicon substartes can be possible. This is a crucial step for the integration of non-reciprocal magneto-optical isolating devices into photonic circuits. To increase the magneto-optical response beyond the compositional limits, ferrimagnetic garnets can be prepared in the form of photonic nanostructures. We showed that utilizing the Mie resonances results not only in notable enhancements, but also in the appearance of unconventional magneto-optical phenomena non-existing in simple thin films.

Chapter 4 demonstrated the possibility to use magneto-optical spectroscopy to investigate various material interfaces and their changes with external modifications. This was possible because of the tight link between structural properties and electronic structure in investigated materials. Since the magneto-optical phenomena are sensitive even to small changes in electronic structure, the combination of experimental data with theoretical calculations provided a detailed description of the interface properties from compositional and magnetic point of view. Such results are very important for the design of magnetic nanostructures with precisely chosen magnetic properties for applications in spintronics.

Future perspectives:
With respect to its universality, magneto-optical spectroscopy will remain a powerful experimental tool to probe magnetism and electronic structure of materials and nanostructures down to nanometer scale. With recent advances in the field of topological photonics [176], one can expect to employ topologically protected photonic states to improve the transmittance and isolation ratio in future integrated magneto-optical isolators. Moreover, recent progress in all optical switching of ferrimagnetic garnets [177] and in plasmonic optical field amplification [178] might bring together all optical control of the polarization state of light via magneto-optical material.

The field of spintronics is slowly moving from ferromagnetic materials to materials with antiferromagnetic order. This is motivated by their faster magnetization dynamics, which attacks THz frequencies. Non-collinear antiferromagnets and recently discovered "altermagnets" are especially interesting because they exhibit a spin-split band structure, mimicking the effect of exchange coupling in ferromagnets. As a result, linear magneto-optical phenomena can be observed in such systems, as was shown in our very recent work on MnTe [179]. The very high sensitivity of magneto-optical phenomena to magnetism makes them also suitable for the research in the field of 2D magnetic materials, which represents yet not fully explored scientific territory. Recent developments of our magneto-optical spectrometers allowed to apply magnetic fields up to 14 T in the temperature range from 2 to 400 K. This is suitable for systematic studies of e.g. spin-flop phases of 2D antiferromagnets or topology and symmetry related phenomena, which I together with my collaborators are really looking forward to explore!

Bibliography

[1] Masud Mansuripur. *Classical Optics and Its Applications.* Cambridge University Press, Cambridge, UK, second edition, 2009.

[2] Michael Faraday. On the magnetization of light and the illumination of magnetic lines of force. *Philosophical Transactions of the Royal Society of London*, 136:1–20, 1846.

[3] Paul Fumagalli and Joachim Schoenes. *Magneto-optics: An Introduction.* De Gruyter, Berlin/Boston, 2021.

[4] W Wettling. Magneto-optics of ferrites. *J. Magn. Magn. Mater.*, 3(1-2):147–160, March 1976.

[5] Lars Onsager. Reciprocal relations in irreversible processes. I. *Phys. Rev.*, 37(4):405–426, February 1931.

[6] P Bruno, Y Suzuki, and C Chappert. Magneto-optical kerr effect in a paramagnetic overlayer on a ferromagnetic substrate: A spin-polarized quantum size effect. *Phys. Rev. B Condens. Matter*, 53(14):9214–9220, April 1996.

[7] Stefan Visnovsky. *Optics in Magnetic Multilayers and Nanostructures.* Optical Science and Engineering. CRC Press, Boca Raton, FL, March 2006.

[8] A K Zvezdin and V A Kotov. *Modern Magnetooptics and Magnetooptical Materials.* CRC Press, January 1997.

[9] M Gibertini, M Koperski, A F Morpurgo, and K S Novoselov. Magnetic 2D materials and heterostructures. *Nat. Nanotechnol.*, 14(5):408–419, May 2019.

[10] Bevin Huang, Genevieve Clark, Efrén Navarro-Moratalla, Dahlia R Klein, Ran Cheng, Kyle L Seyler, Ding Zhong, Emma Schmidgall, Michael A McGuire, David H Cobden, Wang Yao, Di Xiao, Pablo Jarillo-Herrero, and Xiaodong Xu. Layer-dependent ferromagnetism in a van der waals crystal down to the monolayer limit. *Nature*, 546(7657):270–273, June 2017.

[11] Yujun Deng, Yijun Yu, Yichen Song, Jingzhao Zhang, Nai Zhou Wang, Zeyuan Sun, Yangfan Yi, Yi Zheng Wu, Shiwei Wu, Junyi Zhu, Jing Wang, Xian Hui Chen, and Yuanbo Zhang. Gate-tunable room-temperature ferromagnetism in two-dimensional Fe3GeTe2. *Nature*, 563(7729):94–99, November 2018.

[12] Jing Xia, Peter T Beyersdorf, M M Fejer, and Aharon Kapitulnik. Modified sagnac interferometer for high-sensitivity magneto-optic measurements at cryogenic temperatures. *Appl. Phys. Lett.*, 89(6):062508, August 2006.

[13] Lukáš Beran. *Optical and magneto-optical studies of ferrimagnetic garnets for photonic and spintronic applications.* Phd dissertation, Charles University, 2020.

[14] M Hubert, C Ross, and M Veis. Unpublished results, 2025.

[15] B Caballero, A García-Martín, and J C Cuevas. Generalized scattering-matrix approach for magneto-optics in periodically patterned multilayer systems. *Phys. Rev. B Condens. Matter Mater. Phys.*, 85(24), June 2012.

[16] L Halagačka, K Postava, M Vanwolleghem, F Vaurette, J Ben Youssef, B Dagens, and J Pištora. Mueller matrix optical and magneto-optical characterization of bi-substituted gadolinium iron garnet for application in magnetoplasmonic structures. *Opt. Mater. Express*, 4(9):1903, September 2014.

[17] T H J Loughran, P S Keatley, E Hendry, W L Barnes, and R J Hicken. Enhancing the magneto-optical kerr effect through the use of a plasmonic antenna. *Opt. Express*, 26(4):4738, February 2018.

[18] Soheila Kharratian, Hakan Urey, and Mehmet C Onbaşlı. RGB magnetophotonic crystals for high-contrast magnetooptical spatial light modulators. *Sci. Rep.*, 9(1):644, January 2019.

[19] Pochi Yeh. Optics of anisotropic layered media: A new 4×4 matrix algebra. *Surf. Sci.*, 96(1-3):41–53, June 1980.

[20] Š Višňovský. Magneto-optical ellipsometry. *Czechoslov. J. Phys.*, 36(5):625–650, May 1986.

[21] Frederic J Kahn, P S Pershan, and J P Remeika. Ultraviolet magneto-optical properties of single-crystal orthoferrites, garnets, and other ferric oxide compounds. *Phys. Rev.*, 186(3):891–918, October 1969.

[22] S Wittekoek, T J A Popma, J M Robertson, and P F Bongers. Magneto-optic spectra and the dielectric tensor elements of bismuth-substituted iron garnets at photon energies between 2.2-5.2 ev. *Phys. Rev.*, 12(7):2777–2788, October 1975.

[23] Herbert S Bennett and Edward A Stern. Faraday effect in solids. *Phys. Rev.*, 137(2A):A448–A461, January 1965.

[24] R Kubo. A general expression for the conductivity tensor. *Can. J. Phys.*, 34(12A):1274–1277, December 1956.

[25] COHERENT. What are faraday rotators and isolators?, 2024. https://www.coherent.com/news/glossary/faraday-rotators-and-isolators.

[26] Yan Zhang, Qingyang Du, Chuangtang Wang, Takian Fakhrul, Shuyuan Liu, Longjiang Deng, Duanni Huang, Paolo Pintus, John Bowers, Caroline A Ross, Juejun Hu, and Lei Bi. Monolithic integration of broadband optical isolators for polarization-diverse silicon photonics. *Optica*, 6(4):473, April 2019.

[27] Wei Yan, Yucong Yang, Shuyuan Liu, Yan Zhang, Shuang Xia, Tongtong Kang, Weihao Yang, Jun Qin, Longjiang Deng, and Lei Bi. Waveguide-integrated high-performance magneto-optical isolators and circulators on silicon nitride platforms. *Optica*, 7(11):1555, November 2020.

[28] Lei Bi, Juejun Hu, Peng Jiang, Dong Hun Kim, Gerald F Dionne, Lionel C Kimerling, and C A Ross. On-chip optical isolation in monolithically integrated non-reciprocal optical resonators. *Nat. Photonics*, 5(12):758–762, December 2011.

[29] Yuya Shoji, Yuya Shirato, and Tetsuya Mizumoto. Silicon Mach–Zehnder interferometer optical isolator having 8 nm bandwidth for over 20 db isolation. *Jpn. J. Appl. Phys. (2008)*, 53(2):022202, February 2014.

[30] Ryusuke Yamaguchi, Yuya Shoji, and Tetsuya Mizumoto. Low-loss waveguide optical isolator with tapered mode converter and magneto-optical phase shifter for TE mode input. *Opt. Express*, 26(16):21271, August 2018.

[31] Karthik Srinivasan, Cui Zhang, Prabesh Dulal, Cosmin Radu, Thomas E Gage, David C Hutchings, and Bethanie J H Stadler. High-gyrotropy seedlayer-free Ce:TbIG for monolithic laser-matched SOI optical isolators. *ACS Photonics*, 6(10):2455–2461, October 2019.

[32] Michiru Nishita, Seung-Yeol Park, Tadashi Nishio, Koki Kamizaki, Zhichao Wang, Kota Tamada, Toru Takumi, Ryuju Hashimoto, Hiroki Otani, Gregory J Pazour, Victor W Hsu, and Yasuhiro Minami. Ror2 signaling regulates golgi structure and transport through IFT20 for tumor invasiveness. *Sci. Rep.*, 7(1):1, January 2017.

[33] Karthik Srinivasan and Bethanie J H Stadler. Review of integrated magneto-optical isolators with rare-earth iron garnets for polarization diverse and magnet-free isolation in silicon photonics [invited]. *Opt. Mater. Express*, 12(2):697, February 2022.

[34] Bethanie J H Stadler and Tetsuya Mizumoto. Integrated magneto-optical materials and isolators: A review. *IEEE Photonics J.*, 6(1):1–15, February 2014.

[35] Shuang Xia, Daria O Ignatyeva, Qing Liu, Jun Qin, Tongtong Kang, Weihao Yang, Yiqin Chen, Huigao Duan, Longjiang Deng, Di Long, Martin Veis, Vladimir I Belotelov, and Lei Bi. Enhancement of the faraday effect and magneto-optical figure of merit in all-dielectric metasurfaces. *ACS Photonics*, 9(4):1240–1247, April 2022.

[36] INNOVENT. Principle - magnetic and optical systems, 2024. https://www.innovent-jena.de/en/magnetic-and-optical-systems/principle.

[37] Yosuke Nagakubo, Qi Liu, Gengjian Lou, and Takayuki Ishibashi. Magneto-optical color imaging of magnetic field distribution. *AIP Adv.*, 7(5):056803, May 2017.

[38] J M Teixeira, R Lusche, J Ventura, R Fermento, F Carpinteiro, J P Araujo, J B Sousa, S Cardoso, and P P Freitas. Versatile, high sensitivity, and automatized angular dependent vectorial kerr magnetometer for the analysis of nanostructured materials. *Rev. Sci. Instrum.*, 82(4):043902, April 2011.

[39] E Jiménez, N Mikuszeit, J L F Cuñado, P Perna, J Pedrosa, D Maccariello, C Rodrigo, M A Niño, A Bollero, J Camarero, and R Miranda. Vectorial kerr magnetometer for simultaneous and quantitative measurements of the in-plane magnetization components. *Rev. Sci. Instrum.*, 85(5):053904, May 2014.

[40] Miguel A Cascales Sandoval, A Hierro-Rodríguez, D Sanz-Hernández, L Skoric, C N Christensen, C Donnelly, and A Fernández-Pacheco. Fourier-space generalized magneto-optical ellipsometry. *Phys. Rev. B.*, 107(17), May 2023.

[41] M C Onbasli, A Kehlberger, D H Kim, G Jakob, M Kläui, A V Chumak, B Hillebrands, and C A Ross. Pulsed laser deposition of epitaxial yttrium iron garnet films

with low gilbert damping and bulk-like magnetization. *APL Mater.*, 2(10):106102, October 2014.

[42] Lichuan Jin, Kancheng Jia, Yujie He, Gang Wang, Zhiyong Zhong, and Huaiwu Zhang. Pulsed laser deposition grown yttrium-iron-garnet thin films: Effect of composition and iron ion valences on microstructure and magnetic properties. *Appl. Surf. Sci.*, 483:947–952, July 2019.

[43] J Daval, B Ferrand, D Challeton, and J C Peuzin. Liquid phase epitaxy of ferrimagnetic garnet double-layers for magneto-optics. *Mater. Res. Bull.*, 11(8):1031–1036, August 1976.

[44] Carsten Dubs, Oleksii Surzhenko, Ralf Linke, Andreas Danilewsky, Uwe Brückner, and Jan Dellith. Sub-micrometer yttrium iron garnet LPE films with low ferromagnetic resonance losses. *J. Phys. D Appl. Phys.*, 50(20):204005, May 2017.

[45] Qing-Hui Yang, Huai-Wu Zhang, Qi-Ye Wen, Ying-Li Liu, and John Q Xiao. Tuning magnetic properties of yttrium iron garnet film with oxygen partial pressure in sputtering and annealing process. *J. Appl. Phys.*, 105(7):07A501, April 2009.

[46] J H Stadler and Anand Gopinath. Integration of yttrium iron garnet films via reactive RF sputtering bethanie. *Mater. Res. Soc. Symp. Proc.*, 517(481), January 1998.

[47] M. Gomi, H. Furuyama, and M. Abe. Strong magneto-optical enhancement in highly ce-substituted iron garnet films prepared by sputtering. *Journal of Applied Physics*, 70(11):7065–7071, 1991.

[48] M Veis, E Lišková, R Antoš, Š Višňovský, Naresh Kumar, D S Misra, N Venkataramani, Shiva Prasad, and R Krishnan. Polar and longitudinal magneto-optical spectroscopy of bismuth substituted yttrium iron garnet films grown by pulsed laser deposition. *Thin Solid Films*, 519(22):8041–8046, September 2011.

[49] T Kim and M Shima. Reduced magnetization in magnetic oxide nanoparticles. *J. Appl. Phys.*, 101(9):09M516, May 2007.

[50] Yu P Sukhorukov, A V Telegin, I D Lobov, S V Naumov, S S Dubinin, K A Merencova, M S Artemyev, and A P Nosov. Magnetooptical gyrotropic effects in nanosized BiYIG films and diamagnetic YAG substrates. *J. Appl. Phys.*, 136(19), November 2024.

[51] Yu P Sukhorukov, A V Telegin, I D Lobov, S V Naumov, S S Dubinin, K A Merencova, M S Artemiev, and A P Nosov. Magnetooptical faraday and kerr effects in nanosized BiYIG/GGG structures. *J. Magn. Magn. Mater.*, 608(172415):172415, October 2024.

[52] Ganesh Gurjar, Vinay Sharma, S Patnaik, and Bijoy K Kuanr. Growth parameters of Bi0.1Y2.9Fe5O12 thin films for high frequency applications. *Thin Solid Films*, 758(139446):139446, September 2022.

[53] Vladimir Berzhansky, Tatyana Mikhailova, Alexander Shaposhnikov, Anatoly Prokopov, Andrey Karavainikov, Viacheslav Kotov, Dmitry Balabanov, and Vladimir Burkov. Magneto-optics of nanoscale Bi:YIG films. *Appl. Opt.*, 52(26):6599–6606, September 2013.

[54] T. Ishibashi, T. Kawata, T. H. Johansen, J. He, N. Harada, and K. Sato. Magneto-optical indicator garnet films grown by metal-organic decomposition method. *Journal of the Magnetics Society of Japan*, 32(2-2):150–153, 2008.

[55] T Okuda, T Katayama, H Kobayashi, N Kobayashi, K Satoh, and H Yamamoto. Magnetic properties of Bi3Fe5O12 garnet. *J. Appl. Phys.*, 67(9):4944–4946, May 1990.

[56] Ming-Yau Chern, Fang-Yuh Lo, Da-Ren Liu, Kuang Yang, and Juin-Sen Liaw. Red shift of faraday rotation in thin films of completely bismuth-substituted iron garnet $Bi_3Fe_5O_{12}$. *Jpn. J. Appl. Phys. (2008)*, 38(12R):6687, December 1999.

[57] M Deb, E Popova, A Fouchet, and N Keller. Magneto-optical faraday spectroscopy of completely bismuth-substituted Bi3Fe5O12garnet thin films. *J. Phys. D Appl. Phys.*, 45(45):455001, November 2012.

[58] Gerald F Dionne and Gary A Allen. Spectral origins of giant faraday rotation and ellipticity in bi-substituted magnetic garnets. *J. Appl. Phys.*, 73(10):6127–6129, May 1993.

[59] Gerald F Dionne and Gary A Allen. Molecular-orbital analysis of magneto-optical Bi-O-Fe hybrid excited states. *J. Appl. Phys.*, 75(10):6372–6374, May 1994.

[60] Atsushi Syouji, Hiroshi Higuchi, and Hiroki Tominaga. Magneto-optical property of ce-substituted YIG films fabricated by metal–organic deposition method. *J. Magn. Magn. Mater.*, 563(169918):169918, December 2022.

[61] R Urakawa, W Asano, M Nishikawa, M Kawahara, T Nishi, D Oshima, T Kato, and T Ishibashi. Magneto-optical property and magnetic anisotropy of (100) oriented R0.5Bi2.5Fe5O12 (r = eu, sm, and pr) thin films prepared by metal–organic decomposition. *AIP Adv.*, 12(9), September 2022.

[62] Issatay Nadinov, Oleksandr Kovalenko, Jean-Luc Rehspringer, Mircea Vomir, and Loïc Mager. Limits of the magneto-optical properties of bi: YIG films prepared on silica by metal organic decomposition. *Ceram. Int.*, 45(17):21409–21412, December 2019.

[63] William O F Carvalho and J R Mejía-Salazar. All-dielectric magnetophotonic gratings for maximum TMOKE enhancement. *Phys. Chem. Chem. Phys.*, 24(9):5431–5436, March 2022.

[64] Da Yan, Han Chen, Qing Cheng, and Han Wang. Enhanced faraday effect by magneto-plasmonic structure design composed of bismuth-iron garnet. *Opt. Laser Technol.*, 161(109193):109193, June 2023.

[65] Wei-Kuo Li and Guang-Yu Guo. First-principles study on magneto-optical effects in the ferromagnetic semiconductorsY3Fe5O12andBi3Fe5O12. *Phys. Rev. B.*, 103(1), January 2021.

[66] Eva Jesenska, Tomohiko Yoshida, Kenji Shinozaki, Takayuki Ishibashi, Lukas Beran, Martin Zahradnik, Roman Antos, Miroslav Kučera, and Martin Veis. Optical and magneto-optical properties of bi substituted yttrium iron garnets prepared by metal organic decomposition. *Opt. Mater. Express*, 6(6):1986, June 2016.

[67] M Kucera, J Bok, and K Nitsch. Faraday rotation and MCD in ce doped yig. *Solid State Commun.*, 69(11):1117–1121, March 1989.

[68] You Xu, Jie Hui Yang, and Guojying Zhang. A theoretical investigation on the strong magneto-optical enhancement in ce-substituted yttrium iron garnet. *J. Phys. Condens. Matter*, 5(47):8927–8934, November 1993.

[69] G J Diercks and S Samuelson. Magneto-optical properties of y/sub 3-x-y/ce/sub x/la/sub y/fe/sub 5/o/sub 12/. *IEEE Trans. Magn.*, 31(6):3328–3330, 1995.

[70] Mehmet C Onbasli, Lukáš Beran, Martin Zahradník, Miroslav Kučera, Roman Antoš, Jan Mistrík, Gerald F Dionne, Martin Veis, and Caroline A Ross. Optical and magneto-optical behavior of cerium yttrium iron garnet thin films at wavelengths of 200-1770 nm. *Sci. Rep.*, 6(1):23640, March 2016.

[71] Liming Duan, Dongling Yang, Zujian Wang, Rongbing Su, Chao He, Xiaoming Yang, and Xifa Long. Growth and characterization of holmium-doped yttrium iron garnet single crystal. *J. Alloys Compd.*, 966(171527):171527, December 2023.

[72] Manik Kuila, Archna Sagdeo, Lanuakum A Longchar, R J Choudhary, S Srinath, and V Raghavendra Reddy. Robust perpendicular magnetic anisotropy in ce substituted yttrium iron garnet epitaxial thin films. *J. Appl. Phys.*, 131(20):203901, May 2022.

[73] Marwa H El Makdah, Mohammad H El-Dakdouki, Rami Mhanna, Jamalat Al Boukhari, and Ramadan Awad. Effects of neodymium substitution on the structural, optical, and magnetic properties of yttrium iron garnet nanoparticles. *Appl. Phys. A Mater. Sci. Process.*, 127(5), May 2021.

[74] Manik Kuila, Uday Deshpande, R J Choudhary, Parasmani Rajput, D M Phase, and V Raghavendra Reddy. Study of magneto-optical activity in cerium substituted yttrium iron garnet (Ce:YIG) epitaxial thin films. *J. Appl. Phys.*, 129(9):093903, March 2021.

[75] Yucong Yang, Tao Liu, Lei Bi, and Longjiang Deng. Recent advances in development of magnetic garnet thin films for applications in spintronics and photonics. *J. Alloys Compd.*, 860(158235):158235, April 2021.

[76] Alex J Grede, Nina Krainova, and Noel C Giebink. Exceptional point magneto-optic isolators. *Opt. Express*, 29(14):22614–22622, July 2021.

[77] Banoj Kumar Nayak, Cijy Mathai, Dekel Meirom, Oleg Shtempluck, and Eyal Buks. Optical interface for a hybrid magnon–photon resonator. *Appl. Phys. Lett.*, 120(6):062404, February 2022.

[78] Yuma Kawaguchi, Mengyao Li, Kai Chen, Vinod Menon, Andrea Alù, and Alexander B Khanikaev. Optical isolator based on chiral light-matter interactions in a

ring resonator integrating a dichroic magneto-optical material. *Appl. Phys. Lett.*, 118(24):241104, June 2021.

[79] Khadidja Saker, Mahieddine Lahoubi, and Shengli Pu. Optimized magneto-optical isolator design based on cerium-substituted yttrium iron garnet fiber. *Opt. Quantum Electron.*, 53(6), June 2021.

[80] William O F Carvalho and J R Mejía-Salazar. Magneto-optical micro-ring resonators for dynamic tuning of add/drop channels in dense wavelength division multiplexing applications. *Opt. Lett.*, 46(10):2396–2399, May 2021.

[81] Andreas Kehlberger, Kornel Richter, Mehmet C Onbasli, Gerhard Jakob, Dong Hun Kim, Taichi Goto, Caroline A Ross, Gerhard Götz, Günter Reiss, Timo Kuschel, and Mathias Kläui. Enhanced magneto-optic kerr effect and magnetic properties ofCeY2Fe5O12Epitaxial thin films. *Phys. Rev. Appl.*, 4(1), July 2015.

[82] Enno Lage, Lukas Beran, Andy Udo Quindeau, Lukas Ohnoutek, Miroslav Kucera, Roman Antos, Sohrab Redjai Sani, Gerald F Dionne, Martin Veis, and Caroline A Ross. Temperature-dependent faraday rotation and magnetization reorientation in cerium-substituted yttrium iron garnet thin films. *APL Mater.*, 5(3):036104, March 2017.

[83] Ying Meng, Peng Chen, Wenqing He, Haoyu Zhuang, Jiahui Li, Jing Dong, Xiangfei Li, Luyao Wang, Qinwen Guo, Junkai Yang, Yu Ji, Xi Shen, Xiaohui Yu, Guoqiang Yu, Junjie Li, Xiufeng Han, and Richeng Yu. A strategy for enhancing perpendicular magnetic anisotropy in yttrium iron garnet films. *Small*, 20(25):e2308724, June 2024.

[84] Sreeveni Das, Rhodri Mansell, Lukáš Flajšman, Lide Yao, and Sebastiaan van Dijken. Perpendicular magnetic anisotropy in bi-substituted yttrium iron garnet films. *J. Appl. Phys.*, 134(24), December 2023.

[85] Nanxi Lin, Fangliang Sheng, Xin Chen, Xiaolin Hu, and Naifeng Zhuang. Epitaxy growth of pure phase CeFeO3 thin films with high magneto-optical performance and strong vertical magnetic anisotropy. *J. Rare Earths*, March 2023.

[86] Kishori Lal, Ravinder Kumar, Pramod Ghising, B Samantaray, and Z Hossain. Oblique magnetic anisotropy and domain texture in Bi3Fe5O12 films. *Phys. Rev. B.*, 108(1), July 2023.

[87] Lei Bi, Juejun Hu, Peng Jiang, Hyun Suk Kim, Dong Hun Kim, Mehmet Cengiz Onbasli, Gerald F Dionne, and Caroline A Ross. Magneto-optical thin films for on-chip monolithic integration of non-reciprocal photonic devices. *Materials (Basel)*, 6(11):5094–5117, November 2013.

[88] Lei Bi. Materials for nonreciprocal photonics. *MRS Bull.*, 43(6):408–412, June 2018.

[89] Hideki Yokoi, Tetsuya Mizumoto, and Yuya Shoji. Optical nonreciprocal devices with a silicon guiding layer fabricated by wafer bonding. *Appl. Opt.*, 42(33):6605–6612, November 2003.

[90] Karthik Srinivasan and Bethanie J H Stadler. Magneto-optical materials and designs for integrated TE- and TM-mode planar waveguide isolators: a review [invited]. *Opt. Mater. Express*, 8(11):3307, November 2018.

[91] Xue Yin Sun, Qingyang Du, Taichi Goto, Mehmet C Onbasli, Dong Hun Kim, Nicolas M Aimon, Juejun Hu, and Caroline A Ross. Single-step deposition of cerium-substituted yttrium iron garnet for monolithic on-chip optical isolation. *ACS Photonics*, 2(7):856–863, July 2015.

[92] Naresh Kumar, D S Misra, N Venkataramani, Shiva Prasad, and R Krishnan. Magnetic properties of pulsed laser ablated YIG thin films on different substrates. *J. Magn. Magn. Mater.*, 272-276:E899–E900, May 2004.

[93] Junxian Wang, Songgang Cai, Yucong Yang, Zixuan Wei, Tianchi Zhang, Wei Yan, and Lei Bi. Crystallization of $Y_3Fe_5O_{12}$ thin films on silicon photonic waveguides using CO_2 laser annealing. *Opt. Mater. Express*, 14(6):1579, June 2024.

[94] Lihong Shi, Xuliang Wang, Kaifang Gao, Hongjian Chen, and Wenbo Yan. Growth of homogeneous-phase YIG grains on si substrates and their optical properties on a micron scale. *Ceram. Int.*, 47(10):14067–14074, May 2021.

[95] Y Zhang, C T Wang, X Liang, B Peng, H P Lu, P H Zhou, L Zhang, J X Xie, L J Deng, M Zahradnik, L Beran, M Kucera, M Veis, C A Ross, and L Bi. Enhanced magneto-optical effect in Y1.5Ce1.5Fe5O12 thin films deposited on silicon by pulsed laser deposition. *J. Alloys Compd.*, 703:591–599, May 2017.

[96] Takian Fakhrul, Stana Tazlaru, Lukáš Beran, Yan Zhang, Martin Veis, and Caroline A Ross. Magneto-optical Bi:YIG films with high figure of merit for nonreciprocal photonics. *Adv. Opt. Mater.*, 7(13):1900056, July 2019.

[97] Meng-Li Liu, Cheng Wang, Xuan Wu, Jin-Ru Shen, Teng Gao, Xin Chen, Xiao-Lin Hu, and Nai-Feng Zhuang. Greatly enhanced magnetic and magneto-optical properties of bismuth iron oxide sillenite crystal with cobalt–iron codoping. *Adv. Opt. Mater.*, 12(10), April 2024.

[98] Junsheng Li, Youwen Liu, and Xiao Li. Enhancement of transverse Magneto-Optic kerr effect in subwavelength all-dielectric guided mode gratings with a buffer layer. *Results Phys.*, 59(107597):107597, April 2024.

[99] Takian Fakhrul, Bharat Khurana, Hans Toya Nembach, Justin M Shaw, Yabin Fan, Grant A Riley, Luqiao Liu, and Caroline A Ross. Substrate-dependent anisotropy and damping in epitaxial bismuth yttrium iron garnet thin films. *Adv. Mater. Interfaces*, 10(30), October 2023.

[100] Jackson J Bauer, Ethan R Rosenberg, Subhajit Kundu, K Andre Mkhoyan, Patrick Quarterman, Alexander J Grutter, Brian J Kirby, Julie A Borchers, and Caroline A Ross. Dysprosium iron garnet thin films with perpendicular magnetic anisotropy on silicon. *Adv. Electron. Mater.*, 6(1):1900820, January 2020.

[101] Yan Zhang, Qingyang Du, Chuangtang Wang, Wei Yan, Longjiang Deng, Juejun Hu, Caroline A Ross, and Lei Bi. Dysprosium substituted Ce:YIG thin films with perpendicular magnetic anisotropy for silicon integrated optical isolator applications. *APL Mater.*, 7(8):081119, August 2019.

[102] Takian Fakhrul, Stana Tazlaru, Bharat Khurana, Lukáš Beran, Jackson Bauer, Michal Vančík, Ariane Marchese, Ekaterina Tsotsos, Miroslav Kučera, Yan Zhang, Martin Veis, and Caroline A Ross. High figure of merit magneto-optical ce- and bi-substituted terbium iron garnet films integrated on si. *Adv. Opt. Mater.*, 9(16):2100512, August 2021.

[103] Ethan R Rosenberg, Lukáš Beran, Can O Avci, Cyrus Zeledon, Bingqian Song, Claudio Gonzalez-Fuentes, Johannes Mendil, Pietro Gambardella, Martin Veis, Carlos Garcia, Geoffrey S D Beach, and Caroline A Ross. Magnetism and spin transport in rare-earth-rich epitaxial terbium and europium iron garnet films. *Phys. Rev. Mater.*, 2(9), September 2018.

[104] P Hansen and J-P Krumme. Magnetic and magneto-optical properties of garnet films. *Thin Solid Films*, 114(1-2):69–107, April 1984.

[105] N P Thuy, Š Višňovský, V Prosser, R Krishnan, and T K Vien. Magnetooptical polar kerr effect and reflectivity of terbium iron garnet between 2 and 6 ev. *J. Appl. Phys.*, 52(3):2292–2294, March 1981.

[106] Han Li, Ding Zhang, Yuanjing Zhang, Jingyan Yu, Ihor Syvorotka, Feng Wang, Shuting Yang, Qiye Wen, Huaiwu Zhang, and Qinghui Yang. Giant reduced magnetic anisotropy in magneto-optical garnet. *Results Phys.*, 60(107625):107625, May 2024.

[107] Hui Shen, Yu Zhao, Leifan Li, Qixin Li, Heyan Geng, Yasheng Li, Xuanbing Shen, Jiayue Xu, Ding Zhou, Tian Tian, Yunfeng Ma, Jiamin Shang, and Anhua Wu. Recent advances of rare earth iron garnet magneto-optical single crystals. *J. Cryst. Growth*, 631(127626):127626, April 2024.

[108] Tianchi Zhang, Yucong Yang, Di Wu, Junxian Wang, Zixuan Wei, Wei Yan, and Lei Bi. Silicon integrated $Bi_2TbFe_5O_{12}$ thin films for o-band nonreciprocal photonic device applications. *Opt. Mater. Express*, 14(3):767, March 2024.

[109] Svetlana V Eliseeva, Vladimir A Ostatochnikov, and Dmitrij I Sementsov. Control of defect mode in magnetophotonic crystals in the magnetic resonance region. *J. Magn. Magn. Mater.*, 354:267–271, March 2014.

[110] T Goto, A V Dorofeenko, A M Merzlikin, A V Baryshev, A P Vinogradov, M Inoue, A A Lisyansky, and A B Granovsky. Optical tamm states in one-dimensional magnetophotonic structures. *Phys. Rev. Lett.*, 101(11):113902, September 2008.

[111] A B Khanikaev, A B Baryshev, P B Lim, H Uchida, M Inoue, A G Zhdanov, A A Fedyanin, A I Maydykovskiy, and O A Aktsipetrov. Nonlinear verdet law in magnetophotonic crystals: Interrelation between faraday and borrmann effects. *Phys. Rev. B Condens. Matter Mater. Phys.*, 78(19), November 2008.

[112] Shuang Xia, Daria O Ignatyeva, Qing Liu, Jun Qin, Tongtong Kang, Weihao Yang, Yiqin Chen, Huigao Duan, Longjiang Deng, Di Long, Martin Veis, Vladimir I Belotelov, and Lei Bi. Enhancement of the faraday effect and magneto-optical figure of merit in all-dielectric metasurfaces. *ACS Photonics*, 9(4):1240–1247, April 2022.

[113] Hao Pan, Mu Ku Chen, Din Ping Tsai, and Shubo Wang. Nonreciprocal Pancharatnam-Berry metasurface for unidirectional wavefront manipulations. *Opt. Express*, 32(15):25632–25643, July 2024.

[114] Xue Yin Sun, Martin Veis, Jaroslav Kousal, Eva Jesenska, Chen Zhang, Nicolas M Aimon, Taichi Goto, Mehmet C Onbasli, Dong Hun Kim, Hong Kyoon Choi, and C A Ross. SrGa(0.7)Co(0.3)O(3-δ) perovskite-cobalt oxide-metal nanocomposite films: magnetic and optical properties. *Nanotechnology*, 26(11):115701, March 2015.

[115] Alexey Kimel, Anatoly Zvezdin, Sangeeta Sharma, Samuel Shallcross, Nuno de Sousa, Antonio García-Martín, Georgeta Salvan, Jaroslav Hamrle, Ondřej Stejskal, Jeffrey McCord, Silvia Tacchi, Giovanni Carlotti, Pietro Gambardella, Gian Salis, Markus Münzenberg, Martin Schultze, Vasily Temnov, Igor V Bychkov, Leonid N Kotov, Nicolò Maccaferri, Daria Ignatyeva, Vladimir Belotelov, Claire Donnelly, Aurelio Hierro Rodriguez, Iwao Matsuda, Thierry Ruchon, Mauro Fanciulli, Maurizio Sacchi, Chunhui Rita Du, Hailong Wang, N Peter Armitage, Mathias Schubert, Vanya Darakchieva, Bilu Liu, Ziyang Huang, Baofu Ding, Andreas Berger, and Paolo Vavassori. The 2022 magneto-optics roadmap. *J. Phys. D Appl. Phys.*, 55(46):463003, November 2022.

[116] Daria O Ignatyeva, Denis M Krichevsky, Vladimir I Belotelov, François Royer, Sushree Dash, and Miguel Levy. All-dielectric magneto-photonic metasurfaces. *J. Appl. Phys.*, 132(10):100902, September 2022.

[117] Xiaoqiang Zhang, Yunqing Jiang, Qiuyue Li, Yong Xu, Qiwen Zhan, and Weishneg Zhao. Giant magneto-optical kerr effects governed by the quasi-bound states in the continuum. *Opt. Express*, 32(22):38720–38729, October 2024.

[118] An Chang, Yanlin Zhu, Shulei Li, Lei Chen, Jindong Chen, Yi Zhou, Gaofeng Liang, Zhongquan Wen, Jin Xiang, and Gang Chen. Strong transverse magneto-optical kerr effect at normal incidence based on hybrid bound states in the continuum. *Phys. Rev. B.*, 108(23), December 2023.

[119] R von Helmolt, J Wecker, B Holzapfel, L Schultz, and K Samwer. Giant negative magnetoresistance in perovskitelikeLa2/3Ba1/3MnOxferromagnetic films. *Phys. Rev. Lett.*, 71(14):2331–2333, October 1993.

[120] Clarence Zener. Interaction between thed-shells in the transition metals. II. ferromagnetic compounds of manganese with perovskite structure. *Phys. Rev.*, 82(3):403–405, May 1951.

[121] G H Jonker and J H Van Santen. Ferromagnetic compounds of manganese with perovskite structure. *Physica*, 16(3):337–349, March 1950.

[122] M Bowen, M Bibes, A Barthélémy, J-P Contour, A Anane, Y Lemaıtre, and A Fert. Nearly total spin polarization in La2/3Sr1/3MnO3 from tunneling experiments. *Appl. Phys. Lett.*, 82(2):233–235, January 2003.

[123] H L Liu, K S Lu, M X Kuo, L Uba, S Uba, L M Wang, and H-T Jeng. Magneto-optical properties of La0.7Sr0.3MnO3 thin films with perpendicular magnetic anisotropy. *J. Appl. Phys.*, 99(4):043908, February 2006.

[124] M Veis, Š Višňovský, Ph Lecoeur, A-M Haghiri-Gosnet, J-P Renard, P Beauvillain, W Prellier, B Mercey, J Mistrík, and T Yamaguchi. Magneto-optic spectroscopy of La2/3Sr1/3MnO3films on SrTiO3(1 0 0) and (1 1 0) substrates. *J. Phys. D Appl. Phys.*, 42(19):195002, October 2009.

[125] Y Tokura and N Nagaosa. Orbital physics in transition-metal oxides. *Science*, 288(5465):462–468, April 2000.

[126] Teruo Kanki, Hidekazu Tanaka, and Tomoji Kawai. Anomalous strain effect inLa0.8Ba0.2MnO3epitaxial thin film: Role of the orbital degree of freedom in stabilizing ferromagnetism. *Phys. Rev. B Condens. Matter*, 64(22), November 2001.

[127] S Yamaguchi, Y Okimoto, K Ishibashi, and Y Tokura. Magneto-optical kerr effects in perovskite-type transition-metal oxides:La1xSrxMnO3andLa1xSrxCoO3. *Phys. Rev. B Condens. Matter*, 58(11):6862–6870, September 1998.

[128] Yu E Samoshkina, I S Edelman, M V Rautskii, and M S Molokeev. Correlation between magneto-optical and transport properties of sr doped manganite films. *J. Alloys Compd.*, 782:334–342, April 2019.

[129] Manuel Monecke, Peter Richter, Daniel Bülz, Peter Robaschik, Dietrich R T Zahn, and Georgeta Salvan. La $_{1x}$ sr $_{x}$ MnO $_{3}$ thin films on silicon prepared by magnetron sputtering: Optimization of the film structure and magnetic properties by postdeposition annealing. *Phys. Status Solidi B Basic Res.*, 258(12):2100307, December 2021.

[130] Yulia Samoshkina, Dmitriy Petrov, Andrei Telegin, Dmitry Neznakhin, and Andrey Kaul. The visible magneto-optical response of RE1-xAxMnO3manganites: relationship with the charge component of the material. *J. Phys. Condens. Matter*, 36(47):475701, August 2024.

[131] Z F Zi, Q C Liu, X W Tang, J G Lv, J M Dai, and Y P Sun. Effects of magnetic-field annealing on the morphology and magnetic properties of La0.7Sr0.3MnO3 film. *J. Low Temp. Phys.*, 170(5-6):302–306, March 2013.

[132] Tingxian Li, Kuoshe Li, Dunbo Yu, Feipeng Zhang, Ming Zhang, and Fengjun Yu. Effect of oxygen pressure on electrical transport properties for (110) oriented La2/3Sr1/3MnO3 films directly deposited on silicon. *J. Rare Earths*, 31(4):376–380, April 2013.

[133] Marie-Bernadette Lepetit, Bernard Mercey, and Charles Simon. Interface effects in perovskite thin films. *Phys. Rev. Lett.*, 108(8):087202, February 2012.

[134] M Veis, M Zahradnik, R Antos, S Visnovsky, Ph Lecoeur, D Esteve, S Autier-Laurent, J-P Renard, and P Beauvillain. Interface effects and the evolution of ferromagnetism in La2/3Sr1/3MnO3 ultrathin films. *Sci. Technol. Adv. Mater.*, 15(1):015001, February 2014.

[135] A Tebano, C Aruta, S Sanna, P G Medaglia, G Balestrino, A A Sidorenko, R De Renzi, G Ghiringhelli, L Braicovich, V Bisogni, and N B Brookes. Evidence of orbital reconstruction at interfaces in ultrathin La0.67Sr0.33MnO3 films. *Phys. Rev. Lett.*, 100(13):137401, April 2008.

[136] Jörg Schöpf, Paul H M van Loosdrecht, and Ionela Lindfors-Vrejoiu. Disentangling the magneto-optic kerr effect of manganite epitaxial heterostructures. *AIP Adv.*, 13(3), March 2023.

[137] Li-Yong Chen, Meng-Zhen Han, Tian-Jun Zhang, You Xie, and Jian-Min Zhang. Favorable optical response for non-ferromagnetic (La2/3Sr1/3MnO3)n/SrTiO3 (001) ultrathin heterojunction: a potential photomagnetoelectric device. *Eur. Phys. J. Plus*, 137(8), August 2022.

[138] Lin Yang, Lei Jin, Lena Wysocki, Jörg Schöpf, Daniel Jansen, Brajagopal Das, Lior Kornblum, Paul H M van Loosdrecht, and Ionela Lindfors-Vrejoiu. Enhancing the ferromagnetic interlayer coupling between epitaxial SrRuO3 layers. *Phys. Rev. B.*, 104(6), August 2021.

[139] Zhipeng Li, Dongsheng Song, Rong Yu, Binghui Ge, Zhenyu Liao, Yueliang Li, Shuai Dong, and Jing Zhu. Competing interfacial reconstruction mechanisms in $la_{0.7}Sr_{0.3}MnO_3/SrTiO_3$ heterostructures. *ACS Appl. Mater. Interfaces*, 8(36):24192–24197, September 2016.

[140] Daisuke Kan, Ryotaro Aso, Riko Sato, Mitsutaka Haruta, Hiroki Kurata, and Yuichi Shimakawa. Tuning magnetic anisotropy by interfacially engineering the oxygen coordination environment in a transition metal oxide. *Nat. Mater.*, 15(4):432–437, April 2016.

[141] Xiaoyan Li, Ionela Lindfors-Vrejoiu, Michael Ziese, Alexandre Gloter, and Peter A van Aken. Impact of interfacial coupling of oxygen octahedra on ferromagnetic order in La0.7Sr0.3MnO3/SrTiO3 heterostructures. *Sci. Rep.*, 7(1), January 2017.

[142] Z Liao, M Huijben, Z Zhong, N Gauquelin, S Macke, R J Green, S Van Aert, J Verbeeck, G Van Tendeloo, K Held, G A Sawatzky, G Koster, and G Rijnders. Controlled lateral anisotropy in correlated manganite heterostructures by interface-engineered oxygen octahedral coupling. *Nat. Mater.*, 15(4):425–431, April 2016.

[143] S Thomas, B Kuiper, J Hu, J Smit, Z Liao, Z Zhong, G Rijnders, A Vailionis, R Wu, G Koster, and J Xia. Localized control of curie temperature in perovskite oxide film by capping-layer-induced octahedral distortion. *Phys. Rev. Lett.*, 119(17), October 2017.

[144] Martin Zahradník, Thomas Maroutian, Martin Zelený, Lukáš Horák, Georg Kurij, Tomáš Maleček, Lukáš Beran, Štefan Višňovský, Guillaume Agnus, Philippe Lecoeur, and Martin Veis. Electronic structure of La2/3Sr1/3MnO3 : Interplay of oxygen octahedra rotations and epitaxial strain. *Phys. Rev. B.*, 99(19), May 2019.

[145] Yingqi Cui, Yiming Liu, Guifang Li, Jiayi Zhang, Yaqi Chu, Xu Li, Shenbo Yang, and Hao Tian. Strain-induced antiferroelectric-ferroelectric-antiferroelectric phase transitions in epitaxial LaTaO4 films. *ACS Appl. Mater. Interfaces*, 16(47):65149–65156, November 2024.

[146] Yulia Samoshkina, Dmitriy Petrov, Andrei Telegin, Dmitry Neznakhin, and Andrey Kaul. The visible magneto-optical response of RE1-xAxMnO3manganites:

relationship with the charge component of the material. *J. Phys. Condens. Matter*, 36(47):475701, August 2024.

[147] Leonard Schüler, Ulrich Ross, and Vasily Moshnyaga. Strain-induced phase transition at the surface of epitaxial La0.65Sr0.35MnO3 films. *Surf. Interfaces*, 45(103906):103906, February 2024.

[148] Kristupas Kazimieras Tikuišis, Lukášs Beran, Petr Cejpek, Klára Uhlířová, Jaroslav Hamrle, Marek Vaňatka, Michal Urbánek, and Martin Veis. OPTICAL AND MAGNETO-OPTICAL PROPERTIES OF PERMALLOY THIN FILMS IN 0.7–6.4 ev PHOTON ENERGY RANGE. *Mater. Des.*, 114:31–39, January 2017.

[149] K Nakajima, H Sawada, T Katayama, and T Miyazaki. Effects of the surface and interface on the magneto-optical properties in (co, Ni)/Cu(001) ultrathin films. *Phys. Rev. B Condens. Matter*, 54(22):15950–15957, December 1996.

[150] Dmitry Murzin, Victor Belyaev, Christina Gritsenko, Vladimir Komanicky, and Valeria Rodionova. Magnetic field sensing elements based on Ni80Fe20 2D magnetoplasmonic crystals. *Sens. Actuators A Phys.*, 377(115773):115773, October 2024.

[151] B Choi and M Aryal. Spectroscopic investigations on plasmonic enhancement of magneto-optical effect in Ni80Fe20 thin films incorporating gold-nanoparticles. *Curr. Appl. Phys.*, 49:138–142, May 2023.

[152] Dmitry V Murzin, Aleksandr Yu Frolov, Karen A Mamian, Victor K Belyaev, Andrey A Fedyanin, and Valeria V Rodionova. Low coercivity magnetoplasmonic crystal based on a thin permalloy film for magnetic field sensing applications. *Opt. Mater. Express*, 13(1):171, January 2023.

[153] P Monalisha, Shengyao Li, Tianli Jin, P S Anil Kumar, and S N Piramanayagam. Synaptic plasticity investigation in permalloy based channel material for neuromorphic computing. *J. Phys. D Appl. Phys.*, 56(1):015302, January 2023.

[154] V B Novikov, A M Romashkina, D A Ezenkova, I A Rodionov, K N Afanasyev, A V Baryshev, and T V Murzina. Surface plasmon driven enhancement of linear and nonlinear magneto-optical kerr effects in bimetallic magnetoplasmonic crystals in conical diffraction. *Phys. Rev. B.*, 105(15), April 2022.

[155] Hidekazu Kinjo, Kenji Machida, Koichi Matsui, Ken-Ichi Aoshima, Daisuke Kato, Kiyoshi Kuga, Hiroshi Kikuchi, and Naoki Shimidzu. Low-current-density spin-transfer switching in Gd22Fe78-MgO magnetic tunnel junction. *J. Appl. Phys.*, 115(20):203903, May 2014.

[156] Eva Jesenská, Takayuki Ishibashi, Lukáš Beran, Martin Pavelka, Jaroslav Hamrle, Roman Antoš, Jakub Zázvorka, and Martin Veis. Optical and magneto-optical properties of GdxFe(100-x) thin films close to the compensation point. *Sci. Rep.*, 9(1):16547, November 2019.

[157] A Chanda, J E Shoup, N Schulz, D A Arena, and H Srikanth. Tunable competing magnetic anisotropies and spin reconfigurations in ferrimagnetic Fe100xGdx alloy films. *Phys. Rev. B.*, 104(9), September 2021.

[158] N Yamashita, E Shigematsu, S Honda, R Ohshima, M Shiraishi, and Y Ando. Realization of efficient tuning of the fermi level in iron-based ferrimagnetic alloys. *Phys. Rev. Mater.*, 6(10), October 2022.

[159] Yuzhi Xing, Ruofei Xing, Xiaonan Zhao, Zhenfa Wu, Dong Wang, Houning Song, Chen Qi, Lin Wei, Shishen Yan, Yufeng Tian, Lihui Bai, and Yanxue Chen. Voltage control of magnetic properties in Gd_xFe_{100-x} films by hydrogen migration. *Appl. Phys. Lett.*, 121(26):262403, December 2022.

[160] Mojtaba Mohammadi, Satoshi Sumi, Kenji Tanabe, and Hiroyuki Awano. Boosting domain wall velocity and stability in ferrimagnetic GdFe nanowires by applying laser-annealing process. *Appl. Phys. Lett.*, 123(20), November 2023.

[161] A Maziewski, P Mazalski, Z Kurant, M O Liedke, J McCord, J Fassbender, J Ferré, A Mougin, A Wawro, L T Baczewski, A Rogalev, F Wilhelm, and T Gemming. Tailoring of magnetism in Pt/Co/Pt ultrathin films by ion irradiation. *Phys. Rev. B Condens. Matter Mater. Phys.*, 85(5), February 2012.

[162] E Lišková, M Veis, Š Višňovský, J Ferré, A Mougin, P Mazalski, A Maziewski, M O Liedke, and J Fassbender. Effect of ga+ irradiation on the magneto-optic spectra of Pt/Co/Pt sandwiches. *Thin Solid Films*, 520(24):7169–7172, October 2012.

[163] P Mazalski, L Ohnoutek, I Sveklo, L Beran, Z Kurant, W Powroźnik, A Wawro, M O Liedke, M Butterling, A Wagner, J Fassbender, J Hamrle, R Antoš, V Kletecka, M Veis, and A Maziewski. Ultrathin co films with pt and au covers—magnetic and structural properties driven by ga+ ion irradiation. *New J. Phys.*, 23(2):023015, February 2021.

[164] Chen-Yuan Hsieh, Pei-Cheng Jiang, Wei-Hsiang Chen, and Jyh-Shen Tsay. Strain driven phase transition and mechanism for Fe/Ir(111) films. *Sci. Rep.*, 11(1):21909, November 2021.

[165] D Ourdani, Y Roussigné, S M Chérif, M S Gabor, and M Belmeguenai. Correlation between interface perpendicular magnetic anisotropy and interfacial Dzyaloshinskii–Moriya interactions in Pt/Pd(t $_{Pd}$)/Co(t $_{Co}$)/Au. *J. Phys. D Appl. Phys.*, 55(48):485004, December 2022.

[166] M Kowacz, M Matczak, M Schmidt, F Stobiecki, and P Kuświk. Correlation between anisotropy and concentration profiles of Ir/Co/Pt system modified by ga+ bombardment with different energies. *J. Magn. Magn. Mater.*, 587(171271):171271, December 2023.

[167] Roman Pedan, Ivan Kruhlov, Pavlo Makushko, Oleksandr Dubikovskyi, Oleksandr Kosulya, Andrii Orlov, Andrii Bodnaruk, Vladimir Golub, Frans Munnik, René Hübner, Denys Makarov, and Igor Vladymyrskyi. The effect of ar+ and n+ ion irradiation on the thermally induced evolution of the structural and magnetic properties of Co/Pt and Pt/Co bilayered stacks. *Mater. Chem. Phys.*, 327(129862):129862, November 2024.

[168] Berthold H Rimmler, Banabir Pal, and Stuart S P Parkin. Non-collinear antiferromagnetic spintronics. *Nat. Rev. Mater.*, August 2024.

[169] Satoru Nakatsuji, Naoki Kiyohara, and Tomoya Higo. Large anomalous hall effect in a non-collinear antiferromagnet at room temperature. *Nature*, 527(7577):212–215, November 2015.

[170] Tomoya Higo, Huiyuan Man, Daniel B Gopman, Liang Wu, Takashi Koretsune, Olaf M J van 't Erve, Yury P Kabanov, Dylan Rees, Yufan Li, Michi-To Suzuki, Shreyas Patankar, Muhammad Ikhlas, C L Chien, Ryotaro Arita, Robert D Shull, Joseph Orenstein, and Satoru Nakatsuji. Large magneto-optical kerr effect and imaging of magnetic octupole domains in an antiferromagnetic metal. *Nat. Photonics*, 12(2):73–78, February 2018.

[171] David Boldrin, Andrei P Mihai, Bin Zou, Jan Zemen, Ryan Thompson, Ecaterina Ware, Bogdan V Neamtu, Luis Ghivelder, Bryan Esser, David W McComb, Peter Petrov, and Lesley F Cohen. Giant piezomagnetism in Mn3NiN. *ACS Appl. Mater. Interfaces*, 10(22):18863–18868, June 2018.

[172] F Johnson, J Zázvorka, L Beran, D Boldrin, L F Cohen, J Zemen, and M Veis. Room-temperature weak collinear ferrimagnet with symmetry-driven large intrinsic magneto-optic signatures. *Phys. Rev. B.*, 107(1), January 2023.

[173] Ken-Ichi Aoshima, Nobuhiko Funabashi, Kenji Machida, Yasuyoshi Miyamoto, Kiyoshi Kuga, Takayuki Ishibashi, Naoki Shimidzu, and Fumio Sato. Submicron magneto-optical spatial light modulation device for holographic displays driven by spin-polarized electrons. *J. Display Technol.*, 6(9):374–380, September 2010.

[174] Freya Johnson, Frederic Rendell-Bhatti, Bryan D Esser, Aisling Hussey, David W McComb, Jan Zemen, David Boldrin, and Lesley F Cohen. The impact of local strain fields in noncollinear antiferromagnetic films. *Adv. Mater.*, 36(27):e2401180, July 2024.

[175] Sebastian Beckert, João Godinho, Freya Johnson, Jozef Kimák, Eva Schmoranzerová, Jan Zemen, Zbyněk Šobáň, Kamil Olejník, Jakub Železný, Joerg Wunderlich, Petr Němec, Dominik Kriegner, Andy Thomas, Sebastian T B Goennenwein, Lesley F Cohen, and Helena Reichlová. Anomalous nernst effect in Mn3NiN thin films. *Phys. Rev. B.*, 108(2), July 2023.

[176] Tomoki Ozawa, Hannah M Price, Alberto Amo, Nathan Goldman, Mohammad Hafezi, Ling Lu, Mikael C Rechtsman, David Schuster, Jonathan Simon, Oded Zilberberg, and Iacopo Carusotto. Topological photonics. *Rev. Mod. Phys.*, 91(1), March 2019.

[177] A Stupakiewicz, K Szerenos, D Afanasiev, A Kirilyuk, and A V Kimel. Ultrafast nonthermal photo-magnetic recording in a transparent medium. *Nature*, 542(7639):71–74, February 2017.

[178] Paolo Biagioni, Matteo Savoini, Jer-Shing Huang, Lamberto Duò, Marco Finazzi, and Bert Hecht. Near-field polarization shaping by a near-resonant plasmonic cross antenna. *Phys. Rev. B Condens. Matter Mater. Phys.*, 80(15), October 2009.

[179] Michal Hubert, Tomáš Maleček, Kyo-Hoon Ahn, Martin Míšek, Jakub Železný, František Máca, Gunther Springholz, Martin Veis, and Karel Výborný. Anomalous

spectroscopical effects in an antiferromagnetic semiconductor: The case of magneto-optical kerr effect. *Phys. Status Solidi B Basic Res.*, February 2025.

Selected publications

* corresponding author

[A1] **M. Veis***, E. Lišková, R. Antoš, Š. Višňovský, Naresh Kumar, D.S. Misra, N. Venkataramani, Shiva Prasad, R. Krishnan, *Polar and longitudinal magneto-optical spectroscopy of bismuth substituted yttrium iron garnet films grown by pulsed laser deposition*, Thin Solid Films **519**, 8041–8046 (2011), DOI: 10.1016/j.tsf.2011.06.007

Contribution of M. Veis: Performed all experiments and theoretical modeling, wrote the manuscript.

[A2] E. Jesenska, T. Yoshida, K. Shinozaki, T. Ishibashi, L. Beran, M. Zahradnik, R. Antos, M. Kučera, and **M. Veis***, *Optical and magneto-optical properties of Bi substituted yttrium iron garnets prepared by metal organic decomposition*, Optical Materials Express **6**, 261138 (2016), DOI: 10.1364/OME.6.001986

Contribution of M. Veis: Planned and guided the study, supervised E. Jesenská, who did all the experimental measurements, wrote the manuscript.

[A3] M. C. Onbasli1, L. Beran, M. Zahradník, M. Kučera, R. Antoš, J. Mistrík, G. F. Dionne, **M. Veis***, C. A. Ross, *Optical and magneto-optical behavior of Cerium Yttrium Iron Garnet thin films at wavelengths of 200–1770 nm*, Scientific Reports **6**, 23640 (2016), DOI: 10.1038/srep23640

Contribution of M. Veis: Planned and guided the study together with C. A. Ross, completed the optical measurements and magneto-optical fitting and co-wrote the manuscript.

[A4] E. Lage, L. Beran, A. U. Quindeau, L. Ohnoutek, M. Kucera, R. Antos, S. R. Sani, G. F. Dionne, **M. Veis**, and C. A. Ross, *Temperature-dependent Faraday rotation and magnetization reorientation in cerium-substituted yttrium iron garnet thin films*, APL Materials **5**, 036104 (2017), DOI: 10.1063/1.4976817

Contribution of M. Veis: Planned and supervised the magneto-optical characterization and analyzed the data together with C. A. Ross, co-wrote the manuscript.

[A5] Y. Zhang, C.T. Wang, X. Liang, B. Peng, H.P. Lu, P.H. Zhou, L. Zhang, J.X. Xie, L.J. Deng, M. Zahradnik, L. Beran, M. Kucera, **M. Veis**, C. A. Ross, L. Bi, *Enhanced magneto-optical effect in $Y_{1.5}Ce_{1.5}Fe_5O_{12}$ thin films deposited on silicon by pulsed laser deposition*, Journal of Alloys and Compounds **703**, 591-599 (2017), DOI: 10.1016/j.jallcom.2017.01.315

Contribution of M. Veis: Supervised the optical and magneto-optical characterization and analyzed the data, contributed to the writing of the manuscript.

[A6] T. Fakhrul, S. Tazlaru, L. Beran, Y. Zhang, **M. Veis**, C. A. Ross, *Magneto-Optical Bi:YIG Films with High Figure of Merit for Nonreciprocal Photonics*, Advanced Optical

Materials **7**, 1900056 (2019), DOI: 10.1002/adom.201900056

Contribution of M. Veis: Planned and supervised the optical and magneto-optical characterization together with C. A. Ross, analyzed the experimental data, co-wrote the manuscript.

[A7] T. Fakhrul, S. Tazlaru, B. Khurana, L. Beran, J. Bauer, M. Vančík, A. Marchese, E. Tsotsos, M. Kučera, Y. Zhang, **M. Veis**, C. A. Ross, *High Figure of Merit Magneto-Optical Ce- and Bi-Substituted Terbium Iron Garnet Films Integrated on Si*, Advanced Optical Materials **9**, 2100512 (2021), DOI: 10.1002/adom.202100512

Contribution of M. Veis: Planned and supervised the optical and magneto-optical characterization together with C. A. Ross, analyzed the experimental data, co-wrote the manuscript.

[A8] S. Xia, D. O. Ignatyeva, Q. Liu, J. Qin, T. Kang, W. Yang, Y. Chen, H. Duan, L. Deng, D. Long, **M. Veis**, V. I. Belotelov, L. Bi, *Enhancement of the Faraday Effect and Magneto-optical Figure of Merit in All-Dielectric Metasurfaces*, ACS Photonics **9**, 1240–1247 (2022), DOI: 10.1021/acsphotonics.1c01692

Contribution of M. Veis: Contributed to the analysis of the experimental data, contributed to the writing of the manuscript.

[A9] S. Xia, D. O. Ignatyeva, Q. Liu, H. Wang, W. Yang, J. Qin, Y. Chen, H. Duan, Y. Luo, O. Novák, **M. Veis***, L. Deng, V. I. Belotelov, L. Bi, *Circular Displacement Current Induced Anomalous Magneto-Optical Effects in High Index Mie Resonators*, Laser & Photonics Reviews **16** 2200067 (2022), DOI: 10.1002/lpor.202200067

Contribution of M. Veis: Designed the magneto-optical experiments, contributed to the analysis of the data, co-wrote the manuscript.

[A10] X. Y. Sun, **M. Veis**, J. Kousal, E. Jesenska, Ch. Zhang, N. M Aimon, T. Goto, M. C Onbasli, D. H. Kim, H. K. Choi, C. A. Ross, *$SrGa_{0.7}Co_{0.3}O_{3-\delta}$ perovskite-cobalt oxide-metal nanocomposite films: magnetic and optical properties*, Nanotechnology **26**, 115701 (2015), DOI: 10.1088/0957-4484/26/11/115701

Contribution of M. Veis: Performed spectroscopic ellipsometry measurements, analyzed the experimental data, contributed to the writing of the manuscript.

[A11] **M. Veis***, Š. Višňovský, Ph. Lecoeur, A.-M. Haghiri-Gosnet, J.-P. Renard, P. Beauvillain, W. Prellier, B. Mercey, J. Mistrík and T. Yamaguchi, *Magneto-optic spectroscopy of $La_{2/3}Sr_{1/3}MnO_3$ films on $SrTiO_3$ (100) and (110) substrates*, Journal of Physics D: Applied Physics **42**, 195002 (2009), DOI: 10.1088/0022-3727/42/19/195002

Contribution of M. Veis: Performed all magneto-optical experiments and theoretical modeling, wrote the manuscript.

[A12] **M. Veis***, M. Zahradnik, R. Antos, S. Visnovsky, Ph. Lecoeur, D. Esteve, S.

Autier-Laurent, J.-P. Renard, and P. Beauvillain, *Interface effects and the evolution of ferromagnetism in* $La_{2/3}Sr_{1/3}MnO_3$ *ultrathin films*, Science and Technology of Advanced Materials **15**, 015001 (2014), DOI: 10.1088/1468-6996/15/1/015001

Contribution of M. Veis: Planned and supervised the study, performed theoretical modeling, wrote the manuscript.

[A13] M. Zahradník, T. Maroutian, M. Zelený, L. Horák, G. Kurij, Tomáš Maleček, L. Beran, Š. Višňovský, G. Agnus, P. Lecoeur, and **M. Veis***, *Electronic structure of* $La_{2/3}Sr_{1/3}MnO_3$*: Interplay of oxygen octahedra rotations and epitaxial strain*, Physical Review B **99**, 195138 (2019), DOI: 10.1103/PhysRevB.99.195138

Contribution of M. Veis: Planned and supervised the study, analyzed the experimental data, co-wrote the manuscript.

[A14] K. K. Tikuišis, L. Beran, P. Cejpek, K. Uhlířová, J. Hamrle, M. Vaňatka, M. Urbánek, **M. Veis***, *OPTICAL AND MAGNETO-OPTICAL PROPERTIES OF PERMALLOY THIN FILMS IN 0.7–6.4 eV PHOTON ENERGY RANGE*, Materials & Design **114**, 31-39 (2017), DOI: 10.1016/j.matdes.2016.10.036

Contribution of M. Veis: Planned and supervised the study, analyzed the experimental data, wrote the manuscript.

[A15] E. Jesenská, T. Ishibashi, L. Beran, M. Pavelka, J. Hamrle, R. Antoš, J. Zázvorka, **M. Veis***, *Optical and magneto-optical properties of* $Gd_xFe_{(100-x)}$ *thin films close to the compensation point*, Scientific Reports **9**, 16547 (2019), DOI: doi.org/10.1038/s41598-019-52252-z

Contribution of M. Veis: Planned and supervised the study, analyzed the experimental data, wrote the manuscript.

[A16] P. Mazalski, L. Ohnoutek, I. Sveklo, L. Beran, Z. Kurant, W. Powróznik, A. Wawro, M. O. Liedke, M. Butterling, A. Wagner, J. Fassbender, J. Hamrle, R. Antoš, V. Kletecka, **M. Veis***, and A. Maziewski, *Ultrathin Co films with Pt and Au covers—magnetic and structural properties driven by* Ga^+ *ionirradiation*, New Journal of Physics **23**, 023015 (2021), DOI: 10.1088/1367-2630/abde6d

Contribution of M. Veis: Supervised the magneto-optical characterization, provided the theoretical modeling of the interfaces, co-wrote the manuscript.

[A17] F. Johnson, J. Zázvorka, L. Beran, D. Boldrin, L. F. Cohen, J. Zemen, and **M. Veis***, *Room-temperature weak collinear ferrimagnet with symmetry-driven large intrinsic magneto-optic signatures*, Physical Review B **107**, 014404 (2023), DOI: 10.1103/PhysRevB.107.014404

Contribution of M. Veis: Planned and supervised the study together with L. Cohen, provided the magneto-optical models, co-wrote the manuscript.